POLYPUBLIE
Polytechnique Montréal

POLYTECHNIQUE MONTRÉAL
UNIVERSITÉ D'INGÉNIERIE

Titre: Title:	The Lab-Scale Fluidized Bed Reactor Transforms Thermo-Catalytically Poly(Methyl Methacrylate) (PMMA) to Methacrylic Acid (MAA)
Auteur: Author:	Olga Chub
Date:	2022
Type:	Mémoire ou thèse / Dissertation or Thesis
Référence: Citation:	Chub, O. (2022). The Lab-Scale Fluidized Bed Reactor Transforms Thermo-Catalytically Poly(Methyl Methacrylate) (PMMA) to Methacrylic Acid (MAA) [Thèse de doctorat, Polytechnique Montréal]. PolyPublie. https://publications.polymtl.ca/10712/

Document en libre accès dans PolyPublie
Open Access document in PolyPublie

URL de PolyPublie: PolyPublie URL:	https://publications.polymtl.ca/10712/
Directeurs de recherche: Advisors:	Gregory Scott Patience
Programme: Program:	Génie chimique

Ce fichier a été téléchargé à partir de PolyPublie, le dépôt institutionnel de Polytechnique Montréal
This file has been downloaded from PolyPublie, the institutional repository of Polytechnique Montréal

https://publications.polymtl.ca

POLYTECHNIQUE MONTRÉAL
affiliée à l'Université de Montréal

The lab-scale fluidized bed reactor transforms thermo-catalytically poly(methyl methacrylate) (PMMA) to methacrylic acid (MAA)

OLGA CHUB
Département de génie chimique

Thèse présentée en vue de l'obtention du diplôme de *Philosophiæ Doctor*
Génie chimique

Octobre 2022

© Olga Chub, 2022.

POLYTECHNIQUE MONTRÉAL
affiliée à l'Université de Montréal

Cette thèse intitulée :

The lab-scale fluidized bed reactor transforms thermo-catalytically poly(methyl methacrylate) (PMMA) to methacrylic acid (MAA)

présentée par **Olga CHUB**
en vue de l'obtention du diplôme de *Philosophiæ Doctor*
a été dûment acceptée par le jury d'examen constitué de :

Abdellah AJJI, président
Gregory PATIENCE, membre et directeur de recherche
Nick VIRGILIO, membre
Cathy CHIN, membre externe

DEDICATION

To my beloved parents and family
for your endless love and support
...

ACKNOWLEDGEMENTS

I express my gratitude to my supervisor Prof. G.S. Patience for giving me a chance to be a part of his team, to complete my Ph.D., for support, motivation, and lessons he gave me during my research, which goes far beyond the scope of the project that I was carrying out.

Thanks to Jean-Luc Dubois (Scientific Director at Arkema; linked with Catalysis, Processes, Renewables, and Recycling) for his critical appraisal and fruitful discussions of the results of my research.

I am sincerely grateful to Amir for his constant support, as well as for his invaluable help in correcting my English.

My sincere gratitude to Fede, Jacopo, for their sincere and professional support during my research and out of it, and for scientific discussions and taking coffee together.

Special thanks to Adrien d'Oliveira and Marie-Thérèse, for helping me with translation in French.

My deep gratitude to all my lab colleagues, with whom we exchanged experience, shared office, thanks for our joint pieces of training and emotional support.

A special thanks to all technical staff of Polytechnique Montréal for their professional assistance, and to our laboratory technicians, namely, Jean-Francois without whom my setup wouldn't exist, to Jean Ghantous – for his kind and professional daily technical assistance, to Martine Lamarche and Gino Robin for their technical support and positive emotions.

Thanks to the grant awarding authority for the financial support.

In the end, I would like to express my gratitude to all my family, and especially to my parents for their endless love, believe and support during these past four years.

RÉSUMÉ

Le polyméthacrylate de méthyle (PMMA) est un polymère thermoplastique léger et transparent. C'est une matière première pour de nombreux plastiques composés, des feux d'automobiles, de l'électronique et autres, en raison de sa grande transparence, de sa rigidité et d'autres propriétés. Selon le rapport Statista, la production mondiale annuelle de plastique a dépassé 3.6 Mt en 2020. Moins de 9 % des déchets plastiques (divers plastiques) sont recyclés au Canada. La majorité du PMMA est mise en décharge ou subit une récupération de chaleur. L'industrie est motivée à découvrir une voie rentable pour produire du PMMA de qualité supérieure. Le PMMA se transforme en monomère avec un rendement de >90 % à partir de 300 °C to 600 °C en inerte. L'industrie pratique la chaîne de retraitement: déchets de PMMA - r-MMA - r-PMMA tout en pyrolysant le PMMA en son monomère. La formation concomitante de sous-produits de réaction, tels que les oligomères, dont le point d'ébullition est similaire à celui du MMA, affecte la qualité du r-PMMA obtenu (odeur, opacité) et nécessite des coûts supplémentaires pour sa séparation.

Notre objectif était de développer un procédé de conversion du PMMA en MAA dans un réacteur à échelle laboratoire, dans lequel nous commençons par introduire le MAA comme produit final de la conversion du PMMA et impliquons les déchets de PMMA contenant des additifs, qui étaient auparavant considérés comme un traitement non rentable dans le futur. Le recentrage sur le retraitement des déchets de PMMA, qui se divise en une dépolymérisation en monomère (MMA) suivie d'une hydrolyse catalytique de l'ester en MAA, permettra à l'industrie de minimiser les investissements dans la purification du produit en raison de la différence significative entre les points d'ébullition du MAA (161 °C) et du MMA (100 °C) en obtenant du r-MMA de qualité supérieure.

Nous avons d'abord étudié les performances de catalyseurs industriels ou synthétisés en laboratoire aux propriétés physico-chimiques variées dans un réacteur à lit fluidisé de 13 mm de diamètre lors de la dégradation du PMMA. Des tests TGA isothermes préliminaires ont démontré que $\leq 6\%$ du PMMA s'est décomposé à 230 °C, alors que tout le polymère s'est complètement thermalisé à 350 °C. Dans le réacteur à lit fluidisé, avec un mélange et un transfert de chaleur améliorés, la conversion a augmenté de plus de 20 pourcent à 230 °C et 350 °C. Le PMMA s'est dégradé en 10 min. Le rendement maximal de MAA a été observé avec une zéolite Y acide (33 pourcent) et sur $CsxH_3-xPW_{12}O_{40}/SiO_2$ (20 pourcent), tandis que les autres catalyseurs ont produit moins de 8 pourcent de MAA. Malgré le rendement relativement élevé de MAA sur la zéolite Y, par rapport aux autres catalyseurs, la couche

externe de SiO_2 à la surface du catalyseur, formée pendant le séchage par pulvérisation des micro-tamis moléculaires de zéolite, a recouvert les sites acides du catalyseur. La décarboxylation partielle du MMA à 350 °C et la formation de coke sur la surface du catalyseur ont réduit le rendement en MAA.

Dans l'étape suivante, nous avons hydrolysé le MMA dans un réacteur à lit fixe et identifié les paramètres apparents de la réaction chimique. Nous avons agrandi les micro-tamis moléculaires de zéolite Y en les encapsulant dans la matrice de gel de silice, ce qui a permis d'augmenter la surface spécifique du catalyseur de 780 metersquared/g à 962 meter^2/g, de disperser de manière homogène les micro-nervures de zéolite Y dans la matrice de SiO_2 et d'améliorer les propriétés hydrophobes du catalyseur. Différentes techniques analytiques ont confirmé la présence de sites acides de Brønsted sur la zéolite Y/SiO_2. Le MMA s'est hydrolysé dans l'intervalle de 160 °C to 300 °C, la conversion a approché 96 % au-dessus de 250 °C. Le modèle de second ordre (premier ordre par le MMA et premier ordre par l'eau) correspondait au mieux à la courbe expérimentale, et l'énergie d'activation apparente était juste au-dessus de 100 kJ mol^{-1}.

Un réacteur tandem pyrolyse le PMMA dans la partie inférieure du tube de quartz de 13 mm ID et hydrolyse ensuite le MMA dans le lit fixe de zéolite Y suspendu entre une couche de laine de verre - dans sa partie supérieure. Nous avons fait varier la température dans la gamme de 270 °C to 370 °C dans le lit fluidisé, alors qu'elle ne dépassait pas 300 °C dans le lit fixe. Le rendement en MAA après le lit fixe a atteint 48 % à 50 % de la conversion du PMMA à des régimes de température modérés. Dans le lit fluidisé de sable, il s'est formé 0.001 g de coke par gramme de sable, alors qu'il était 15 fois plus élevé sur le gel de silice. Le procédé est sensible à la concentration en eau. Ainsi, à 370 °C et en l'absence d'eau, des composés organiques aromatiques se sont formés sur les parois du réacteur et dans les conduites après le lit fixe. Le coke s'est formé dans la gamme de 5 % to 6 % par masse du catalyseur dans le lit fixe à haute température et en l'absence d'eau, mais il était deux fois moins à 250 °C dans le lit fluidisé. Au cours des expériences, le lit fluidisé s'est défluidisé lorsque la température du réacteur a atteint le point de fusion du PMMA, mais le réacteur ne s'est pas arrêté et la fluidisation a repris lorsque la température a atteint le point de dégradation du PMMA.

ABSTRACT

Polymethyl methacrylate (PMMA) is a lightweight, transparent, thermoplastic polymer. It is a raw material for many compounding plastics, automobile rare lights, electronics, and others due to its high transparency, stiffness, and other properties. Annual global plastic production exceeded 3.6 Mt in 2020 according to the Statista report. Less than 9 % of plastic wastes (various plastics) is recycled in Canada. The majority of PMMA is land-filled or underwent heat recovery. The industry is motivated to discover a cost-effective route to produce premium-grade PMMA. PMMA converts to monomer with the yield >90 % from 300 °C to 600 °C in inert. Industry practices the reprocessing chain: scrap PMMA - r-MMA - r-PMMA while pyrolyzing PMMA into its monomer. The concomitant formation of reaction by-products, such as oligomers, with similar to MMA boiling points, affects the quality of the resulting r-PMMA (odor, opacity) and requires additional costs for separation.

We aimed to develop a process for PMMA conversion into MAA in a lab-scale reactor, in which we lay the stone for introducing MAA as the end product of PMMA conversion and involve the scrap PMMA-containing additives, which was previously considered unprofitable processing in the future. Refocusing on the reprocessing of scrap PMMA, consisting of its depolymerization to monomer (MMA) followed by catalytic hydrolysis of the ester to MAA, will allow the industry to minimize investment in product purification due to the significant difference in boiling points of MAA (161 °C) and MMA (100 °C) by obtaining premium quality r-MMA.

We, first, studied the performance of industrial and home-made catalysts of various physico-chemical properties in a 13 mm fluidized bed reactor at PMMA degradation. Preliminary isothermal TGA tests demonstrated that $\leq 6\%$ of the PMMA decomposed at 230 °C, whereas all the polymer completely thermalized at 350 °C. In the fluidized bed reactor, at enhanced mixing and heat transfer, conversion raised by more than 20 percent at 230 °C and 350 °C PMMA degraded in 10 min. The maximum yield of MAA was observed over the acidic zeolite Y (33 percent) and $CsxH_3-xPW_{12}O_{40}/SiO_2$ (20 percent), while the rest of catalysts produced less than 8 percent of MAA. Despite the relatively high yield of MAA over the zeolite Y, compared to other catalysts, the outer layer of SiO_2 on the catalyst surface formed during the spray-drying of zeolite micro-sieves, covered catalyst acid sites. Partial MMA decarboxylation at 350 °C and above as well as coke formation on the catalyst surface reduced MAA yield.

In the next step, we hydrolyzed MMA in a fixed-bed reactor and identified the apparent

parameters of the chemical reaction. We enlarged zeolite Y micro-sieves via their encapsulation into the matrix of silica gel, which increased the catalyst surface area from $780\,m^2\,g^{-1}$ to $962\,m^2\,g^{-1}$, homogeneously dispersed the zeolite Y micro-sieves in the matrix of SiO_2, and enhanced the catalyst's hydrophobic properties. Different analytical techniques confirmed the presence of Brønsted acid sites over the zeolite Y/SiO_2. MMA hydrolyzed in the range from 160 °C to 300 °C, the conversion approached 96 % above 250 °C. The second-order model (first order by MMA and first order by water) approximated best the experimental curve, and the apparent activation energy was right above $100\,kJ\,mol^{-1}$.

The tandem reactor pyrolyzed PMMA in the down part of the 13 mm ID quartz tube and then hydrolyzed MMA in the fixed bed of zeolite Y suspended between the glass wool layers - in its upper part. We varied the temperature in the range from 270 °C to 370 °C in the fluidized bed, while it did not exceed 300 °C in the fixed bed. The MAA yield after the fixed bed reached 48 % at 50 % of PMMA conversion at moderate temperature regimes. In the fluidized bed of sand, $0.001\,g\,g^{-1}$ of coke formed per gram of sand, while over the silica gel it was 15 times higher. The process is sensitive to water concentration. Thus, at 370 °C and in the absence of water, aromatic organics formed on the reactor walls and in the lines after the fixed bed. The coke formed in the range from 5 % to 6 % per mass of the catalyst in the fixed bed at high temperatures and absence of water, but it was twice less at 250 °C in the fluidized bed. During the experiments, the fluidized bed defluidized when the temperature in the reactor reached the PMMA melted point, however, the reactor did not shut down and the fluidization recommenced when the temperature reached the PMMA degradation point.

TABLE OF CONTENTS

DEDICATION iii

ACKNOWLEDGEMENTS iv

RÉSUMÉ v

ABSTRACT vii

TABLE OF CONTENTS ix

LIST OF TABLES xii

LIST OF FIGURES xiii

LIST OF SYMBOLS AND ACRONYMS xvii

LIST OF APPENDICES xx

CHAPTER 1 INTRODUCTION 1
- 1.1 Background and problem identification 1
- 1.2 Objectives 3

CHAPTER 2 COHERENCE OF THE CHAPTERS 6

CHAPTER 3 LITERATURE REVIEW 8
- 3.1 PMMA recycling 8
  - 3.1.1 Mechanical recycling 8
  - 3.1.2 Non-catalytic pyrolysis 8
  - 3.1.3 Degradation of PMMA with fillers and additives 13
  - 3.1.4 Catalytic pyrolysis 14
- 3.2 The effect of T and softening of PMMA in fluidized bed reactors 14
- 3.3 MAA synthesis routs 15
- 3.4 Theoretical background. Reaction mechanisms 16
  - 3.4.1 PMMA degradation mechanism 16
  - 3.4.2 Hydrolysis of esters by acidic mechanism 17
- 3.5 Catalysts for PMMA transformation to MAA 19

3.6 Processes and phenomena in fluidized bed 21
3.6.1 PMMA feeding methods in FB 22
3.6.2 Defluidization 22
3.7 Hydrodynamics studies 23
3.7.1 Minimum fluidization velocity 23
3.7.2 Residence time distribution 24
3.8 Kinetics 25
3.8.1 Benefits of PMMA degradation in FB 28

CHAPTER 4 ARTICLE 1 : FLUIDIZED BED POLY(METHYL METHACRYLATE) THERMOLYSIS TO METHYL METHACRYLATE FOLLOWED BY CATALYTIC HYDROLYSIS TO METHACRYLIC ACID 29
4.1 Abstract 29
4.2 Introduction 29
4.3 Experimental 32
4.3.1 Materials 32
4.3.2 Methods 33
4.3.3 DOE 34
4.3.4 Catalyst synthesis 34
4.3.5 Lab Set-up 35
4.4 Results and Discussions 35
4.4.1 Catalyst characterization 35
4.4.2 TGA 38
4.4.3 Catalytic degradation in FB 40
4.4.4 Reaction mechanism 49
4.5 Conclusions 49

CHAPTER 5 ARTICLE 2 : ZEOLITE Y HYDROLYSES METHYL METHACRYLATE TO METHACRYLIC ACID IN THE GAS PHASE 52
5.1 Abstract 52
5.2 Introduction 52
5.3 Experimental 54
5.3.1 Materials 54
5.3.2 Catalyst synthesis 54
5.3.3 Characterization 54
5.3.4 MMA hydrolysis tests 55
5.4 Results and discussion 56

5.4.1 BET 56
5.4.2 SEM 57
5.4.3 DR-UV–vis 57
5.4.4 XPS 59
5.4.5 MAS-NMR 61
5.4.6 TPD 62
5.4.7 MMA hydrolysis to MAA 63
5.5 Conclusions 69

CHAPTER 6 ARTICLE 3 : TANDEM FLUIDIZED BED/MILLI-SECOND FIXED BED REACTOR PRODUCES METHACRYLIC ACID FROM POLY(METHYL METHACRYLATE) 71
6.1 Abstract 71
6.2 Introduction 71
6.3 Experimental 73
6.3.1 Materials 73
6.3.2 Catalyst Characterization 73
6.3.3 Laboratory set-up 74
6.4 Results and discussion 75
6.4.1 Powder characteristics 75
6.4.2 Degradation of PMMA in a tandem reactor 76
6.5 Conclusions 81

CHAPTER 7 GENERAL DISCUSSION 83

CHAPTER 8 CONCLUSION 87
8.1 Conclusion 87
8.2 Limitations of the solution proposed 88
8.3 Recommendations for future research 89

REFERENCES 90

APPENDICES 113

LIST OF TABLES

Table 4.1 Catalyst physical properties. 36

Table 4.2 Experimental conditions and performance data: $Q_{\text{in}} = 70\,\text{mm}\,\text{min}^{-1}$ 1 g PMMA. We completed 20 tests at a nominal temperature of 350 °C and the standard deviation was ±7 °C. The percent standard deviation on conversion was 10 % based on twelve runs at 350 °C: two repeat runs for Al_2O_3 and FCC with 10 mL of catalyst and one repeat for Al_2O_3, FCC, and Mo−Zr/SiO_2 with 4 mL of catalyst. 42

Table 5.1 Identification and quantification of elements in zeolite Y/SiO_2 catalyst 60

Table 5.2 Experimental conditions and MAA and MeOH selectivity and yield . 65

Table 5.3 Thermodynamic parameters of MMA hydrolysis 66

Table 5.4 Activation energies of liquid phase esterification of various acids . . . 70

Table 6.1 Physical properties of silica gel and sand. 76

Table 6.2 Average temperatures (°C) in the fluidized and fixed beds. 78

Table 6.3 Experimental conditions and MAA and CH_3OH yields. 79

Table 6.4 The products composition after thermolysis of PMMA (run 3, 4) at 370 °C (boiling points from NIST database). 80

Table A.1 Apparent kinetic parameters obtained by different models 123

LIST OF FIGURES

Figure 3.1 Industrial methods of PMMA reprocessing into MMA 9

Figure 3.2 Processes of synthesis MMA and MAA, adopted from [1] 16

Figure 3.3 Principal steps of PMMA degradation: a - initiation in chains with head-head linking's, b - chain end scission, c - random chain scission, copy-pasted from [2] 18

Figure 3.4 Acid-catalyzed hydrolysis of MMA to MAA 19

Figure 3.5 Scheme of catalytic hydrolysis of MMA to MAA 20

Figure 3.6 Fluidization regimes and Geldart particles classification, adopted from [3]. 23

Figure 4.1 Scheme of the lab-scale fluidized bed reactor: 1-Quartz reactor, 2 - Catalyst bed, 3 - Gas distributor, 4 - PMMA injection and fluidizing gas nozzle 36

Figure 4.2 Optical photos of a - FCC catalyst; b - MoO_3-ZrO_2/SiO_2; c - sand; d - Al_2O_3; e - Zeolite Y, spray-dried; f - $Cs_xH_{1-x}PW_{12}O_{40}/SiO_2$ 37

Figure 4.3 SEM-EDS image of spray dried Zeolite Y (CBV 720 from Zeolyst, Ludox AS-40, and polyvinyl alcohol). This was the most active catalyst and was generally spherical. The image shows a rigid outer shell encasing smaller crystals of CBV 720 and silica. 38

Figure 4.4 XRD diffratogram of Al_2O_3, FCC, MoO_3-ZrO_2/SiO_2, $Ce_xH_{3-x}PW_{12}O_{40}$ and zeolite Y: triangles - γ-Al_2O_3, circles - ZrO_2; stars - Faujasite; rhombuses—Keggin-type structure 39

Figure 4.5 PMMA-1 mass loss in a TGA (M_w=1 × 10^5 kmol kg^{-1}) at a heating rate of 20 °C min^{-1} as a function of d_p. 40

Figure 4.6 Isothermal PMMA mass loss in a TGA at 230 °C, 280 °C, 300 °C, and 350 °C: solid line–PMMA-1, dashed line–PMMA-2. 41

Figure 4.7 Selectivity parity: x-axis is the ratio of mole MAA detected in the quench and moles PMMA converted and the y-axis is the ratio of the mole MAA and the total mole of products (Eqs. 4.2, 4.6) ($R^2 = 0.89$). 43

Figure 4.8 Conversion as a function of catalyst composition. Excluding the zeolite Y data the correlation coefficient, R, for the conversion based on PMMA reacted and products detected was 0.95. 44

Figure 4.9 Products composition obtained at 350 °C, $V_{catalyst}$ 4 mL and water in excess. 45

Figure 4.10 Products composition obtained at 350 °C, V_{catalyst} 10 mL and water in excess. 46
Figure 4.11 Products composition at 280 °C, V_{catalyst} 4 mL and water in excess. . . 46
Figure 4.12 Products composition at 300 °C, V_{catalyst} 4 mL and water in excess. . . 47
Figure 4.13 Mechanism of PMMA degradation and side reactions resulting formation of CO, CO_2, acetone and CH_3O- radical [4] leading to methanol formation on protonated sides of catalyst. 48
Figure 4.14 Yield MeOH versus MAA. The parity line is what we expect based on the MMA hydrolysis stoichiometry. 50
Figure 5.1 The experimental setup consisted of an 8 mm ID quartz tube housed in an electrical furnace, two HPLC pumps, quench, pH meter to monitor the acid concentration with time, Ar as the carrier gas, and air to regenerate the catalyst after an experiment. 56
Figure 5.2 EDS mapping of silicon, aluminum and oxygen in the catalyst sample (on the left) and N_2 adsorption-desorption isotherms (on the right). . 57
Figure 5.3 SEM image of zeolite Y encapsulated in silica gel. The white inclusions are zeolite Y. 58
Figure 5.4 DR UV-visible spectra of absorbance vs wavelength and Kubelka-Munk function multiplied proton energy ($(F(R') \cdot E^{0.5})$ vs E) (inclusion) for zeolite Y particles size less than 1 µm (green, line) and zeolite Y encapsulated in silica gel (blue, dash) 59
Figure 5.5 DR UV-Visible spectra of absorbance vs wavelength for fresh zeolite Y micro-sieve encapsulated in silica-gel (black) and after the reaction at different temperatures 200 °C (blue), 250 °C (pink), 300 °C (green). Spectrum of carbon black (red) represented as a reference. 60
Figure 5.6 XPS spectrum of Si_2p (a), Al_2p (b), O_1s (c) and C_1s ions. 61
Figure 5.7 ^1H MAS-NMR spectrum of catalyst. The chemical shifts 0.9 ppm, 2.86 ppm belong to AlOH species located in supercages of zeolite and extra-framework, respectively; 1.58 ppm and 2.02 ppm represent AlOH external to the framework or defects located at silanol groups; 4.57 ppm belongs to SiO_3HAl species [5]. The chemical shift 6.22 ppm is due to adsorbed carbonyl groups on the catalyst surface. 62
Figure 5.8 NH_3-TPD curve of zeolite Y encapsulated in silica gel 63
Figure 5.9 MMA conversion as a function of temperature. Experimental data are illustrated with symbols while the model fit at the two Ar feed rates are depicted with lines. 69

Figure 6.1 The tandem reactor system with a 13 mmID quartz reactor (2) located in an electrical furnace (1). The PMMA degraded in the lower fluidized bed (4) of inert (sand or silica gel) supported on the glass-wool distributor (3), and the MMA hydrolyzed in the upper fixed bed (5) of zeolite Y (hydrogen form). 74
Figure 6.2 The scanning electron microscopy of zeolite Y catalyst (10^4 and $5{\cdot}10^4$ magnification) and distribution of silica, alumina and oxygen in the sample. 75
Figure 6.3 Optical images of sand (a), silica gel (b) and grinded PMMA (c). . . 75
Figure 6.4 Time evolution of PMMA powder (d_p of 65 µm) back-mixing with sand at argon flow rate 40 mL min^{-1}; a - 0 s, b - 5 s, c - 10 s, d - 20 s, e - 30 s. 77
Figure 6.5 Defluidized bed of sand and PMMA in a temperature range from 130 °C to 270 °C (a) and agglomerates of sand and PMMA on the bottom at recommencement of fluidization above 280 °C. 77
Figure 6.6 The distribution of coke in the fixed bed of zeolite Y located in the upper part of the tandem reactor. 81
Figure A.1 TG and DTG curves obtained at HRR, 25 °C min^{-1} 118
Figure A.2 TGA (red), DTG (black) curves correspond to mass-loss of PMMA at 10 °C min^{-1}. 119
Figure A.3 The DTG curve (black, dashed line) and the MS spectra of liquid products of PMMA thermolysis registered at heating rate 10 °C min^{-1}: MMA (red), acetone (cyan), methanol (pink), dimethyl ether (DME) (green), water (light-blue), methacrylic acid (MAA) (orange). 120
Figure A.4 The DTG curve (black dashed line) corresponds to the mass-loss of PMMA at 10 °C min^{-1}. The MS signals: CO_2 (green), propene (pink), hydrogen (light blue), ethane (dark yellow), methane (orange), and ethylene (red). 121
Figure A.5 TG curves of PMMA pyrolysis demonstrated at heating rates 5 °C min^{-1}, 15 °C min^{-1} and 40 °C min^{-1} and inert flow rate 60 mL min^{-1}. 122
Figure A.6 DTG curves of PMMA pyrolysis demonstrated at heating rates 5 °C min^{-1}, 15 °C min^{-1} and 40 °C min^{-1} and inert flow rate 60 mL min^{-1}. 123
Figure A.7 Simulated results (lines) versus experimental (dots) for the first order model 124

Figure A.8 The linearized experimental data by Coats-Redfern method at variation of heating rates from 5 °C min^{-1} to 40 °C min^{-1} (dots) and extrapolated curves: 1 °C min^{-1} - blue and 400 °C min^{-1} black assuming the pyrolysis of micronized PMMA. 125

LIST OF SYMBOLS AND ACRONYMS

ATH	aluminum trihydroxide
BET	Brunauer– Emmett–Teller method
CSBR	conical spouted Bed reactor
DME	dimethyl ester
DOE	design of experiments
DTG	the derivative of mass loss by temperature
DRS	diffuse reflectance spectra
DQ	double quantum
EDS	energy dispersive spectroscopy
EDXRF	energy eispersive X-ray fluorescence method
FB	fluidized bed
FCC	fluid catalytic cracking
FID	flame ionization detector
GC	gas chromatography
HPLC	High Performance Liquid Chromatography
HRR	high resolution ramp technique
LCD	liquid crystal display
LECO	carbon analysis method
MAA	methacrylic acid
MAS	magic angle spinning
MFB	mechanically fluidized beds
MMA	methyl methacrylate
MS	mass spectrometer
NMR	nuclear magnetic resonance
PMMA	poly(methyl methacrylate)
PVA	polyvinyl alcohol
r-MAA	recycled methacrylic acid
r-MMA	recycled methyl methacrylate
r-PMMA	recycled poly(methyl methacrylate)
SEM	scanning electron microscopy
TEOS	tertaethyl orthosilicate
TGA	thermogravimetric analysis
TPD	thermo-programmed desorption

XPS	X-ray photoelectron spectroscope
XRD	X-ray diffraction
ZSM-5	zeolite Socony Mobil–5
USY	ultra stable Y zeolite
UV	ultra violet
C	concentration
E_{a}	activation energy
E	band gap energy
k	reaction rate constant
$k^{'}$	absorption coefficient
k_0	pre-exponent of reaction rate constant
k_{diff}	mass transfer coefficient
j_D	mass transfer factor
M_{w}	molecular weight
m_0	initial sample weight
m_t	instantaneous sample weight
m_{inf}	final sample weight
m_i	mass of component
N_{exp}	number of experiments
n_i	mole of component
n	reaction order
R	gas constant
$R^{'}$	reflectance
Re	Reynolds number
s	scattering coefficient
Sc	Schmidt number
S_{sp}	ratio of catalyst surface area to its volume
$StDev$	standard deviation
t	time
T	temperature
T_g	glass transition temperature
T_m	melting temperature
T_{Ref}	reference temperature
Q	flow rate
u	gas linear velocity
y	fraction of component

α	conversion extent function
ϵ	particles porosity
μ	weight coefficient

LIST OF APPENDICES

Appendix A Degradation kinetics of poly(methyl methacrylate) at non-isothermal conditions 113

CHAPTER 1 INTRODUCTION

According to an announcement by the Canadian government released in 2022, only 9 % of total annual plastic waste is recycled in Canada, 4 % undergoes heat recovery, and the rest ends up in landfills [6]. Among high-valued polymer wastes, the growing global volume of accumulated PMMA presents a problem for its disposal. But at the same time, it is an opportunity for recycling.

1.1 Background and problem identification

PMMA is known as a raw material for many compounding plastics, automobile tail-lights, and electronics like LCD-TVs [7]. Its global market is expected to reach 14 billion USD by 2027 [8], with a compounded annual growth rate close to 5 % and sales from 4.5 $/kg ("Global Market Insights"). Industry recycles PMMA in different ways such as (1) mechanical, (2) incineration to recover heat, and (3) chemical feed-stock recovery [9].

Mechanical recycling focuses on producing powders from PMMA wastes to re-shape plastic for new applications. The low quality of the final product and uneconomical processing limits the application of this method. Heat recovery from PMMA incineration is unattractive economically.

The chemical reprocessing into MMA is based on pyrolysis of PMMA into monomer – MMA from 350 °C to 550 °C [10, 11]. At present, the industry mostly employs different types of reactors as baths with molten metal (lead or tin) [12], single or twin extruders [13,14], rotating drums [8]. Despite significant advances in reactor design and even pilot testing - as in the case of fluidized bed reactors [11], mechanically agitated [15], spouted bed (CSBR) [16], driven by mechanical excitation or vibration, or by electromechanical or ultrasonic force [17–19] - these reactor systems are still under development.

Based on the review of the open literature, most of the technologies, such as molten metal baths and extruders, ignore the end-of-life PMMA, which contains reinforcement materials, pigments, fibers, etc. This significantly reduces the potential volumes of plastic waste to be reprocessed. Compared to other reactors, fluidized bed reactors are able digesting polymers containing additives at increased heat and mass transfer rates and high conversion due to good mixing of polymer with a fluidizing agent, approaching the maximal possible monomer recovery to 97 % [11, 12, 20, 21].

Such industrial giants as Arkema, Mitsubishi Rayon et al. seek alternative technologies to

derive more value from PMMA thermal degradation and produce high purity monomers. However, besides the target monomer, thermolysis of PMMA produces by-products like co-monomers, oligomers, and higher molecular weight volatile compounds. Small amounts of other organic compounds like methyl esters (introduced to lower the glass transition temperature) are also produced [22]. Some by-products of PMMA pyrolysis has boiling points similar to MMA, which increases the cost of their separation.

PMMA depolymerizes to MMA following a radical mechanism [23, 24], degradation starts above the glass transition temperature [22] and unzipping depends on the chain length and the synthesis method (free-radical or anionic). In this regard, many studies on PMMA thermolysis are devoted to the influence of individual factors such as the spatial arrangement of PMMA molecule (isotactic, syndiotactic or atactic) and dispersity (branching degree) [25, 26], the influence of co-polymers and stabilizers, which are added to PMMA during its preparation to improve the commercial quality [27–33]. The main degradation steps with respect to bond strength can be distinguished as the least stable head-to-head scission at around 160 °C, scission of unsaturated ends at 270 °C and random scission at 370 °C [24,34–37]. Later studies expanded the knowledge about the reaction mechanism for a variety of PMMA molecular weight, physical properties and experimental conditions [25, 26, 38, 39] as well as initial particle size [40–43] and shape [44]. However, the mechanism of PMMA degradation is still under the discussion and study of the gas phase composition will shed light on its clarification.

Many studies demonstrated the effect of catalysts, especially zeolites, on PMMA cracking and selectivity to MMA [45–47], metal oxides [48, 49], and sulfates [7]. The MMA yield depends on the number and acid strength of the catalyst acid sites [45].

The methacrylic acid is a precursor for methyl methacrylate and also one of the side products of industrial PMMA pyrolysis of higher boiling point (161 °C versus 100 °C of MMA). The esterification of MAA by methyl alcohol is a reverse reaction to MMA hydrolysis and a simplest way to produce MMA [50].

In this context, reprocessing of PMMA to methacrylic acid can solve the the problem of purity of reaction products for the expense of the difference between boiling points of MAA and by-products on the one hand and will allow to involve in the reprocessing of low-quality end-of-life PMMA , which is ignored by existing industrial methods on the other hand.

We expect that in a fluidized bed reactor, in the presence of water vapors and catalyst, PMMA will convert into MMA at an increased temperature followed by catalytic hydrolysis of MMA into MAA. The acid-catalyzed hydrolysis is a well-studied reaction where the activation of the ester molecule is the limiting step and previous studies demonstrated that Brønsted acids

catalyze the reaction to form carboxylic acids [51, 52]. Gas phase hydrolysis is more selective and the solvation effect which affects the acid-solid interaction is lower compared to liquid phase acid-solid interaction [53]. However, previous studies on esterification of carboxylic acids in the liquid phase reported high yield of the target product when exploiting the acidic catalysts [50,54–56]. Among different solid acids, super acids like Ce salts of hetero-poly acids, as well as zeolites represent the highest activity and stability to water poisoning [52, 57–59].

Many research groups summarized that the yield and the selectivity in hydrolysis by zeolites is a function of catalyst acid sites strength, and hydrophobicity (defined by crystallinity and Si/Al ratio) [52, 58, 60–62].

Although the two processes mentioned above (PMMA thermolysis and MMA hydrolysis) are well studied, the combination of them in one reactor volume represents a completely new type of process and has not been studied before. In addition, the kinetics of MMA hydrolysis by zeolites Y in the gas phase is not well represented in the literature.

Although in chemistry the term "degradation" covers all variety of processes to break the structure of the polymer [33, 63], in this work, this term is applied to cover all the processes in an inert atmosphere to convert PMMA to its monomer (MMA).

Questions related to the search for the appropriate reaction conditions (temperature, the catalyst to polymer ratio, particle size of the polymer, residence time, type of catalyst, kinetic parameters of thermolysis, and hydrolysis) require clarification. Answering these questions will help to develop an efficient reactor design to maximize MAA yield, and will become significant when scaling up industrial reactors for this process.

1.2 Objectives

The main objective of this project is to introduce MAA as an end value-added product of PMMA depolymerization in fluidized bed reactor as part of a novel approach to producing high-quality r-PMMA in the polymer-based industry.

The specific objectives are:

1. Determine reaction conditions that maximize MAA yield from PMMA in a micro-fluidized bed (13 mm inner diameter)
    - Synthesize home catalysts, choose the industrial catalysts for study;
    - Characterize home-made and industrial catalysts via N-adsorption porosimetry, XRF, XRD, SEM techniques to identify their physico-chemical properties, and morphology;

- Study the PMMA behavior via its mass loss at isothermal conditions at the variation of temperatures;
- Identify an appropriate particle size of PMMA via its thermolysis in TGA at different heating rates (in terms of heat and mass transfer);
- Test catalysts activity and selectivity in the reaction of PMMA degradation into MAA in a FB at variation of temperatures, catalyst volumes, and water feeding;
- Compare catalysts' performance and identify the most active and selective one;
- Identify the reaction mechanism to produce MAA from PMMA.

2. Investigate performance of the zeolite-based catalyst in hydrolysis of MMA to MAA in an 8 mm ID fixed bed reactor, study reaction kinetics, and identify the apparent kinetic parameters:

   (a) Synthesize catalyst via encapsulation of acidic Zeolite Y (Faujasite type) microsieve in silica gel matrix;

   (b) Characterize catalyst via N-adsorption porosimetry, SEM, XPS, MAS-NMR, TPD, UV-Vis techniques to identify their physico-chemical properties and morphology;

   (c) Study activity of the catalyst at constant contact times and variation of temperature regimes and flow rates to find conditions at which the contribution of the external mass transfer is minimal;

   (d) Design and conduct kinetic experiments;

   (e) Analyze experimental data and estimate kinetic parameters;

3. Study PMMA degradation to MAA in a 13 mm ID tandem reactor where PMMA thermolyzes in the fluidized bed in the down portion of the reactor followed by MMA hydrolysis in the upper fixed bed of acidic zeolite Y (Faujasite) suspended between glass wool:

   (a) Design and conduct kinetic experiments at variation of temperatures, flow rates, fluidizing agent;

   (b) Analyze reaction products via GC-MS

   (c) Analyze experimental data and estimate the yield of MAA.

4. Study thermolysis of PMMA by TGA method in an inert atmosphere and clarify details of the reaction mechanism, identify the reaction products and the apparent kinetic parameters in a wide range of heating rates :

- Degrade PMMA using a TGA technique in a broad range of heating rates with simultaneous analysis of gas-phase products, and at high-resolution ramp technique;
- Identify kinetic parameters of PMMA pyrolysis (activation energy and pre-exponential factor) applying the different reaction models.

CHAPTER 2 COHERENCE OF THE CHAPTERS

Below are the brief descriptions and the integrity of the chapters.

Chapter 1 introduces the problem of global PMMA accumulation, with a background in the area of its industrial processing methods, focusing on specifics of PMMA reprocessing in fluidized bed reactors, namely, reprocessing of scrap PMMA by different methods. In this chapter, the main and specific objectives of the current research are established. Also, the hypothesis, scientific approaches, and methods to achieve the research objectives are suggested.

Chapter 2 briefly describes the chapters of the current research and their consistency and integrity.

Chapter 3 is the literature review. At the beginning, it embraces current industrial methods of PMMA recycling, and summarizes their advantages and disadvantages, with the emphasis on PMMA pyrolysis, including catalytic. It introduces the basics of polymer behavior phenomena in fluidized bed reactors and the hydrodynamics of fluidized bed, demonstrates basic concepts of catalytic hydrolysis of esters by acids, and outlines theoretical aspects for modeling apparent kinetics.

Chapter 4 represents the pioneer studies in the chemical reprocessing of PMMA in 13 mm fluidized bed of catalyst, in flow of inert and water co-feeding to obtain methacrylic acid. This part of the study covers the synthesis and characterization of the home-made and industrial catalysts, which represents their activity at the variation of temperature, water concentration, the proportion of polymer/catalyst, and the type of catalyst. This study demonstrates that the acidic catalysts – zeolite Y and Cs-HPA – enhance MAA yield. Based on the reaction product distribution , we proposed the reaction mechanism. In addition, we developed a method to inject PMMA into a 13 mm lab-scale reactor. The results of our findings are published in **Applied catalysis A: General**.

Chapter 5 this chapter represents a continuation of the studies in PMMA depolymerization into MMA (Chapter 5) with the specific focusing on the gas-phase hydrolysis of MMA to MAA by acidic zeolite Y (Faujasite). We developed a method for synthesizing a zeolite-based catalyst. We also studied its catalytic activity in a stationary bed, and kinetics of

MMA hydrolysis at equilibrium conditions. The zeolite Y micro-sieves were encapsulated in the matrix of silica gel. The analytical methods like N_2 adsorption, TPD, NMR, UV-Vis, and XPS characterized the physico-chemical properties of the catalyst. Then, we designed and performed the experiments to study the kinetics of the gas-phase MMA hydrolysis in a plug-flow 8 mm ID reactor, as well as identifying the apparent kinetic parameters. The results of this research have passed the reviewing process and are ready to be published in **Chemical Engineering Journal**.

Chapter 6 summarizes previous studies on PMMA degradation in the fluidized bed and the gas-phase MMA hydrolysis in the stationary bed and demonstrates the results of the pioneer study on PMMA conversion to MAA in a tandem reactor. We studied the performance of both reactor beds and demonstrated that PMMA thermolyzed the best in the fluidized bed of sand at high temperatures, while the maximal yield of MAA after the fixed bed was observed at moderate temperatures and the excess of water. The results of this study are submitted to **Applied catalysis A: General**.

Chapter 7 is a general discussion of the research topic with an accent on the major conclusions of the main research results and their originality.

Chapter 9 summarizes the whole results, with an emphasis on the originality of the current research and its potential contribution to industry development. It also describes challenges and provides recommendations for future studies.

Annex A covers the fourth specific objective of the research and describes the results of PMMA thermolysis in an inert atmosphere obtained by a thermogravimetric method. We demonstrated that PMMA thermally degrades by the random scission and MMA, acetone, methanol, dimethyl ether, water and methacrylic acid as liquid-phase products and CO_2, propene, hydrogen, ethane, methane, and ethylene are the gas-phase products. We identified the apparent activation energy of PMMA thermolysis as well as the temperature regimes for the fluidized bed reactor.

CHAPTER 3 LITERATURE REVIEW

This chapter embraces known industrial methods to recycle PMMA (and their challenges) with an accent to PMMA pyrolysis to MMA including catalytic, basic aspects of polymer behavior in fluidized bed reactors, concepts of catalytic hydrolysis of esters, outlined principal requirements to catalysts properties for hydrolysis and theoretical aspects to identification and modeling of apparent kinetics.

3.1 PMMA recycling

Poly(methyl methacrylate) (PMMA) is a thermoplastic polymer known by different trade names and uses as a raw material in different industries like automobile, construction, medicine, electronics et al. due to its perfect physico-chemical, mechanical and optical characteristics.

The global market of PMMA is expected to reach 14 billion USD by 2027 [8], with a compounded annual growth rate close to 5 % and sells from 4.5 $/kg ("Global Market Insights"). The recent pandemic enhanced the demand for PMMA in 2020, which will also contribute to increasing PMMA annual waste.

The increasing worldwide production of PMMA on the one hand and its value on the other challenges the industry to reprocess PMMA rather than dispose of it. Due to both its high value and environmental burden, land-filling PMMA is economically and environmentally irresponsible. Waste recycling is categorized as mechanical, incineration and chemical feedstock recovery [9].

3.1.1 Mechanical recycling

Method aimed to produce powders by milling with the following forming polymeric concrete resins for bathroom washbasins (a substitute for white dolomite filler) [64,65]. The application limitations of this method are end-of-life polymers containing various fillers, fibers, and copolymers.

3.1.2 Non-catalytic pyrolysis

Polymer decomposes in various reactor types such as a rotary kiln, puddle, Auger, spouted or fluidized bed, molten metal bath, single or twin-screw extruder, microwave or induction, at

temperature range from 350 °C to 600 °C, with the recovery of monomer, methyl methacrylate (MMA-R) [11, 66, 67]. Some of these processes, the most common in the industry, are represented schematically (Figure 3.1) and discussed below.

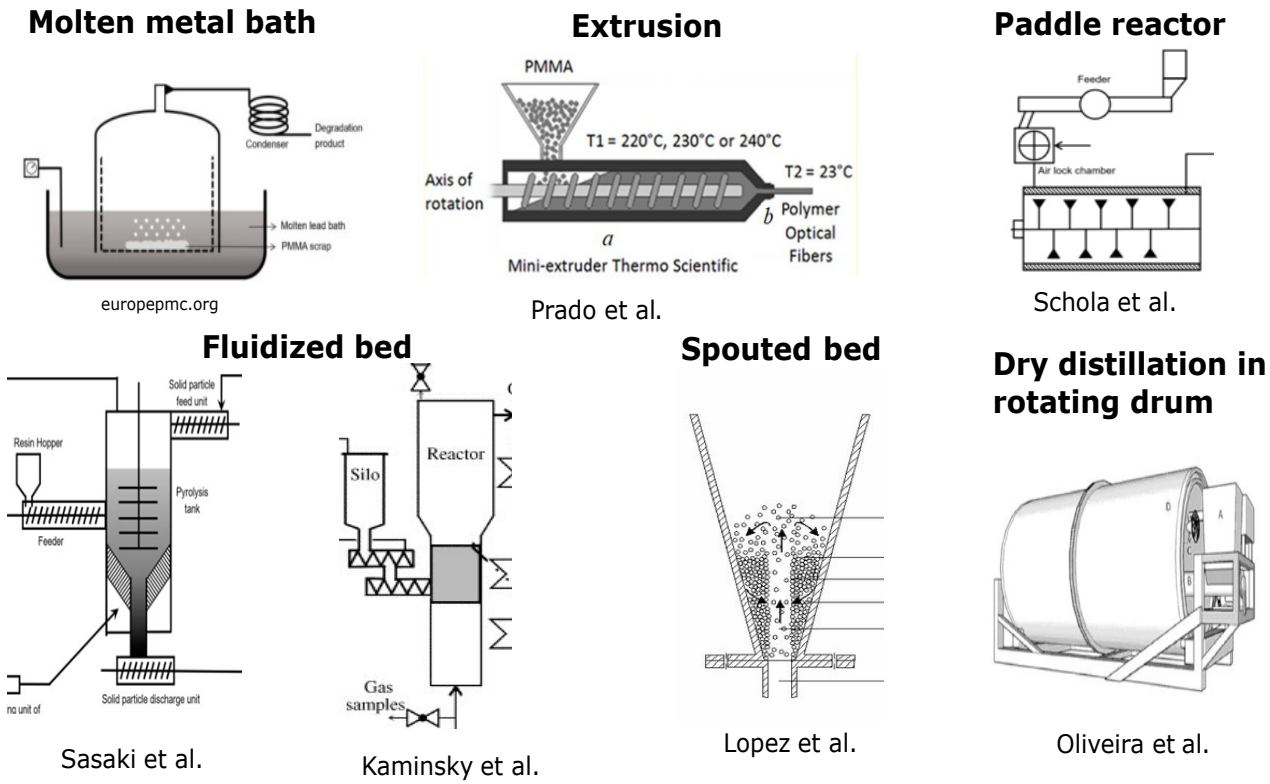

Figure 3.1 Industrial methods of PMMA reprocessing into MMA

Metal baths

The process of depolymerization of PMMA in a molten lead (or tin) bath operates at 450 °C to 550 °C. Coarsely ground plastic parts feed a heated molten metal bath and depolymerize in the absence of oxygen. The yield of gaseous MMA is about 97 % of MMA condensed [12]. The main disadvantages are economic and environmental considerations, namely, traces of metal in r-MMA and the toxicity of the process as a whole [4, 8].

Extruders

Thermal degradation of PMMA by extrusion provides a continuous process with more than 90 % of the yield of high-purity monomer. Here, PMMA scrap feeds in a single or twin-screw extruder, and an electric heater maintains the temperature. Plastic contacts with extruder elements, and melting starts already in the first extrusion zone of 200 °C. The

screw pushes the melted polymer along the extrusion zones where depolymerization occurs. Gas-phase products easily remove from the reaction volume, which sufficiently increases the yield of monomer [13]. The reaction by-products are separated and condensed in the hopper. Then, target products separate by distillation. Extrusion treats the scrap PMMA as acrylic plates after disassembling LCD monitors, rear car lights, etc. The extrusion method suffers from high extruder inertia to rapid temperature changes, high-energy consumption, and the impossibility of processing PMMA containing such fillers as glass fibers, granite particles, etc., which can destroy the extruder. However, processing PMMA scraps with minimum additives result in r-PMMA with good optical characteristics [14].

Mechanical agitators

The operating principle of mechanically agitated reactors (or mechanically fluidized beds (MFB)) is almost similar to that one of a fluidized bed reactor but driven by mechanical vibration, electro-mechanical or ultrasonic forces. The absence of any carrier gas opens perspectives for operating under a vacuum, minimizes monomer vapor in the reactor, and simplifies gaseous product removal. The heat consumption in the bed is reduced due to direct contact of the surface of the immersed heater with particles. Heat transfer coefficients at some vibration frequency and atmospheric pressure in MFB reach the same values which could be achieved in presence of carrier gas [17, 18]. MFB reactors provide high purity of monomer recovery (>99 %), the main disadvantage of this method is providing vibratory energy input.

Mistubishi developed a process in which paddles mechanically agitate a tank full of polymer and hot sand operating from 300 °C to 500 °C [15, 19]. The reaction temperature, reactor geometry,process conditions and hydrodynamics directly influence the degradation effectiveness and product quality. Namely, low solid amount improves agitation, reduces power needed to feed fluidized gas, decreases pressure drop, and the necessary amount of sand. Decreasing of the total length of the reactor reduces equipment costs. The effective injection position for PMMA was found to be less than 0.5 of layer height in its stationary constitution. The preferable particle size of plastic was 3 mm to 10 mm to provide stable feeding. The effective size of sand was found to be 0.05 mm to 0.8 mm. The optimal temperature of fluidization agent also varies between 50 °C to 250 °C in order to increase the pyrolysis rate of the resin and quality of pyrolyzed products. The fed resin temperature recommended is less than T_g or T_m, namely (Tg-50) °C or in the range 0 - (Tg-50) °C or 0 - (Tm-50) °C. From one hand, too low temperature of feeding resin will decrease the total temperature in the reactor and effectiveness of the process also will decrease. If the resin temperature is higher than Tg or close

to Tm, it can cause particle fusion, and finally, defluidization. Solid particles maintain the temperature in the reactor and provide a good heat distribution in the reactor. In addition, the proportion between the feeding ratio (kg/hr) of the fluidizing agent and plastic particles should keep in the range 1 to 20 in order to maintain stable pyrolysis and reduce operation cost. The preferable ratio (kg/hr) of the fluidization gas/sand is from 0.04 to 0.3. The low ratio (0.04 or more) improves the flow in the reactor, the ratio less than 0.3 allows reducing of the fluidization gas and the amount of solid particles. The preferable ratio of feeding rate of fluidization gas/resin feeding rate is in the range 0.4 – 3.0. The low ratio decreases the time needed to send the pyrolysis products to a recovery process. The ratio less than 3.0 allows decrease the amount of solid particles and fluidization gas. The optimal residence time of solid particles of 0.5 – 1.5 hr provides sufficient pyrolysis of resin, and decreases the amount of resin discharged along with the solid particles in the reactor. The position of the introduction of polymer particles into the reactor relative to the introduction of the fluidizing agent determines the hydrodynamic situation in the reactor, and therefore, the heat transfer rate. This factor ultimately affects the processes of defluidization and the effectiveness of depolymerization. The particle size of the polymer varies in a fairly wide range and it is shown that it does not affect depolymerization.

Steam, as a fluidizing gas may hydrolyze MMA to methacrylic acid but pressure increases at operation at high temperature. Furthermore, MMA and steam have similar boiling points which complicates their separation. In addition, such problems as necessity of optimization of heat and mass transfer in reactor as well as some thermodynamics issues, related to realization of subsequent reaction steps at different temperatures, do not allow increase reactor performance to the competitive level.

Conical spouted bed reactors

Conical spouted bed reactor (CSBR) described in detail by Lopez [16] operates at a pressure drop half lower than for fluidized bed, wide particle size range, density distribution, and extra short residence time 1 µs to 20 µs. These conditions minimize the secondary reaction products and increase the selectivity by MMA. The optimal temperature in CSBR to achieve the highest degradation rates and avoid defluidization problems is 400 °C what 12.5 % lower than in fluidized bed reactor as concluded by Kang [68].

Nevertheless, the range of bed mass ratio to PMMA flow rate in CSBR is at least twice lower than for fluidized beds according to data obtained by Kang [68] and Kaminsky [20, 47]. Avoiding defluidization problems is possible at increasing particle size, but this limits the recycling of high-viscosity polymers. The total yield of MMA in CSBR is also lower than in

a fluidized bed.

Fluidized bed reactors

Fluidized bed (FB) reactors enhance heat and mass transfer rates and conversion and are sensitive to the hydrodynamic regime in the reactor. However, the monomer recovery is preferable in FB rather than producing syn-gas or hydrocarbons [47, 69, 70]. In the FB method, plastic material feeds in the bed of preheated sand, and inert gas fluidizes the mixture of sand and polymer. The FB reactors can operate at short contact times (which is important to avoid secondary reactions), and allow recovering fillers as fibers, granite particles, aluminum hydroxide [71], and co-polymers. Compared to the spouted bed reactors, the realization of the process in fluidized bed reactors is possible at a wide ratio range of bed mass/PMMA flow rate. Increasing process temperature leads to enlarging of gas phase product formation and decreasing in monomer recovery.

Monomer recovery approaches 97 % in the temperature range 400 °C to 450 °C [10, 11, 20]. The major by-products are CO, CO_2, CH_4, hydrocarbons, esters [71],including propanoic esters [10]. Comparison of product composition after degradation of virgin and waste colored (rear car lights) PMMA shows that waste PMMA gives 5 times more gas phase (7.36 %), 1.05 times less liquid phase (92.13 %), 0.95 times less MMA yield (90.99 %) and 1.76 times more carbon (0.51 %) in comparison with virgin PMMA. The MMA yield keeps at the level of 90 % even at very high temperatures (up to 700 °C). Investigation of the liquid phase in the temperature range 450 °C to 600 °C shown also the presence of methanol and 1,4-cyclohexane dicarboxylic acid dimethyl ester as by-products [12, 70]. Temperatures above 590 °C favor the formation of methane, ethene, propene, carbon monoxide, and dioxide in the gas phase [47, 70].

Pyrolysis in a circulating fluidized bed is a variation of a fluidized bed but allows regenerating fluidization agent and designing contact-free depolymerization [19]. The certain heat transfer value maintains the stable performance of FB [19]. Thus, it is important to maintain the exact temperature in the reactor to promote the thermal degradation of polymer particles and prevent sticking and defluidization [12].

Other reactor types

Pyrolysis of PMMA in closed batch reactors called “dry distillation” is inexpensive and is implemented mainly in Asian countries. The process consists in loading the reactor with plastic, and direct heating of the closed reactor until the end of the process in the range

400 °C to 550 °C followed by the product's condensation and purification. The reactor with a rotating drum represents the improved version of the dry distillation batch reactor but its rotation enhances heat transfer. The principal drawback of these processes is a low-quality r-MMA and formation of coke [4, 8].

The pyrolysis of PMMA is also possible while transferring energy from different sources. Thus, microwave depolymerization is environmentally friendly but necessary to add a susceptor (metal-containing inorganic material) into the reaction volume. Issues connected to equal heating of polymer in the reactor and the presence of co-polymers make this process complicated to realize in industrial scales [72, 73].

3.1.3 Degradation of PMMA with fillers and additives

Aluminum trihydroxide (ATH) is a filler used to produce PMMA composites for bathrooms and kitchens and composes about 67 % in a mixture with PMMA [47]. The presence of ATH at high temperatures causes the release of water and initiates the MMA hydrolysis in the PMMA degradation process. At the same time, one can note that aluminum oxide plays the role of catalyst giving Lewis acid sites. The hydrolysis products are methacrylic, isobutyric acids, and methanol. With this, the yield of MMA decreases to 57 % which is 1.7 times less in comparison with virgin PMMA. A way to suppress the formation of methacrylic acid as an undesired by-product in a fluidized bed reactor is to decrease of partial pressure of monomer and water in the reactor by removing these reactants and changing reaction conditions in the FB reactor by decreasing of temperature to 400 °C and contact time [74]. Another type of common filler is silica oxide (62 %)wt in form of particles of 10 µm to 100 µm diameter and granite particle (71 %wt) of 100 µm to 1000 µm in diameter as reported Kaminsky et al. [20]. The reactor performed at a short residence time, which allowed obtaining the 83 % to 90 % yield of MMA in comparison with virgin polymer (98.4 % of MMA). The authors mentioned that temperature increases up to 480 °C as well as fillers and cross-linking in the PMMA increased the yield of gas, liquid phases, and carbon black. Here, filled PMMA affords the formation of a higher amount of oil products. The main gas products were CO, CO_2, and CH_4, also some amount of methacrylic acid was found in the liquid phase. Fillers after the reaction can be separated by an overflow. In addition, studies of the mechanical properties of PMMA obtained from MMA recycled in an Sn bath [9] revealed that impurities contained in MMA after plastic recycling improve the mechanical strength of newly obtained PMMA but, at the same time, increase its opacity. This study once again confirms the importance and advantages of the fluidized bed process, which allows obtaining a higher quality product.

3.1.4 Catalytic pyrolysis

Catalytic pyrolysis allows decreasing the reaction temperature from 450 °C to 600 °C [10, 11] to 270 °C to 300 °C due to a decrease in activation energy, increasing the yield of MMA. Previous studies reported about the realization of pyrolysis in presence of the zeolite catalysts in fixed or fluidized beds [45, 75–77].

In fluidized beds a solid catalyst serves as a fluidizing agent. PMMA can be mixed with the catalyst in fixed beds or other reactor types which allow presence of solid particles. In addition, realization of catalytic process allows increase PMMA/catalyst ratio comparing to thermolysis without catalyst [78]. The major cracking product is MMA and low-chain hydrocarbons like light oils, and gaseous products [77, 79, 80], while the pyrolysis results in higher portion of heavy oils. Polymers decompose by a radical mechanism. In catalytic cracking, the radicals from the gas phase adsorb on the catalyst surface and diffuse in catalyst pores where the reaction takes place. Different types of catalysts as zeolites, FCC, reforming catalysts (like Pt/SiO_2-Al_2O_3), metal oxides (MoO_3, $Al(OH)_3$) and others were studied during past decades [78,81,82]. Cracking of different plastic wastes over the FCC catalyst resulted in selectivity to gasoline-range hydrocarbons like aromatics and naphthenes [78, 81]. The acidic group of catalyst in atmosphere of inert able to initiate the unzipping and chain cleavage of polymers via interaction of H^+ active sites of catalyst with defect site of polymer, boost isomerization and aromatization reactions [35,78]. The strong acidity of the catalyst due to its high Si/Al ratio favors the C-C bond cleavage [82]. The reforming catalysts are bi-functional and benefit hydrogenation/dehydrogenation reactions on metal oxides and isomerization on acidic active sites and are good catalysts to form hydrocarbons with improved octane number [83]. Zeolites like ZSM-5, BETA, USY are known to be the most effective for this process due to their acidic properties [45, 46]. The main by-products reported in catalytic cracking over BETA catalyst at 300 °C are 2-methyl propionate and methyl 2-methyl butyrate [46].

3.2 The effect of T and softening of PMMA in fluidized bed reactors

Unfortunately, there is a lack of information in literature about the thermal behavior of PMMA (softening, melting, foaming) at polymer cracking in the fluidized bed. The study of PMMA degradation behavior in a conical calorimeter [84] shown that, in general, degradation behavior in oxygen or inert divides into four stages. In the first step, the polymer melts, accompanied by the onset of its active mass loss and, depending on the external heat flux, bubbles may appear on the polymer surface. The second step attributes to the swelling (foaming) of the polymer and the degradation of a bulk sample (thick liquid). This

phenomenon accompanies by the active release of the gas phase and the mass slower loss compared to the first step. Referring to earlier studies of polymers degradation one can assume the prevalence of diffusion processes in the bulk of polymer which are the limiting step of degradation [85, 86].

On another hand, studies of polymer behavior during its burning revealed that PMMA, compared to other polymers, volatilize rapidly after its softening and does not give a lot of melt [87]. The third and fourth stages correspond to particle cracking or/and oxidation (if the process occurs in the air). The authors revealed that effective particle degradation strongly depends on the intensity of irradiance level and time. The higher the heat flux to the polymer surface, the more effective mass loss of the polymer particle and the shorter the time of each stage. Some other researches support the idea of the realization of PMMA degradation in a fluidized bed at maintaining high heat transfer between particles and surrounding gas at short contact times for the account of slightly increased temperature and intensive mixing to prevent bubbling and swelling of the polymer maintain durable reactor operation. Thus, Newborough [12] mentioned heat transfer coefficient to be higher than $600\,\mathrm{W\,m^{-2}\,K^{-1}}$ at bed temperature higher than $400\,^{\circ}\mathrm{C}$ initiate polymer particles ablation. Vaughan et al. demonstrated similar results [86], they mentioned higher monomer purity at the value of the heat transfer coefficient from $500\,\mathrm{W\,m^{-2}\,K^{-1}}$ to $600\,\mathrm{W\,m^{-2}\,K^{-1}}$ and fluidized bed temperature $400\,^{\circ}\mathrm{C}$ to $425\,^{\circ}\mathrm{C}$ and alumina oxide as a fluidization agent.

3.3 MAA synthesis routs

The modern industry produces PMMA from its monomer, in turn, the market for the production of MMA is largely focused on the routes involving different C2 - C4 hydrocarbons as a raw material or ACH, rather than the processing of polymer waste [1, 88, 89] (Figure 3.2) where MAA is mostly a by-product of MMA production. Synthesis of MAA and MMA via the traditional or improved acetone cyanohydrin (ACH) process is not favorable because of the involvement of highly toxic hydrogen cyanide and corrosive, concentrated sulfuric acid [90,91]. The novel MMA/MAA processes (Figure 3.2) have a much less environmental footprint and consider potentially promising [88]. Nevertheless, drawbacks connected to low MAA-MAA yields, also catalysts lifetime, and optimal composition are a subject for further studies [52]. In addition, some reactions, such as isobutane oxidation, require a specific isobutane-oxygen ratio to avoid self-ignition.

The hydrolysis of esters into carboxylic acids is a very slow reversible process. However, the equilibrium shift to the acid formation is possible at the increased temperature and pressure [92] and can be realized in liquid (water) or gas phase (water vapor). An acid

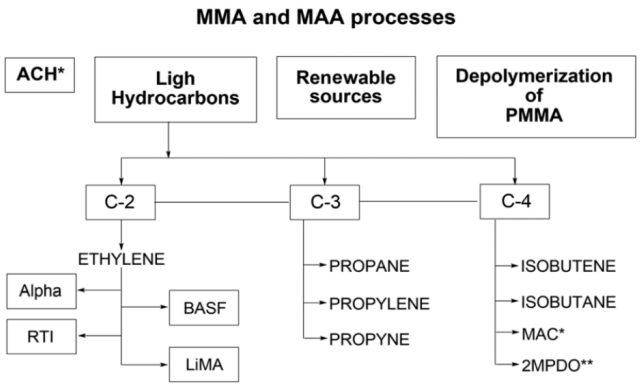

Figure 3.2 Processes of synthesis MMA and MAA, adopted from [1]

catalyst, as a source of additional protons (benzene sulfonic acid, linear alkyl benzene sulfonic acid, or sulfuric acid), can enhance the reaction. The process is realized at low temperatures (70 °C to 130 °C) in a single phase mixture at stoichiometric molar ratio (1:1) of water to ester. Other studies reported the results in the liquid phase where the catalytic process was successfully realized on zeolites, ion-exchange resins and acid amorphous catalysts [93, 94] with presence of dimethylsulfoxide (DMSO) as a solvent.

Packet [95] reported realization of continuous hydrolysis of fatty acids in a gas phase over a fixed bed of catalyst at the optimal range of temperatures 250 °C to 280 °C and pressure of 10 bar to 70 bar. Higher temperatures lead to cracking of the fatty acid ester and acid which minimize selectivity. Among high pressure, the high Si/Al ratios improve conversion and selectivity [95]. Another confirmation of this phenomena obtained at the hydrolysis of substituted benzoic acid in near-critical water (250 °C to 300 °C [96] due to drastic (three orders of magnitude) enhancing of water ionization constant at near-critical conditions with obtaining of high concentration of hydronium and hydroxide ions which initiate acid or base catalytic reaction route. One of the principal disadvantages of processes in the liquid phase is the necessity of reaction product separation [90, 97], low selectivity which is typical for most processes occurring in the liquid phase, and use of toxic liquid acids as catalysts.

3.4 Theoretical background. Reaction mechanisms

3.4.1 PMMA degradation mechanism

The degradation of PMMA starts above the glass transition temperature [22], and refers back to the polymer synthesis way - free radical polymerization or anionic [4]. In general, it strongly depends on the chain length (which is determined by the polymerization method),

spatial arrangement of PMMA molecule (isotactic, syndiotactic or atactic) and dispersity (branching degree) [25, 26]. Some studies reported the range of glass transition temperature of PMMA as 50 °C to 130 °C depending on spacial arrangement of PMMA molecule where the isotactic structure has the lowest Tg and the syndiotactic structure associates with the highest Tg [98]. In another study, the Tg covers the range 42 °C to 207 °C depending on the degree of polymerization apart from the spatial arrangement of PMMA [99]. Co-polymers and stabilizers added to PMMA during its preparation to improve the commercial quality, catalyze or inhibit the depolymerization process [27–32]. Thermal degradation consists of three steps: initiation, propagation and termination [100]. Plastic non-oxidative thermal degradation is endothermic free-radical process. In general terms, the range 140 °C to 200 °C the weakest head-to-head bonds cleave (Figure 3.3, a); unsaturated end groups rupture in the temperature range 210 °C to 280 °C (Figure 3.3, b) following by random chain scission above 300 °C (Figure 3.3, c) [2, 4, 23, 24, 32, 101].

The initiation step consist of the formation of free radicals during the splitting of the main backbone into smaller molecules. Weak site of the macromolecule backbone chain or its chain ends contribute in this step [100]. Thus, primary radical formation triggers propagation reaction with the contribution of various reactions (cross-linking, intra- or inter-molecular hydrogen transfer) until termination which again generates unsaturated polymer chains which are less stable than saturated ones [23]. The second step can consist of disproportionation in the unsaturated ends involving homolytic β-scission of the vinyl group. The last step is also very complicated, it can be a combination of β-scission of unsaturated group and following main or random chain scission [23, 24, 45]. A random scission causes a reduction of polymer molecular weight and chain-end scission generates volatile products [101]. Later studies expanded this idea for a variety of PMMA molecular weight, physical properties, and experimental conditions [25,26,38,39] as well as the initial particle size [40–43] and shape [44].

3.4.2 Hydrolysis of esters by acidic mechanism

Hydrolysis of an ester is the reverse reaction to the esterification. One of the first references to the synthesis of methacrylic acid by hydrolysis of ethyl methacrylate, obtained by dehydrating of ethyl α-hydroxyisobutyrate, became known in 1865. In 1901, thanks to the work of Otto Röhm , the importance of methacrylic monomers, including their potential for industry, was recognized [89]. The nature of catalysis by acids or basics was described in 1928 by Brønsted. In acid catalyzed condition, due to the effect of hydrogen ion, it leads to a carboxylic acid and alcohol formation; a carboxylate ion and an alcohol forms in basic medium due to hydroxyl ions effect [102]. In case of acid catalyzed hydrolysis without catalyst, it needs a very long

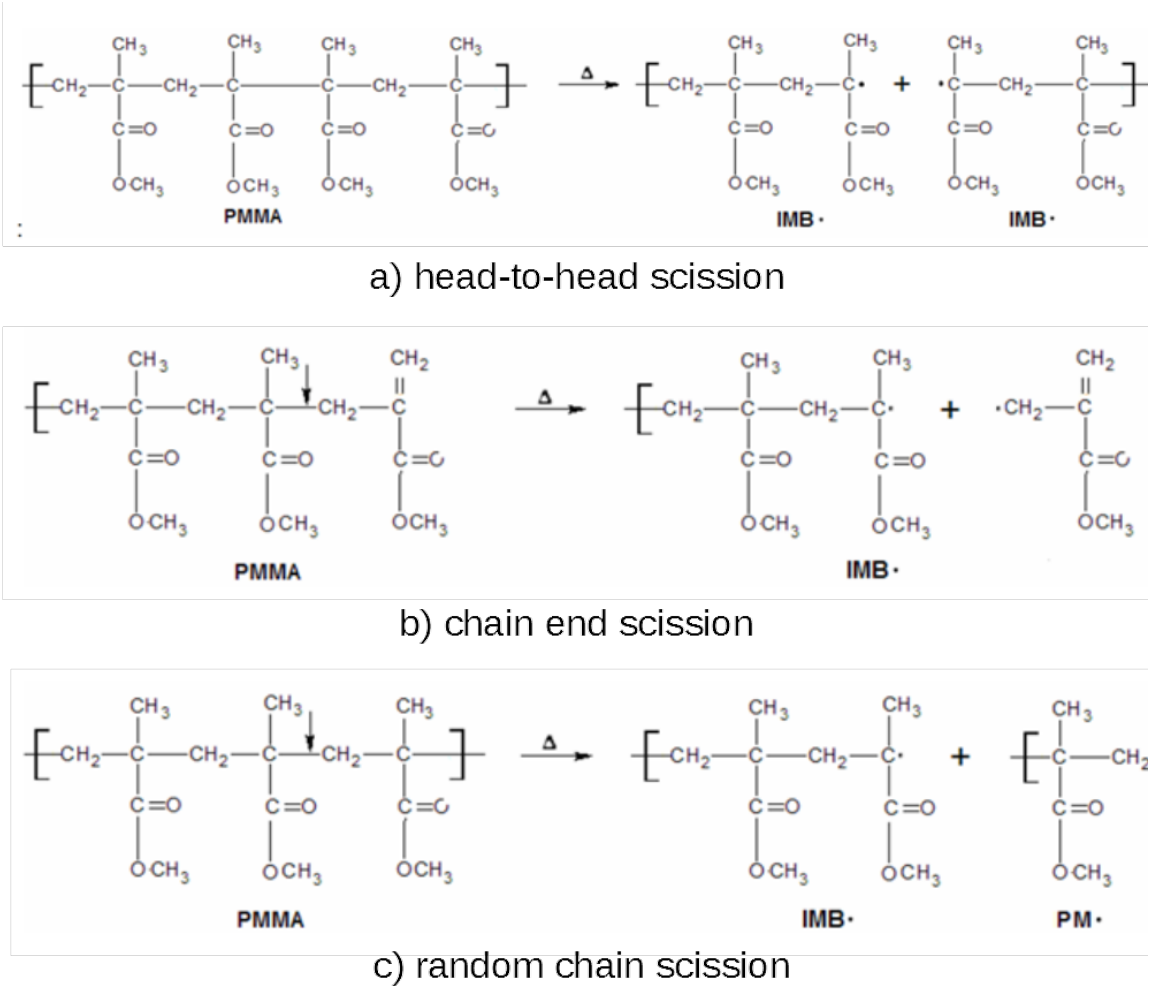

Figure 3.3 Principal steps of PMMA degradation: a - initiation in chains with head-head linking's, b - chain end scission, c - random chain scission, copy-pasted from [2]

time to reach the equilibrium state. In this sense, the advantage of hydrolysis with alkalies is that the reaction is unidirectional. The reaction product is salt and to obtain an acid, the second step of reaction of salt with concentrated acid is necessary [103].

Neutral hydrolysis can be represented as a semantic variation of acid hydrolysis with the clarification that for the initialization of the reaction, the condition of auto-ionization of the water and ester molecules must be satisfied. However, there is still no unified idea of the reaction mechanism along this pathway [104]. Despite of reversibility of the reaction, acid catalysis represents the most interest from an economic point of view.

The general mechanism of acidic hydrolysis includes several steps (Figure 3.4). On the first step, the hydrogen proton attacks double-bonded carbon atom in the ester molecule

(according to Markovnikov's rule) activating it (making it more electrophilic). Then, ion pairs on the oxygen of a water molecules attacks electrophilic carbon atom (with double-bond) with a subsequent transferring of a hydrogen ion from the oxygen atom towards the oxonium ion, creating a tetrahedral intermediate. The last several steps represent an acid-base reaction and deprotonation of the oxonium ion to release the reaction products. Here, a molecule of ethanol is lost from the ion and it is one of the reaction products. The latest ion has a positive charge at double-bonded carbon which is also delocalized (as on the first step). Cleavage of hydrogen ion with it's attachment to oxygen of water ion brings an acid as a second reaction product [105].

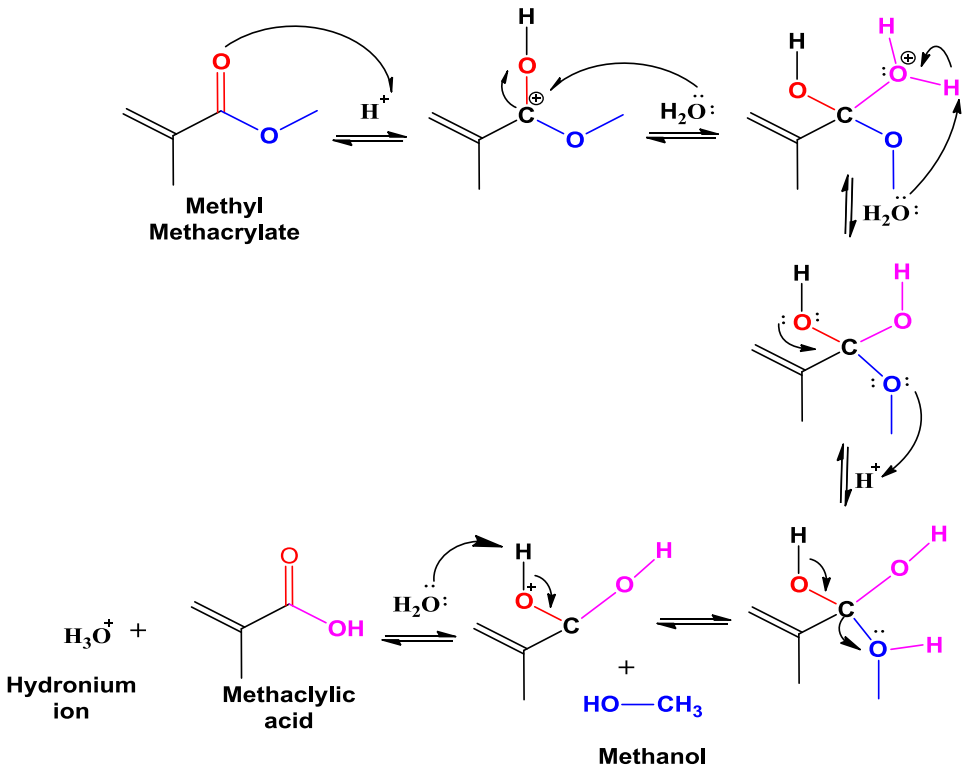

Figure 3.4 Acid-catalyzed hydrolysis of MMA to MAA

3.5 Catalysts for PMMA transformation to MAA

Based on the mechanisms of PMMA thermolysis and MMA hydrolysis mentioned above, one can assume that the combined process can be implemented in two stages. In the first stage, PMMA is radically depolymerized in an inert atmosphere into its monomer - MMA, which, in turn, is hydrolyzed into MAA on the catalytic surface. Previous studies have shown the efficiency of using fluidized bed reactors, in which PMMA is thermalized in the temperature

range of 400 °C to 700 °C. The catalyst is able to reduce the temperature to 300 °C to 600 °C [71] for the account of direct contact with PMMA with catalyst centers (mainly defects of catalyst surface) or adsorption of the thermolysis products. The catalyst increases the reaction rate and the target product yield compared to the thermal pyrolysis [78,106,107] due to reduced activation energy. In addition, the presence of free radical sources (for example H_2O_2) also initiate the radical depolymerization [108]. On the other hand, the catalytic hydrolysis of MMA to MAA proceeds effectively at lower temperatures - 270 °C to 300 °C. The catalytic conversion of MMA to MAA over the acid catalysts is represented schematically (Figure 3.5).

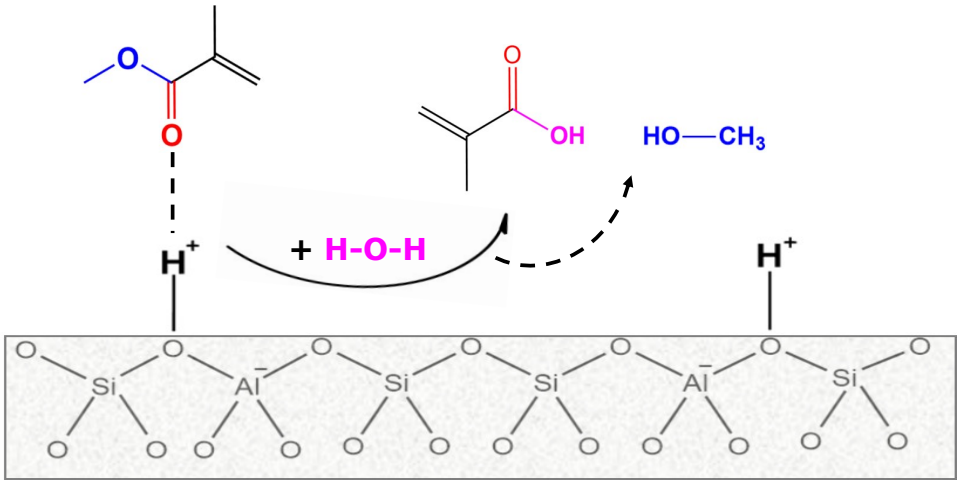

Figure 3.5 Scheme of catalytic hydrolysis of MMA to MAA

It should be noted that most studies are focused on hydrolysis in batch reactors at relatively low temperatures, few studies suggest the implementation of the process in a gas-solid medium in a flow reactor with a fixed catalyst bed under near-critical conditions (10 bar to 70 bar). In both cases, Brønsted acids, namely zeolites, showed the highest activity. The following are some of the catalytic systems that are effective in the hydrolysis process. According to Miskolczi [82] amorphous catalytic sites initiate cracking reactions, while propagation and termination stages take place on the crystalline sites. The high Si/Al ratio is preferred as defined by the scission activity of the catalyst and its higher thermal stability [95]. Among the catalysts of polymer catalytic pyrolysis, the acid-based zeolite catalysts as $ZSM-5$ [82,109], H-ultrastable Y-zeolite (HUSY) [82], FCC [82], MoO_3 [82], $Ni-Mo$ [82], $Al(OH)_3$ [82] are known. Metallic sulfates increase the PMMA depolymerization rate [7, 110], the catalytic activity row for metal sulfates is: $Fe_2(SO_4)_3 > Al_2(SO_4) > MgSO_4 > CuSO_4 > BaSO_4$. A special place among the catalysts is occupied by the FCC catalyst, specially developed for cracking macro-molecular compounds in oil refining. The principal feature of this cata-

lyst is its high activity and selectivity due to its high acidity compared to aluminosilicates, which distinguishes it as a promising catalyst for the depolymerization of plastics [45,78,111]. Miskolczi [82] compared acidic properties of some commercial catalysts and found that FCC has the highest Si/Al ratio and pore radius, its acidity is compatible with Y and β-zeolites and HZSM-5.

Esters hydrolysis is potentially effective with ion-exchange polymers [93,94]. The pore volume of these catalysts varies in the range (2 nm to 40 nm) [112]. The ion-exchange resins have high initial acidity and safety limits for operation at temperatures over 130 °C. USY (UOP), mordenite (Zeocros), J639 (from Grace) and zeolite (ZM510 from Zéocat) and CF815A, CF815B (from Zeolyst) catalysts [95] presented high activity in the temperature range 240 °C to 300 °C. Reforming catalysts based on $SiO_2 - Al_2O_3$ are bifunctional, their metallic sites catalyze hydrogenation/dehydrogenation reactions and acidic sites catalyze isomerization reactions. When reforming catalysts are applied to plastic cracking, the acidic sites in the alumina support are expected to function as an FCC catalyst [78].

3.6 Processes and phenomena in fluidized bed

The FB is a moving mixture of solid and liquid phases, which has properties similar to those of a liquid. The functioning of the FB reactor is very sensitive to changes in the hydrodynamic regime which defines temperature profiles, axial and radial mixing of particles, the intensity of heat and mass transfer, and residence time. A combination of these factors affects the whole process's effectiveness [69].

The formation of bubbles in the fluidized bed can result in bypassing of unreacted species and a subsequent decrease in reactor performance. The residence time for particles in the fluidized bed is different than in fixed bed at the same reaction conditions and geometry. In addition, in most cases fluidized bed reactor performance is far from the regime of ideal mixing or plug flow which becomes very important when modeling the reaction kinetics.

Fixed bed reactors are more simple in operation but heat transfer rates are too low and in highly exothermal reactions they must operate at low conversion to minimize hot spots. Fluidized bed reactors are ideal for catalytic processes such as cracking, oxidation, hydroforming, dehydrogenation etc., compared to fixed beds because the high mixing rates minimize radial concentration gradients, enhance effective thermal conductivity (isothermic conditions) and mass transfer, reducing pressure drop. When carrying out processes in a fluidized bed, the catalyst bears an additional mechanical load due to the contact of the particles between themselves and the walls of the apparatus.

3.6.1 PMMA feeding methods in FB

In general, there are many possible continuous or sequential methods for introducing a polymer into a fluidized bed. Among them, dry injection, injection of dissolved polymer, as well as in a mixture with water, can be noted. Injection of dry powder by pulse injection [113] is attractive due to a fast introduction of fine particles in the reaction zone and the simple design of the particle introduction device. The possible challenges of this method are related to defluidization problems because of the agglomeration of polymer particles with the catalyst. The solution to this problem can be found if injecting dissolved PMMA into a fluidized bed. Morales et al. [114] used PMMA dissolved in the mixture of acetone-to-pentane to simulate behavior at the injection of high-viscous liquids in a fluidized bed. They found that increasing bed temperature, fluidization velocity, and atomization gas flow rate will improve injection.

3.6.2 Defluidization

When polymer particles are introduced into the FB, they heat, and the external surface of the polymer softens which triggers the sticking of the polymer with the particles of fluidizing agent - sand or catalyst. If the hydrodynamic regime doesn't provide the necessary flow rate and good mixing, the FB defluidizes. At sufficient gas supply, the reactor keeps operating and the polymer inside agglomerates melts, covering the sand particle's surface, and degrades. In the case of PMMA, the softening of polymer particles followed by their degradation happens rather than polymer melting. Defluidization takes place because of particle agglomeration. Arena [69] revealed that all initial reactions are related to the phase transition in polymer structure and agglomeration processes and this process finalizes by uniform temperature distribution over the polymer-solid-gas phases.

Bed defluidization issues directly related to polymer injection conditions, material properties (particle diameter, mass, shear modulus, Poisson's ratio - the ratio of the relative transverse compression to the relative longitudinal tension, depending on the nature of the material, and characterizing the elastic properties of an isotropic material) and contact surface area between particles (adhesiveness coefficient) [115–118]. Moseley [117] simulated the defluidization velocity (U_d) necessary to avoid particles' agglomeration. Investigating the composition behavior of PET and PE in fluidized bed Arena [115] concluded that the key defluidization controlling parameters are the ratio between fluidization agent mass and polymer flow rate ($W_{bed}/Q_{polymer}$). Zhong et al. compared the tendency of Fe_2O_3 particles to agglomerate in various fluidizing gases and found that increasing of gas viscosity an increase in the viscosity of gases in a series from hydrogen to helium leads to an increase in the resistance of the layer

to agglomeration and defluidization as H_2 <N_2 <Ar due to increasing gas drag force with increasing its viscosity.

3.7 Hydrodynamics studies

3.7.1 Minimum fluidization velocity

Fluidized bed fluid dynamics is an extensive field of research. In this study, we specify some of the issues necessary for an understanding of the kinetics of the depolymerization processes.

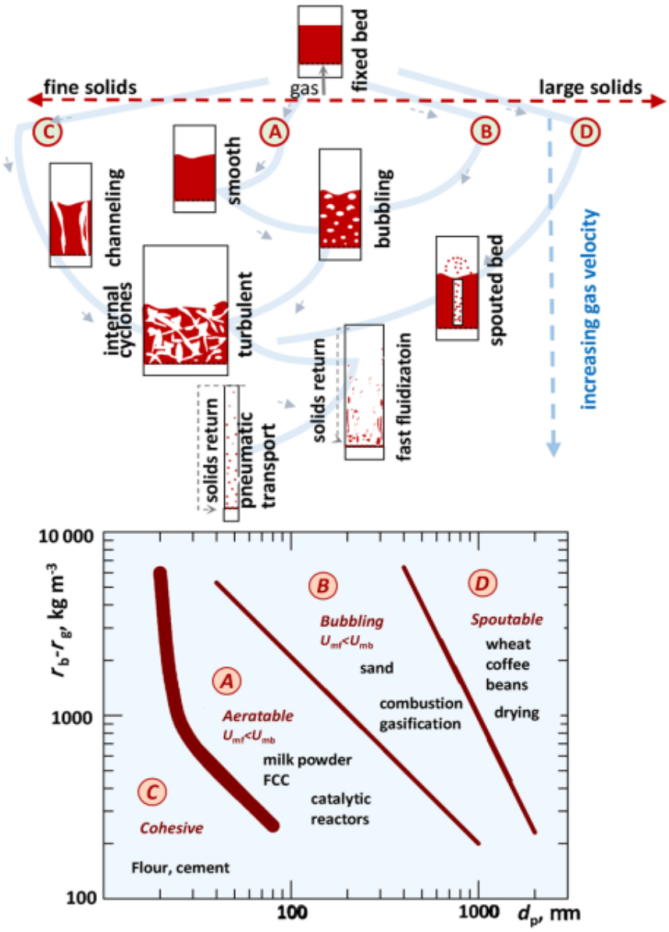

Figure 3.6 Fluidization regimes and Geldart particles classification, adopted from [3].

When varying the fluidization parameters, several operation modes of the apparatus are possible [3] (Figure 3.6), and the fluidization regime depends on which group according to Geldart classification the particles belong to. Minimum fluidization velocity (u_{mf}) reaches when the pressure drop equals the weight of the particles in the bed [3,119]. For Geldart group B particles transition to a bubbling regime occurs when reaching the minimum fluidization

velocity u_{mf}, so $u_{mb} \approx u_{mf}$. For particles of Geldart group A $u_{mb} \approx 2 \cdot u_{mf}$ or more. Pressure drop respects the Ergun equation at velocities under u_{mf}:

$$\frac{\Delta P}{\Delta Z} = \frac{u_g}{\phi d_p} \frac{1-\epsilon_v}{\epsilon_v^3} (150(1-\epsilon_v)\frac{\mu}{\phi d_p} + 1.75\rho_g u_g) \tag{3.1}$$

where u_g - superficial gas velocity, ϵ_v - the void fraction, d_p - the average particle diameter, μ - fluid viscosity, ϕ - particle sphericity, ρ_g - gas density.

3.7.2 Residence time distribution

The hydrodynamics of fluidized bed reactors characterizes by flow back mixing, gas phase bypassing, bubble formation, etc., which leads to significant deviations in the residence time distribution of gas particles in the catalyst bed compared to flow or stirring reactors. To define the real conditions of gas flow in the reactor, one can trace the path of each molecule in the apparatus. For this, theoretically, it is sufficient to have a complete picture of the velocity distribution of the individual liquid elements in this apparatus. However, the realization of this method can cause difficulties. Therefore, for an approximate assessment of the characteristics, one needs to know how long individual molecules present in the vessel. Data on the distribution of time intervals between the moment when molecule enters the reactor and the one when it appears in the effluent stream, in other words, information on the residence time distribution of individual particles in the the reactor can be obtained using direct measurements. For this, a tracer method is used, based on the artificial perturbation and analysis of the consequences caused by them. The residence time distribution function $E(t)$ characterizes the time that the tracer stays in the fluidized bed [120]:

$$E(t) = \frac{QC(t)}{N_0} = \frac{C(t)}{\int_0^\infty C(t)dt} \tag{3.2}$$

the residence time defines as the first moment of the E-function and can be estimated from the experimental measurements of a tracer concentration (C) and real-time (t):

$$\bar{t} = \sum_{t=0}^{\infty} tE(t)\Delta t = \frac{\sum t_i C_i \Delta t_i}{\sum C_i \Delta t_i} \tag{3.3}$$

The spread degree of the curve and deviation from the plug flow can be identified by estimation of the dispersion number ($Pe^{-1} = D(uL)^{-1}$) or variance (σ^2). The large values correspond the more significant deviation from plug flow:

$$\sigma^2 = \frac{\int_0^\infty t^2 E(t)dt}{\int_0^\infty E(t)dt} - \bar{t}^2 \approx \frac{\sum t_i^2 C_i \Delta t_i}{\sum C_i \Delta t_i} - \bar{t}^2 \tag{3.4}$$

There are two approaches to simulating experimental data and identify the concentration profile in the fluidized bed: one-dimensional dispersion model and tanks-in-series model [120]. Here we consider one-dimensional dispersion model to process experimental data:

$$\frac{\partial C}{\partial t} + u\frac{\partial C}{\partial z} = D\frac{\partial^2 C}{\partial z^2} \tag{3.5}$$

with close-open boundary conditions:

$$C_{0,\xi} = 0, 0 \geq \xi \geq 1 \tag{3.6}$$

bringing the equation (3.5) to a dimensionless form:

$$\frac{\partial C}{\partial \theta} + u\frac{\partial C}{\partial \xi} = \frac{1}{N_{Pe}}\frac{\partial^2 C}{\partial \xi^2} \tag{3.7}$$

where θ is dimensionless time, ξ - dimensionless coordinate, we can use analytical solution to identify the profile of dimensionless concentration G(θ) = $\frac{C_{0,\xi}}{C_0}$:

$$G(\theta) = \frac{1}{2}[erfc\sqrt{\frac{N_{Pe}}{4\theta}(1-\theta)} + e^{N_{Pe}} erfc\sqrt{\frac{N_{Pe}}{4\theta}(1+\theta)}] \tag{3.8}$$

Objective function formulates as a sum of squares differences between experimental and calculated values of concentrations, it's minimization allows evaluating the dispersion number (Pe^{-1}) [120]:

$$S = \sum_{i=1}^{N_{exp}} (C_i^{exp} - C_i^{calc})^2 \rightarrow min \tag{3.9}$$

3.8 Kinetics

The solution to the kinetic problem during a chemical reaction usually reduces to solving the inverse problem of chemical kinetics with the determination of numeric values macro-kinetic parameters (E_a and $k(T)$) [121]. In general, the strategy of the experimental kinetic study can be formulated as:

- Choosing of experimental setup type

- Study of reaction conditions in kinetic region
- Balance experiment, estimation of uncertainty and reproducibility, identification of "unknown" side products
- Reducing of mass balances
- Optimal DOE
- Obtaining of information massive of experimental data.

The structure of the chemical model depends on the type of setup, it is the structure of the model that determines the choice of identification methods and computing tools. Among the lab setup types, used for experimental study of kinetics, the most practical meaning has:

- reactors of *ideal mixing*, flow reactors and flow reactors with the circulation of liquid phase
- *Ideal plug-flow* reactors
- *Reactors of closed type* without flow
- *Semi-closed* reactors which usually use for investigation of kinetics in two-phase systems gas-liquid or gas-solid with flow of gas phase (fluidized bed reactors)

In general, the system of algebraic equations for reactor of ideal mixing can be written [121]:

$$N^0 y_i^0 - \left[N^0 + m_{cat} \sum_{i=1}^{N_S} q_i \right] y_i + q_i(y, P, T) m_{cat} = 0 \tag{3.10}$$

where q is the source density:

$$q_i = \sum_{i=1}^{N_R} z_{ij} R_j \tag{3.11}$$

here, z_{ij} matrix of stechiometric coefficients of reaction components, R_j - function of concentration, $N^0 = \sum n_i^0$ total mole flow inlet of the reactor, $N = \sum n_i$ - mole flow, $y_i^0 = n_i^0 / \sum n_i^0$ - mole fraction if i component of mixture inlet of the reactor, $y_i = n_i / \sum n_i$ - mole fraction of i-component out of the reactor, m_{cat} - catalyst mass.
In terms of dimensionless parameters equation 3.11 represents in form:

$$y_i^0 - \gamma y_i + q_i \times \tau = 0 \tag{3.12}$$

where $\tau = m_{cat}/N^0$ fictive contact time $[g \cdot s \cdot mole^{-1}]$, $\gamma = N/N^0$ - coefficient of changing of mixture mole flow.
Equation for the ideal plug flow reactor, operating at isothermal and isobaric conditions, can be written in form [121]:

$$N\frac{dy_i}{dm_{cat}} + y_i\frac{dN}{dm_{cat}} = q_i(y, k, T, P) \tag{3.13}$$

assuming that $dm_{cat} = N^0 d\tau$ and $\gamma = N/N^0$ after corresponding conversions we can present the equation in form of intensive parameters:

$$\frac{dy_i}{d\tau} = \frac{1}{\gamma}\left[q_i - y_i\frac{d\gamma}{d\tau}\right] \tag{3.14}$$

where $\frac{d\gamma}{d\tau} = \sum_{i=1}^{N} q_i$.
Initial conditions are: $\tau = 0$: $y_i = y_i^0$, $\gamma = \gamma_0 = 1$. If the total amount of moles does not change in the reactor, the derivation at all τ will be equal to 0. Both types of equations solve by Gauss-Marquardt method [121]. In this model, apparent kinetic parameters as E_a, $k(T)$ define by minimization of objective function:

$$S = \sum_{j=1}^{N_{exp}}\sum_{i=1}^{N_s}\left[\left(y_{ij}^{exp} - y_{ij}^{calc}\right)^2 + \left(\gamma_j^{exp} - \gamma_j^{calc}\right)^2\right] \longrightarrow min \tag{3.15}$$

where i - component index, j - experiment index. Verification of the adequacy of the model is carried out by analyzing the scaling of the main components of the matrix of eigenvalues [122, 123].

Equation for fluidized bed reactor operating at stationary conditions with first order chemical reaction describes by one-dimensional diffusion model [124]:

$$-u\frac{\partial C}{\partial z} + D\frac{\partial^2 C}{\partial z^2} - kC = 0 \tag{3.16}$$

where u - flow velocity, D - dispersion coefficient, k- reaction constant, C - concentration.
Boundary conditions are: $C|_{z=0} = C_0$, $\frac{dC}{dz}|_{z=H} = 0$. Bringing the equation (3.5) to dimensionless form [124]:

$$\frac{1}{N_{Pe}}\frac{\partial^2 C}{\partial \xi^2} - \frac{\partial C}{\partial \xi} - KC = 0 \tag{3.17}$$

where ξ - dimensionless coordinate, $N_{Pe} = \frac{uZ}{D}$, $K = \frac{kZ}{u}$, $\frac{dC}{d\xi} = 0$ The equation 3.17 can be

transformed to quadratic form by substitution $\frac{dC}{d\xi} = r$:

$$r^2 - N_{Pe}r - K = 0 \tag{3.18}$$

the solution of the equation is:

$$r_{1,2} = \frac{N_{Pe}}{2} \pm \sqrt{\left(\frac{N_{Pe}}{2}\right)^2 + K} \tag{3.19}$$

The general solution of the equation with respect to the concentration profile is:

$$\frac{dN}{dz} = r_1 A_1 exp(r_1 z) + r_2 A_2 exp(r_2 z) \tag{3.20}$$

Coefficients A_1 and A_2 can be found from boundary conditions and substituting them to the concentration equation, we can write the last one with the respect to concentration profile:

$$C = \frac{C_0}{r_1 e^{r_1} - r_2 e^{r_2}} \left(r_1 e^{r_1 + r_2 \xi} - r_2 e^{r_2 + r_1 \xi}\right) \tag{3.21}$$

3.8.1 Benefits of PMMA degradation in FB

Based on the literature review, the main advantages of FB reactors compared to the other types are:

- lower temperature ranges and their equal distribution of the process due to high heat and mass transfer (compared to metal baths, extruders, and microwaves);
- stable fluidization in a wide range of PMMA/sand ratio (compared to the conical spouted beds);
- lower by-products formation (due to lower temperatures range);
- the ability to reprocess PMMA with fillers and additives (possibility to separate contaminants from the reaction zone compared to molten metal baths, extruders);
- the lower probability of breakage because of the absence of moving parts (compared to mechanical agitators, extruders, and microwaves).

CHAPTER 4 ARTICLE 1 : FLUIDIZED BED POLY(METHYL METHACRYLATE) THERMOLYSIS TO METHYL METHACRYLATE FOLLOWED BY CATALYTIC HYDROLYSIS TO METHACRYLIC ACID

Olga V. Chub, Nooshin Saadatkhah, Jean-Luc Dubois, Gregory S. Patience

Applied Catalysis A: General, Published: 25 May 2022

4.1 Abstract

Reprocessing end-of-life polymethyl methacrylate (PMMA) in fluidized beds substitutes fossil fuels as a feedstock for methacrylic acid (MAA). Impurities and high operating and separation costs thwarted the commercialization of the simpler thermolysis PMMA to methyl methacrylate process. In a thermogravimetric analyzer, $\leq$ 6% of the PMMA decomposed at 230 °C, whereas it all reacted at 350 °C. In a 13 mm diameter micro-fluidized bed, all the PMMA reacted within 10 min at 350 °C while at 230 °C $\leq$ 30% reacted. Catalysts like γ-Al_2O_3, FCC, MoO_3-ZrO_2/SiO_2, zeolite Y, and $CsxH_3-xPW_{12}O_{40}/SiO_2$ hydrolyze MMA to MAA. The maximum MAA yield was less than 8% for γ-Al_2O_3, FCC, MoO_3-ZrO_2/SiO_2, while it reached 20% for the Cs heteropoly acid over SiO_2 at 280 °C and exceeded 30% with zeolite Y. Coking on the catalyst and product decomposition along the reactor wall reduced MAA yield. A tandem reactor configuration–thermolysis followed by hydrolysis–will maximize MAA yield.

4.2 Introduction

Poly(methyl methacrylate) (PMMA) is a thermoplastic polymer known by trade names like Altuglas, Crylux, Plexiglas, Acrylite, Lucite, and Perspex. It is transparent, stiff, and UV and abrasion resistant [1, 22]. It is as a raw material for many compounding plastics, automobile tail lights, and electronics like LCD-TVs [7]. The PMMA global market is expected to reach 14 billion USD by 2027 [8], with a compounded annual growth rate close to 5 % and sells from 4.5 $/kg ("Global Market Insights"). Demand has increased since 2020, particularly because of its application as transparent barriers to aerosols that carry the COVID-19 virus. This will increase the PMMA waste that currently exceeds 2.5 million tons annually.

PMMA thermally degrades to its monomer with yields >90 % at 350 °C to 550 °C in an inert atmosphere [47, 125, 126]. In air, oxidation products yield are as low as 5 % [24] Society requires industry to re-purpose and recycle scrap and end-of-life plastics. Catalytic or thermal

pyrolysis, extrusion, and molten lead or tin baths are among the various technologies to depolymerize end-of-life PMMA to its monomer (MMA) rather than processing it into low-value hydrocarbons or synthesis gas [23, 70]. Industry is seeking the high-quality r-MMA [8]. However, fillers contained in end-of-life PMMA (pigments, metals, glass fibres, granite etc.) make recycling uneconomic for industry.

PMMA thermally degrades to MMA oligomers, cyclic compounds C_7-C_{14} [75], methyl isobutyrate, pyruvate, 2,3-butanedione [21, 71], 1,4-cyclohexane dicarboxylic acid dimethyl ester [12, 70], which negatively affect the quality of the r-MMA. In addition, by-products like 2,3-butanedione give a pungent odor to the r-PMMA [21]. Separation costs, including distillation, to extract these by-products increase capital expenditures particularly since some of the compounds have similar physico-chemical properties as MMA, like boiling-point. Rather than MMA as a target compound, reacting PMMA to MAA reduces costs related to product purification. MAA is a primary feedstock for polymers, ion-exchange resins [127], esters, lubricant additives [128], leather treatment agents [129], paints, and adhesives. Its higher boiling point (161 °C) compared to MMA (100 °C), makes it easier to separate from byproducts.

PMMA depolymerizes to MMA following a radical mechanism at 300 °C to 400 °C [23]. Zeolites [45, 46], metal oxides [48, 49], and sulfates [7] accelerate the reaction rate and selectivity to MMA [45, 47]. The MMA yield depends on number and acid strength of acid sites [45]. Radical initiators as H_2O_2 accelerate the reaction rate and decrease the depolymerization temperature [101].

Recycling PMMA in fluidized bed reactors (FB) is attractive for industry due to their high heat and mass transfer and short gas phase residence time, which minimizes investment on the one hand (smaller vessels) and maximizes yield on the other as less PMMA decomposes to by-products and coke [70, 71]. Up to 550 °C, the amount of liquid monomer recovered from fluidized beds exceeds a mass fraction of $0.97\,\mathrm{g\,g^{-1}}$ depending on the pyrolysis temperature. Increasing temperature beyond 550 °C produces more methane, ethane, propane, carbon monoxide and carbon dioxide [47]. At the same time, the size of the plastic particles, the initial average molar mass [126], zip length (which is the number of monomers produced by radical decomposition before radical deactivation by transfer or termination) [130], and polymerization degree are the limiting factors in its thermal decomposition to MMA [24, 34, 35, 131–133].

In a FB reactor, PMMA pyrolyzes through transfer of energy from hot gases and catalyst particles [19]. Thus, it is important to maintain the reactor in a narrow range of temperature to promote thermal ablation of the polymer while minimizing agglomeration and avoiding

defluidization [12]. Some authors identified critical defluidization temperature around 300 °C [16], while others observed stable reactor operation at degradation start temperature (270 °C) and intensive heat transfer [12]. Beside the reactor temperature, the feed rate of polymer with respect to the mass of the solid phase (catalyst) in the reactor are the factors to maintain stable fluidization [16, 115, 117, 134].

Several dozen industrial scale plants already depolymerize PMMA to MMA throughout the world. Most of them are very small capacity units of less than a few hundred tons per year capacity while a few produce more than a few thousand tons per year. All the processes pyrolyze the polymer (heating in the absence of oxygen) usually around 400 °C. The most common technology is "dry-distillation", in which a static reactor is filled with PMMA scraps and heated until no vapor leaves the unit. Solid residues accumulate at the bottom of the reactor during the batch cycles that last a day, and the quality of the produced MMA fluctuates during the cycle. The product is purified in batches. The produced MMA is usually directly used to produce cast PMMA, and only a small fraction of distilled or crude MMA is sold on the open market [135, 136].

A variation of dry-distillation is the "rotating drum" process where PMMA scraps are charged to a partially filled cylinder. It is heated through the wall while it rotates. The solid residue is more easily removed after each cycle and the batch cycle time is one day. This technology is also used to pyrolyze tires. A third variation is the "stirred tank," which is equivalent to dry distillation but is much less common: a shaft in the vessel agitates the solids to improve heat and mass transfer. The difficulty in this process is the high viscosity of the molten PMMA. This process is better designed for continuous process.

The "molten metal" was the prevailing technology to recover PMMA scraps and some plants still operate in Europe, Egypt, and several other countries around the world. Molten lead, tin, or zinc transfers heat to the PMMA above 400 °C. The scraps depolymerize and leave behind a solid residue. Because of its high density, low partial pressure, low cost, and low oxidation rate, molten lead is a good choice. The solid residue accumulates on the surface that is scraped from time to time. With the appropriate scraps, MMA purity reaches 99.0 % (after distillation).

Fluidized bed technology has been implemented at the industrial scale in which an inert material (sand) is circulated between a reactor and a regenerator where it is reheated. High heat and mass transfer in the reactor promotes the depolymerization. One of the drawbacks of this technology is the fluidization gas, which cannot be air (otherwise the PMMA will combust) or nitrogen (as it dilutes the MMA stream). In addition, part of the PMMA is transferred to the regenerator where it is burned with the carbon residues, and reheats the

sand. The fluid bed process operates continuously.

A last technology which is currently investigated more extensively is the twin screw extrusion process where PMMA scraps are fed continuously to an extruder. They first melt and then depolymerize further down the barrel at higher temperature. At the end of the screws the solid residues are captured, and the vapors are condensed. In this process the PMMA has a very short residence time.

Not all processes are appropriate to combine catalytic reactions. The batch processes have long residence times and generate a solid residue. Heat and mass transfer rates are usually very poor. The molten lead process is inappropriate to add an hydrolysis catalyst and to feed water or steam. The twin screw process requires a very active catalyst, since the residence times are rather short. The catalyst is recovered at the end of the screw and reinjected in the feeder, but it would be best operated without a solid catalyst. The stirred tank reactor process could be operated in the presence of steam and might be appropriate for medium-high residence times. The fluid bed process is probably the most appropriate to combine the depolymerization and hydrolysis steps. The fluidization gas can be a mix of nitrogen and steam, and include some combustion gases. The product to be condensed is methacrylic acid, which has a higher boiling point than MMA and a low vapor pressure at room temperature, making it easier to recover. The fluid bed technology is used in multiple catalytic processes, with various catalyst/reagent ratios, residence times, operating temperature. It is also a target, in the current study to use PMMA scraps of lower quality, that would not give high regenerated MMA purity. Through the combined pyrolysis-hydrolysis, the product (methacrylic acid) would address different markets and specifications. In addition, the scraps used would be accessible at lower cost, leaving some opportunities to operate at lower yields.

Here, we tested five catalyst compositions in a micro-fluidized bed (13 mm inner diameter) to determine reaction conditions that maximize MAA yield from PMMA. We characterized the catalyst physico-chemical properties, generated XRD diffractograms for each, and conducted a thermal gravimetric analysis to identify at what temperature PMMA decomposes.

4.3 Experimental

4.3.1 Materials

Poly(methyl methacrylate) in the form of pellets (supplied by Arkema) with $M_{\mathrm{w}} = 100\,000\,\mathrm{kmol\,kg^{-1}}$ (PMMA-1) was milled in liquid N_2. PMMA (purchased from Alfa Aesar) with molecular weight $M_{\mathrm{w}} = 500\,000\,\mathrm{kmol\,kg^{-1}}$ (PMMA-2) and the particle diameter was less than 150 µm. We purchased activated acidic gamma alumina oxide from Sigma Aldrich, faujasite type fluid

catalytic cracking catalyst (FCC) from Grace, zeolite Y (CBV-720, SiO_2/Al_2O_3 mole ratio = 30, the acid form) from Zeolyst. The precursors for the catalyst synthesized in-house included: zirconyl nitrate hydrate (99 %), molybdic acid (>85 %), activated silica gel, cesium carbonate (99 %), phosphotungstic acid hydrate (99 %), Ludox AS-40 (all from Sigma Aldrich).

4.3.2 Methods

We studied PMMA degradation in a TA-Q500 thermogravimetric analyzer (TGA). The PMMA powder was loaded to a platinum pan and heated in 60 mL min^{-1} of N_2. A Platinel II® thermocouple was positioned at 2 mm from the sample to minimize the temperature deviation between the reference and the sample. The thermocouple precision was ±1 °C in the isothermal hold. The measuring precision was ±0.01 % with a sensitivity of 0.1 µg.

An HPR-20 TMS (Hidden Analytical) mass spectrometer (MS) equipped with a quartz inert capillary analyzed CO and CO_2 from the effluent of the fluidized bed. The MS recorded signals at a frequency of 3 Hz. To quantify CO and CO_2, we calibrated the MS with a standard gas bottle of 10.0 % CO and 10.0 % CO_2 (Air Liquide).

A CP3800 Varian gas chromatograph (GC) equipped with a flame ionization detector (FID) and a DB-1ms Ultra Inert column (30 m, 0.25 mm, 0.25 µm, Agilent) quantified the concentrations of condensable products. The chromatographic separated liquid reaction products. The autosampler equipped with 10 µL micro-syringe (Supelco) injected 0.1 µL liquid products in a 30:1 split mode. We first dissolved the reaction products in pure ethanol then filtered the solution with a 0.2 µm filter into 1.6 mL vials.

A LECO CS744 analyzer (LECO), equipped with an IR detector, measure the mass fraction of carbon on the catalyst by induction combustion at 1300 °C to 1400 °C with iron and tungsten accelerators.

An Epsilon 4 (Malvern Panalytical) EDXRF spectrometer with a 50 kV, 3 mA metal-ceramic X-ray tube and Rh/Ag anode quantified the elements in the synthesized catalysts. The EDXRF spectrometer detects elements in the range of fluorine to americium from ppm to 100 % with a sensitivity of µg g^{-1}.

To measure surface area and pore size distribution, we applied the Brunauer– Emmett–Teller (BET) methodology based on data collected in a N_2 porosimeter Gemini VII 5.02 (Micrometrics) [137]. A Jeol JSM-7600TFE scanning electron microscope (SEM) generated images of the surface while an Oxford Intruments X-Max 80 energy dispersive spectroscope (EDS) identified the species distribution on the surface from which we estimated mass ratios. An

XRD D8 advance produced XRD diffractograms [138]. It collected data in the 2θ range of 20°– 90° at a scan speed $0.02\,^{\circ}\,s^{-1}$.

4.3.3 DOE

To identify reaction conditions to maximize PMMA to MAA yield, we completed a fractional factorial experimental design with four factors [139]:

- T (4 levels): 230, 280, 300, 350 °C;
- Molar ratio of PMMA to water (2 levels): 1:1 , excess of water;
- Catalyst volume (2 levels): 4 mL, 10 mL;
- Catalyst type (5 levels): Al_2O_3, MoO_3-ZrO_2/SiO_2, FCC, zeolite Y, $Ce_xH_{3-x}PW_{12}O_{40}$, and sand as a control.

A full factorial design consists of 81 experiments excluding repeats ($4 \cdot 2 \cdot 2 \cdot 5$ plus one for the control with sand). Our fractional design includes 18 conditions, 26 repeats, and a control experiment with sand.

4.3.4 Catalyst synthesis

In the first step of the MoO_3-ZrO_2/SiO_2 synthesis, we impregnated 20 g of SiO_2 support with a 14.8 g aqueous solution of zirconyl nitrate hydrate ($0.4\,g\,g^{-1}$ of ZrO_2). A rotavapor mixed the solution and evaporated the water at 80 °C and 20 kPa vacuum overnight. The sample then dried in a furnace at 120 °C and calcined at 550 °C for 6 h with a mild heating ramp of $5\,^{\circ}C\,min^{-1}$ to minimize particle cracking and breaking. In the second step, we impregnated 0.8 g MoO_3 starting with a molybdic acid solution following the same procedure ($0.04\,g\,g^{-1}$ of MoO_3).

$Cs_xH_{3-x}PW_{12}O_{40}/SiO_2$ was synthesized step-wise by incipient wetness impregnation of phosphotungstic acid followed by drying at 120 °C for 4 h and calcination at 350 °C for 6 h. In the second step, Cs was impregnated on the HPA/SiO_2 by incipient wetness impregnation. It then dried at 120 °C for 4 h and calcined at 350 °C for 6 h [140].

To apply CBV-720 Zeolite Y micro-sieves in a fluidized bed, we spray dried an aqueous solution of Ludox AS-40, CBV-720, and polyvinyl alcohol (PVA) at 200 °C then calcined it at 550 °C for 6 h, and sieved it to collect particles in the range of particle size 70 µm to 100 µm [141]. This high temperature calcination may have been too aggressive for the Zeolite Y and accounts for its lower than expected activity.

4.3.5 Lab Set-up

The laboratory setup consisted of a 13 mm ID quartz tube housed in a Carbolite electrical furnace (Figure 4.1). One gas line, connected at the bottom of the reactor, introduced inert gas to fluidize the catalyst while the other served to inject PMMA powder. The distributor, made of glass wool (3), supported the catalyst bed in the reactor. We loaded the reactor (1) with 2 g to 10 g of catalyst (2) (4 mL to 10 mL) . While ramping the reactor to the design temperature, we fed 30 mL min^{-1} of Ar. When the reactor reached the set-point, a stream of Ar (40 mL min^{-1}) carried 1.0(2) g of PMMA to the bed through a stainless steel nozzle (4). A condenser placed in an ice bath, trapped the condensable reaction products. An Azura 5.1 HPLC pump connected to the fluidization line dosed water to the reactor (0.1 mL min^{-1} to 0.3 mL min^{-1}). We monitored the intensity of the CO and CO_2 MS signals to follow the progression of the reaction. Within 10 min, the concentrations of CO and CO_2 approached zero for active catalysts at 350 °C while it took 45 min at low temperature. To calculate the moles CO and CO_2 produced, we corrected the MS signal with the relative sensitivity from the calibration then multiplied the molar flow rate of the non-condensable gas, Q_{ncg}, by the reaction time, t, and the average concentration $\bar{C}_{\mathrm{COx}}$:

$$n_{\mathrm{COx}} = Q_{\mathrm{ncg}} \cdot t \cdot \bar{C}_{\mathrm{COx}} \tag{4.1}$$

4.4 Results and Discussions

4.4.1 Catalyst characterization

The surface area of the SiO_2 catalytic support for the molybdenum and zirconium oxides was 350 $m^2\,g^{-1}$, with an average pore volume of 0.14 $cm^3\,g^{-1}$, and a pore diameter of 8.6 nm. Impregnating the support with metal oxides reduced the surface area to 197 $m^2\,g^{-1}$ and the drop agrees with previous reports in the literature [142]: at a ratio of Si to Zr of 60:40, the surface area decreased 1.8 times (from 350 $m^2\,g^{-1}$ to 197 $m^2\,g^{-1}$) while for a catalyst with a Si to Zr ratio of 50:50, it decreased 2.5 times(Table 4.1).

All measurements, except surface area, were repeated 3 times. The initial surface area of the zeolite molecular sieve was 780 $m^2\,g^{-1}$. Spray-drying with Ludox reduced the surface area as it covered the catalyst with small particles forming a quasi shell. Spray-dried industrial FCC catalyst and zeolite Y were practically spherical (sphericity approaching 1) (Figure 4.2, 4.3) while other catalysts and sand were irregular shaped polyhedrons some with sharp edges and others with rounded edges (sand - Figure 4.2c).

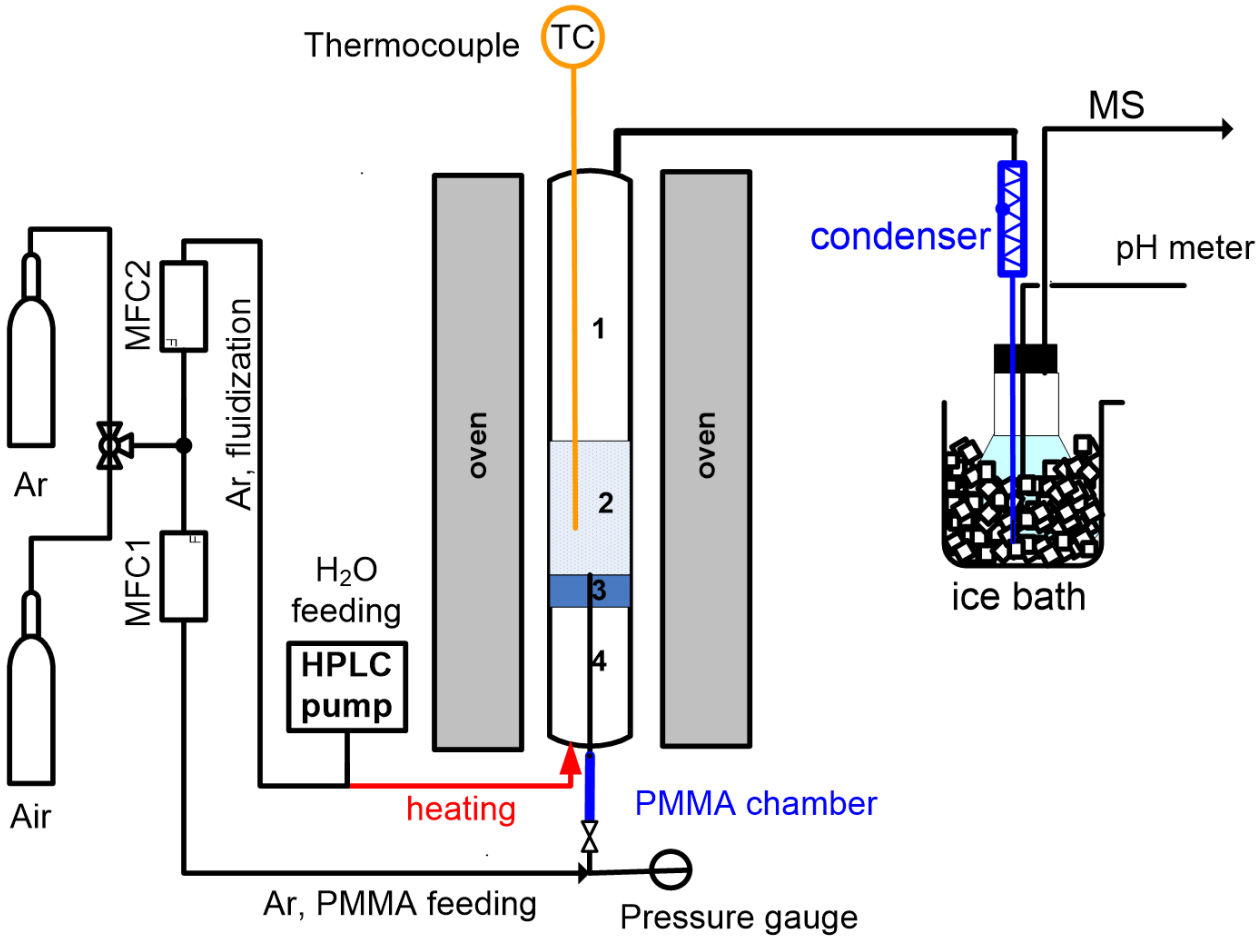

Figure 4.1 Scheme of the lab-scale fluidized bed reactor: 1-Quartz reactor, 2 - Catalyst bed, 3 - Gas distributor, 4 - PMMA injection and fluidizing gas nozzle

Table 4.1 Catalyst physical properties.

Property	γ-Al_2O_3	MoO_3-ZrO_2 on SiO_2	FCC	$Cs_xH_{1-x}PW_{12}O_{40}$ on SiO_2	Zeolite Y	Sand
u_{mf}, mm s^{-1}	4.5	3.4	3.4	6.5	3.3	5.1
ρ_b, g cm^{-3}	0.92	0.51	0.78	1.8	0.77	1.35
d_{10}, µm	65	72	51		68	90
d_{50}, µm	98	99	75		83	117
d_{90}, µm	150	140	110	†	101	168
S_{sp}, m^2 g^{-1}	150	197	275	34	314	-
V_{pore}, cm^3 g^{-1}	0.24	0.65	0.36	0.1	0.29	-
d_{pore}, nm	5.6	6.6	3.1	6.1	7.2	-

† $Cs_xH_{1-x}PW_{12}O_{40}$ sieved from 75-106 µm

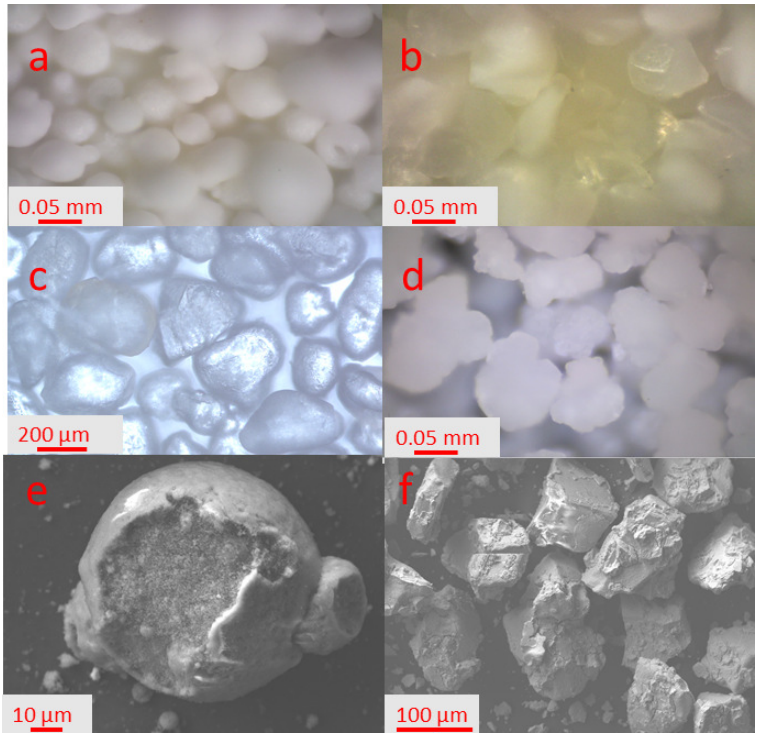

Figure 4.2 Optical photos of a - FCC catalyst; b - MoO_3-ZrO_2/SiO_2; c - sand; d - Al_2O_3; e - Zeolite Y, spray-dried; f - $Cs_xH_{1-x}PW_{12}O_{40}/SiO_2$

The XRD diffractogram of the γ-Al_2O_3 had relatively wide peaks at 2θ= 67°, 46° and 38° due to its amorphous structure (Figure **??**). The silica gel phase has a characteristic re-flection at 26.6° due to its amorphous structure [142, 143] and its weak peak appears only in MoO_3-ZrO_2/SiO_2 catalyst. XRF detected Al_2O_3 and SiO_2 (Si:Al 0.71) and traces of La in La_2O_3 (0.02 g g^{-1}, P in P_2O_5 (0.006 g g^{-1}, Fe in Fe_2O_3 (0.005 g g^{-1}, and Ti in TiO_2 (0.005 g g^{-1}. The faujasite crystalline phase of FCC and zeolite Y appeared at 2θ= 20.4°, 23.6°, 27.0°, 29.6°, 30.7°, 31.4°, 34.0°, and 37.9°, which is consistent with the results of other studies [144]. In the MoO_3-ZrO_2/SiO2 catalyst, the peaks at 30°, 35°, 50°, 60° correspond to ZrO_2 [142]. Peaks related to MoO_3 were inconspicuous due to its low concentration and intercalation of molybdenum in the amorphous matrix of silica during the catalyst calcination [138].

The peaks of $Cs_xH_{1-x}PW_{12}O_{40}/SiO_2$ appeared at 2θ= 21.2°, 23.8°, 26.1°, 30.2°, 35.6°, 38.8°, 43.3°, 47.4°, 54.9°, 61.7°. These angles correspond to the structures x=1.7 and 3.0 (x is a Cs/anion ratio). At x=3.0, the catalyst surface area exceeds 100 $m^2\,g^{-1}$ [145] but it is much lower at x=1.7 because the density of catalyst is higher. The surface area of the synthesized $Cs_xH_{1-x}PW_{12}O_{40}/SiO_2$ was 34 $m^2\,g^{-1}$, which suggests an x closer to 1.7 and a lower activity due to the higher density [145].

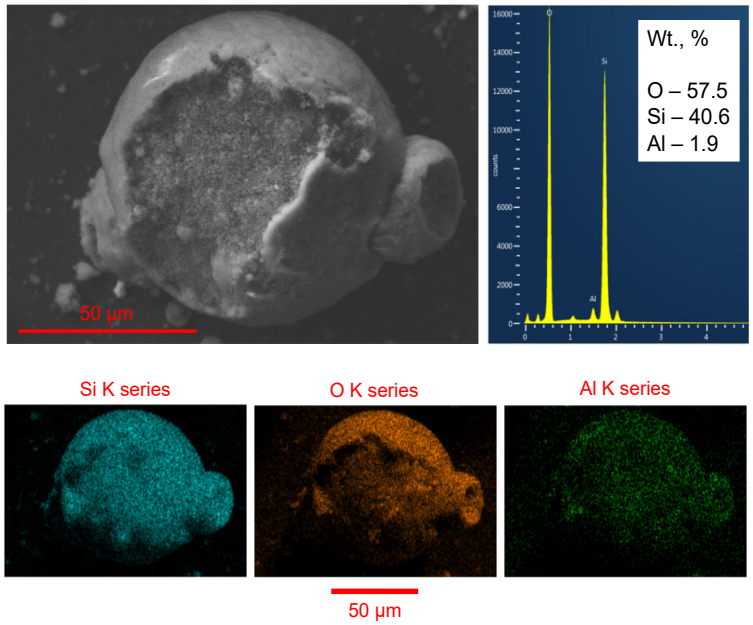

Figure 4.3 SEM-EDS image of spray dried Zeolite Y (CBV 720 from Zeolyst, Ludox AS-40, and polyvinyl alcohol). This was the most active catalyst and was generally spherical. The image shows a rigid outer shell encasing smaller crystals of CBV 720 and silica.

4.4.2 TGA

To identify an appropriate particle size for PMMA thermolysis (in terms of heat and mass transfer), we measured the mass loss of PMMA in a TGA with $0.1\,\mathrm{mm} < d_\mathrm{p} < 0.3\,\mathrm{mm}$, $0.5\,\mathrm{mm} < d_\mathrm{p} < 1\,\mathrm{mm}$, and $d_\mathrm{p} > 1\,\mathrm{mm}$ (Figure 4.5). For these tests, the TGA operated at a ramp of $20\,^\circ\mathrm{C\,min^{-1}}$ with N_2 at a flowrate of $60\,\mathrm{mL\,min^{-1}}$. The DTG peaks demonstrate the temperature at the maximum mass loss as well as the beginning and end of the degradation process. PMMA began to lose mass at $270\,^\circ\mathrm{C}$ for a d_p in the range of 0.1 mm to 0.3 mm while for particles greater than 0.5 mm it was delayed by $10\,^\circ\mathrm{C}$ (Figure 4.5).

In the second set of experiments, the TGA recorded PMMA-1 and PMMA-2 mass loss at a constant temperature (Figure 4.6). The oven temperature ramped at a rate of $40\,^\circ\mathrm{C\,min^{-1}}$ until the set point ($230\,^\circ\mathrm{C}$, $280\,^\circ\mathrm{C}$, $300\,^\circ\mathrm{C}$ and $350\,^\circ\mathrm{C}$), followed by an isotherm of 60 min at $60\,\mathrm{mL\,min^{-1}}$ of N_2. To minimize heat and mass transfer resistance, we loaded not more than 3 mg of $d_\mathrm{p} \leq 100\,\mu\mathrm{m}$ PMMA powder (Alfa Aesar) to the pan. After 60 min at $230\,^\circ\mathrm{C}$, both polymers lost less than 6 % of their mass since the temperature was insufficient to initiate the unzipping process. At $280\,^\circ\mathrm{C}$, the degradation degree reached 10 % for PMMA-1 and 20 % for the PMMA-2.

The initial molecular weight of polymer and its zip length are factors that determine the

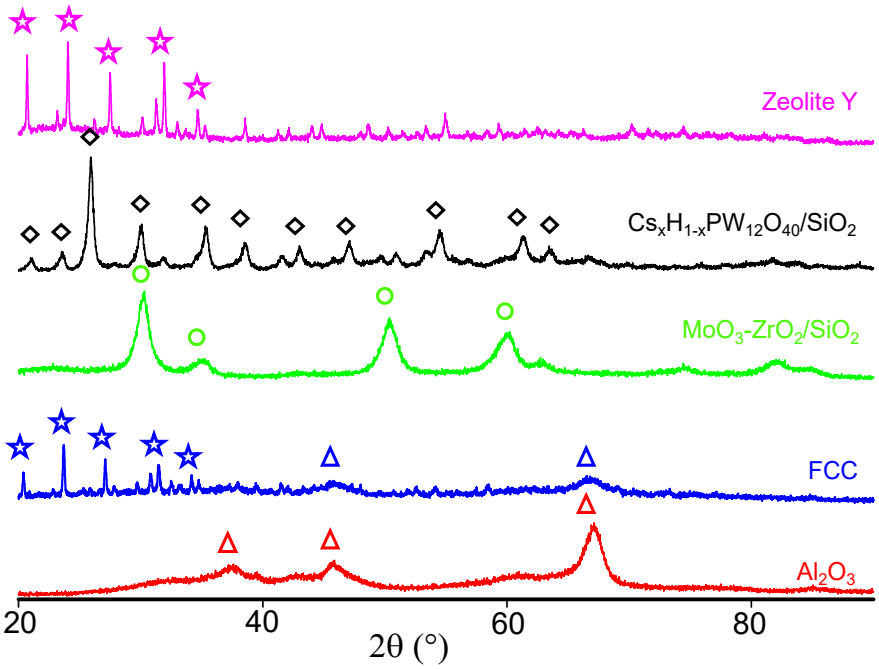

Figure 4.4 XRD diffratogram of Al_2O_3, FCC, MoO_3-ZrO_2/SiO_2, $Ce_xH_{3-x}PW_{12}O_{40}$ and zeolite Y: triangles - γ-Al_2O_3, circles - ZrO_2; stars - Faujasite; rhombuses—Keggin-type structure

extent of degradation as a function of temperature [24, 34, 35]. But the main driver is how it was polymerized and if it contains comonomers. Polymers are synthesized by a radical mechanism or anionic initiation. The end groups and type of defaults in the chain are different. When co-monomers are added (the case for the PMMA supplied by Arkema), their role is to block the depolymerization process at low temperature so that the pellets can be extruded or injected in molds. For that the polymer has to be heated and melted to about 250 °C to avoid depolymerization. The molecular weight depends on the initiators and chain transfer agents, which also create defects in the polymer structure. Finally, the PMMA can be cross-linked and that also affects the depolymerization. The impact of these factors increases with temperature: the mass loss reached 50 % for PMMA-2 while it was only 30 % of PMMA-1 at 300 °C. At 350 °C, both PMMA-1 and -2 degrade completely but it only took 15 min for PMMA-2 while for PMMA-1 it took 60 min (Figure 4.6).

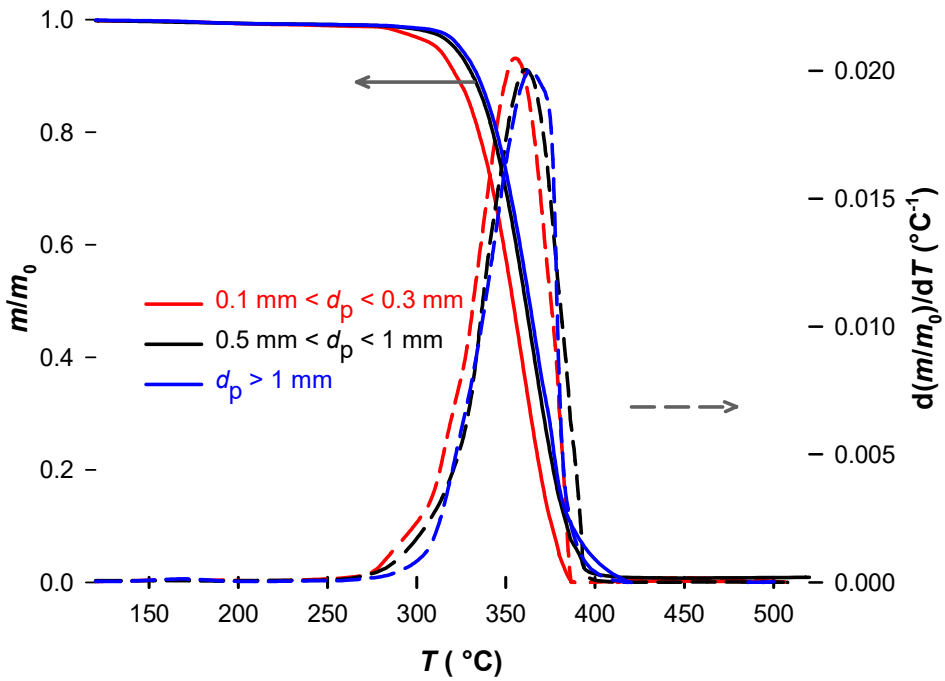

Figure 4.5 PMMA-1 mass loss in a TGA (M_{w}=1 × 10^5 kmol kg^{-1}) at a heating rate of 20 °C min^{-1} as a function of d_{p}.

4.4.3 Catalytic degradation in FB

The temperature ramp in the TGA was 20 °C min^{-1}, while in the fluidized bed the particles heated up more rapidly as we inject them into the vessel at the reaction temperature. The temperature dropped 5 °C immediately after introducing the PMMA. The hot catalyst and gas transfer heat to the surface of the PMMA particles. The polymer on the exterior surface melts and the interior heats via conduction. As a result, the PMMA particles begin to soften and tend to agglomerate with the catalyst and other PMMA particles as they collide. Maintaining a vigorously fluidized bed $U_{\mathrm{g}} >> U_{\mathrm{mf}}$, imparts sufficient kinetic energy to break these agglomerates but this comes at the expense of feeding excess gas and the accompanying compressor cost (at the commercial scale). Ideally, a commercial process would rely exclusively on the produced gas (MMA, MAA, MeOH, CO, and CO_2) to fluidize the bed, thus minimizing compression costs. However, this would be impractical due to the sticky nature of the PMMA and so other mechanical means of mixing are required to impart a shear stress to break up the agglomerates [146].

Injecting particles to our small ID fluidized bed introduces additional challenges with respect

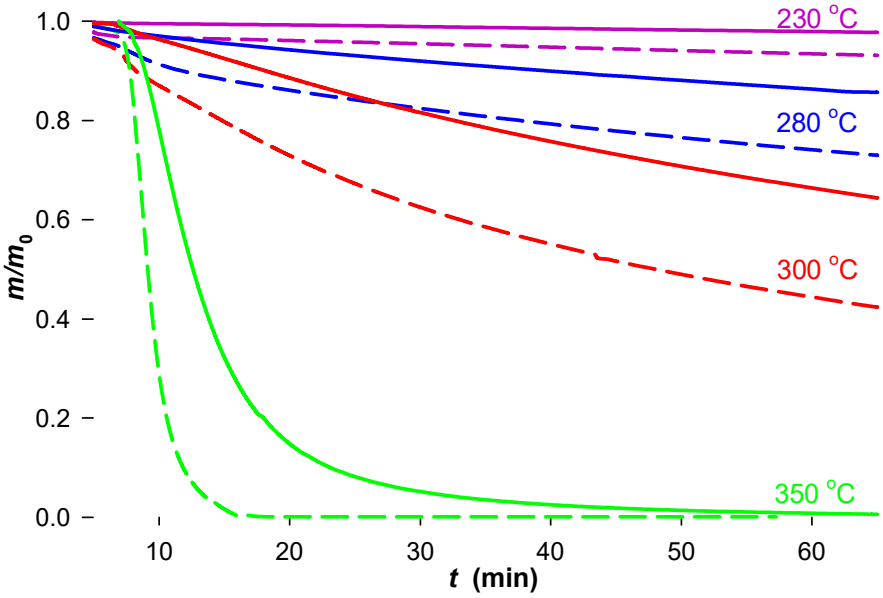

Figure 4.6 Isothermal PMMA mass loss in a TGA at 230 °C, 280 °C, 300 °C, and 350 °C: solid line–PMMA-1, dashed line–PMMA-2.

to mixing. For a commercial process, larger PMMA particles are preferred because this reduces the cost to micronize the polymer. To minimize the formation of agglomerates and maximize the heat transfer rate to the polymer, we chose a d_{p} less than 100 µm, which may be impractical for an industrial process.

We calculated selectivity based on the sum of the moles produced (in the quench and gas phase), $S_{\mathrm{MAA-prod}}$ ($n_{\mathrm{MAA}}, n_{\mathrm{CO}}, n_{\mathrm{CO_2}}, n_{\mathrm{CH_3C(O)CH_3}}$, Eqs. 4.2-4.5) and on total PMMA conversion, $S_{\mathrm{X-PMMA}}$, Eq. 4.6). We equated the carbon LECO measurement to unreacted PMMA and lumped the measure MMA together with it to represent total conversion. Selectivity over Zeolite Y, S_{prod}, was highest and exceeded 90 % (Figure 4.7). However, selectivity based on PMMA conversion was greater than 100 % ($S_{\mathrm{X-PMMA}}$). Besides the Zeolite Y, the molybdenum and Cs-HPA catalysts had the highest selectivity while the FCC and alumina catalysts had the lowest selectivity. A couple of the data points for alumina lie above the parity plot line, indicating $S_{\mathrm{prod}} > S_{\mathrm{X-PMMA}}$. Surprisingly, MAA selectivity with sand (the blank test) was higher than for both the FCC and alumina catalysts, however, conversion to MAA was very low (Figure 4.8).

Below 300 °C the S_{CO} was about double the $S_{\mathrm{CO_2}}$ but at 350 °C it was from 20 times to

Table 4.2 Experimental conditions and performance data: $Q_{\text{in}} = 70\,\text{mm}\,\text{min}^{-1}$ 1 g PMMA. We completed 20 tests at a nominal temperature of 350 °C and the standard deviation was ±7 °C. The percent standard deviation on conversion was 10 % based on twelve runs at 350 °C: two repeat runs for Al_2O_3 and FCC with 10 mL of catalyst and one repeat for Al_2O_3, FCC, and Mo−Zr/SiO_2 with 4 mL of catalyst.

				Mole (%)		Selectivity (%)				
No.	Catalyst	T °C	V_{cat} mL	Ar	H_2O	MAA	MeOH	CO	CO_2	X_{MMA}
1	γ-Al_2O_3	275	4	36	61	42	66	39	19	7
2	FCC	277	4	15	82	50	52	36	12	18
3	CsHPA/SiO_2	287	4	14	83	73	62	24	3	30
4	Zeolite Y	292	4	15	83	93	86	5	1	36
5	Mo-Zr/SiO_2	277	10	25	71	85	83	8	5	10
6	Zeolite Y	278	10	15	82	91	84	6	2	34
7	γ-Al_2O_3	300	4	36	60	36	68	33	31	6
8	FCC	306	4	35	59	37	65	40	19	16
9	CsHPA/SiO_2	297	4	14	82	70	61	26	4	24
10	γ-Al_2O_3	341	4	75	16	0	55	89	0	5
11	FCC	345	4	76	14	4	42	93	2	10
12	Mo-Zr/SiO_2	351	4	86	5	0	0	100	0	6
13	γ-Al_2O_3	352	4	41	50	47	90	52	1	3
14	FCC	346	4	44	50	34	53	55	1	14
15	Mo-Zr/SiO_2	350	4	42	45	60	73	39	0	8
16	γ-Al_2O_3	352	10	41	51	31	91	66	3	2
17	FCC	350	10	44	50	0	16	92	3	14
18	Mo-Zr/SiO_2	357	10	43	50	69	64	29	0	8
19	Sand	352	10	34	61	67	73	30	0	5

100 times higher: the n_{CO_2} detected dropped while the n_{CO} remained about the same. The amount of acetone produced varied little with temperature and was typically from 20 to 100 times lower than n_{CO}.

$$S_{\text{products}} = \frac{5 \cdot n_{\text{MAA}}}{5 \cdot n_{\text{MAA}} + n_{\text{CO}} + n_{\text{CO}_2} + 3 \cdot n_{\text{CH}_3\text{C(O)CH}_3}} \tag{4.2}$$

$$S_{\text{CH}_3\text{OH}} = \frac{5 \cdot n_{\text{CH}_3\text{OH}}}{5 \cdot n_{\text{MAA}} + n_{\text{CO}} + n_{\text{CO}_2} + 3 \cdot n_{\text{CH}_3\text{C(O)CH}_3}} \tag{4.3}$$

$$S_{\mathrm{CO}} = \frac{n_{\mathrm{CO}}}{5 \cdot n_{\mathrm{MAA}} + n_{\mathrm{CO}} + n_{\mathrm{CO_2}} + 3 \cdot n_{\mathrm{CH_3C(O)CH_3}}} \tag{4.4}$$

$$S_{\mathrm{CO_2}} = \frac{n_{\mathrm{CO_2}}}{5 \cdot n_{\mathrm{MAA}} + n_{\mathrm{CO}} + n_{\mathrm{CO_2}} + 3 \cdot n_{\mathrm{CH_3C(O)CH_3}}} \tag{4.5}$$

$$S_{\mathrm{X-PMMA}} = \frac{n_{\mathrm{MAA}}}{n_{\mathrm{MMAin}} - n_{\mathrm{MMAout}} - n_{\mathrm{C,\,reactor}}} \tag{4.6}$$

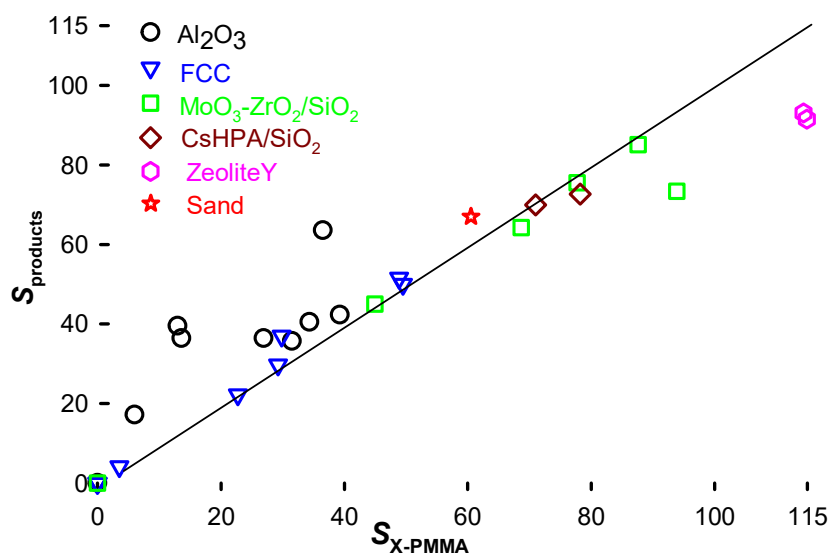

Figure 4.7 Selectivity parity: x-axis is the ratio of mole MAA detected in the quench and moles PMMA converted and the y-axis is the ratio of the mole MAA and the total mole of products (Eqs. 4.2, 4.6) ($R^2 = 0.89$).

Like for selectivity, PMMA conversion was highest over zeolite Y and the second highest conversion was over the Cs-HPA. (Figure 4.8). The conversion calculated based on products (Eq. 4.7) agreed with conversion based on the mass balance around PMMA (Eq. 4.7), where we assume that carbon detected on the catalyst by the Leco was unreacted PMMA ($n_{\mathrm{C,\,reactor}}$).

$$X_{\mathrm{products}} = \frac{n_{\mathrm{MAA}} + n_{\mathrm{CO}}/5 + n_{\mathrm{CO_2}}/5 + n_{\mathrm{CH_3C(O)CH_3}}/1.67}{n_{\mathrm{MMAin}}} \cdot 100 \tag{4.7}$$

$$X_{\mathrm{MMA}} = (1 - \frac{n_{\mathrm{MMAout}} + n_{\mathrm{C,\,reactor}}/5}{n_{\mathrm{MMAin}}}) \cdot 100 \tag{4.8}$$

The conversion (to MAA) across the FCC was second highest and the conversion was lowest

over sand and alumina. Sand is 99.5 % SiO_2 with traces of Fe_2O_3, TiO_2, MgO, CaO, K_2O, NaO_2 and Al_2O_3 oxides (< 0.2 %). It is weakly acid (Lewis acidity) and its low catalytic activity correlates with these low oxide concentrations [147, 148]. Although the selectivity to MAA over sand is low, yield to MMA was the highest of all the samples tested at 0.91 g g^{-1}. Sand has the highest density and largest particle size, which may accelerate heat transfer (higher C_p) and reduce agglomeration. This data supports the hypothesis that the thermolysis of the PMMA is non-catalytic.

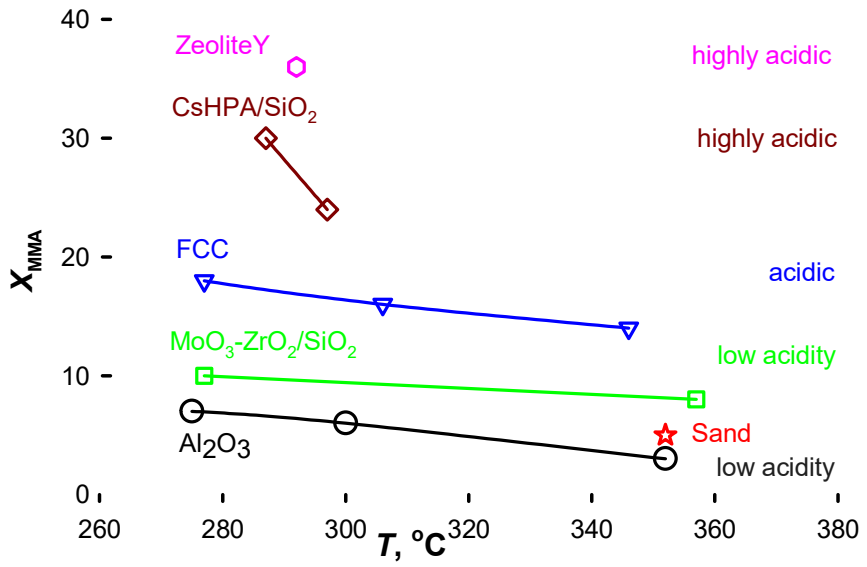

Figure 4.8 Conversion as a function of catalyst composition. Excluding the zeolite Y data the correlation coefficient, R, for the conversion based on PMMA reacted and products detected was 0.95.

The experimental plan first considered high temperature (350 °C) and water concentrations below a mole fraction of 20 % (rows 10, 11, and 12 of Table 4.2). At this condition, all PMMA reacted within 15 min after injection, which agrees with the TGA experiments (Figure 4.6). FCC was the only catalyst to produce a little MAA and methanol in proportion as we would expect from stoichiometery: $S_{prod} = 4\,\%$) and and $S_{MeOH} = 5\,\%$: 1 mol MMA hydroylzes to produce 1 mol MAA and 1 mol methanol (Figure 4.13).

We then increased the water concentration to 50 % at the same temperature as the first series (rows 13, 14, and 15 of Table 4.2). All the catalysts produced MAA. The MAA yield over FCC and MoO_3-ZrO_2/SiO_2 was 5 % γ-Al_2O_3 activity was the lowest with a yield of 1 % (Figure 4.9).

In the third series (rows 16, 17, 18 and 19 of Table 4.2, Figure 4.10), we increased the

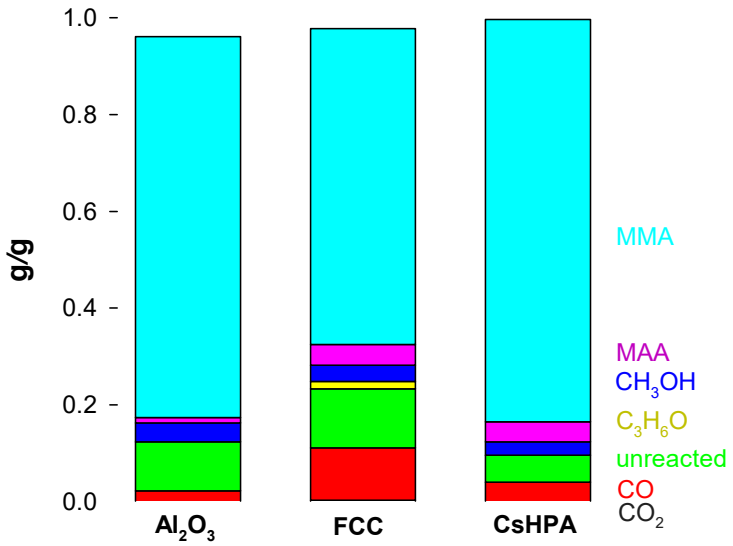

Figure 4.9 Products composition obtained at 350 °C, V_{catalyst} 4 mL and water in excess.

volume of catalyst from 4 mL to 10 mL and operated the reactor with an excess of water and $T = 350\,°\text{C}$. The yield of MAA over MoO_3-ZrO_2/SiO_2 and γ-Al_2O_3 was unchanged, as well as the unreacted PMMA on the catalyst (LECO analysis). Adding more water decreased the CO yield and increased the MAA and MeOH yield (second series). Adding more catalyst at an excess of water affected on MAA yield only for the FCC catalyst. The yield of MeOH decreased by two times for FCC and MoO_3-ZrO_2/SiO_2 catalysts and slightly increased for γ-Al_2O_3.

In the fourth series (rows 1 to 9 in Table 4.2), the reactor operated at 300 °C and 280 °C (all under isothermal conditions with a temperature variation of ±3 °C), while maintaining an excess of water and catalyst volume of 4 mL, increased the amount of carbon remaining with the catalyst 10 % to 15 % for the α-Al_2O_3, FCC, and MoO_3-ZrO_2/SiO_2, (Figure 4.11). PMMA mixed with a catalyst at 280 °C formed a bed that might be termed incipient agglomeration: the bed appeared more viscous but it continued to be fluidized as the PMMA melted. At the end of the experiment, after unloading catalyst from the reactor, we noted that some particle had agglomerated ($< 10\,\%$). Despite these agglomerates, the bed did not slump. The CO and CO_2 MS signals rose to a maximum after about 7-10 min and then gradually fell with time until the concentration approached zero (45 min). Selectivity over γ-Al_2O_3 at these conditions decreased by 5 % versus the third series of tests while for FCC it was in the range 37 % to 50 % that is similar to the results obtained in second series. S_{prod}

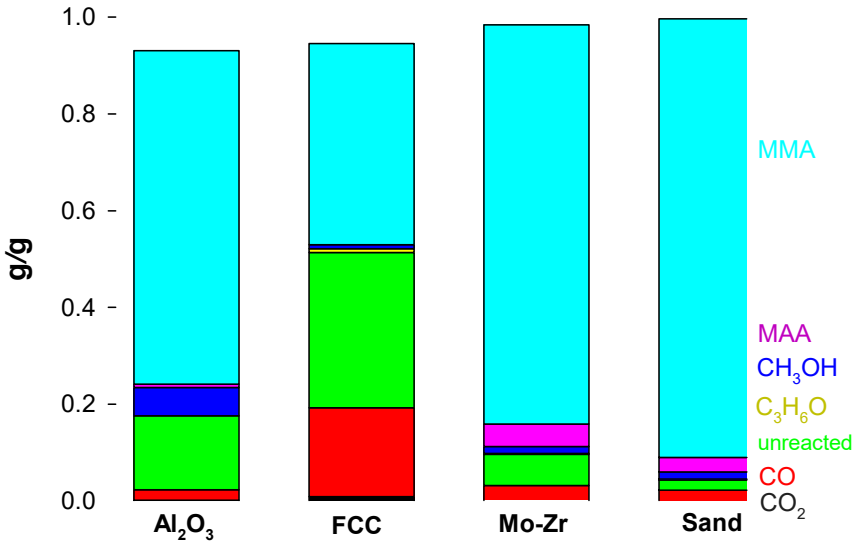

Figure 4.10 Products composition obtained at 350 °C, V_{catalyst} 10 mL and water in excess.

over MoO_3-ZrO_2/SiO_2 increased by 1.5 times.

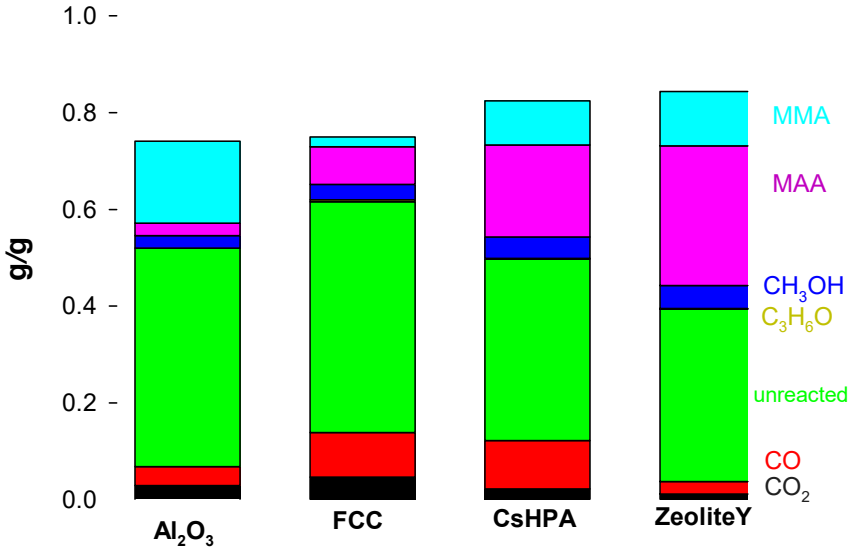

Figure 4.11 Products composition at 280 °C, V_{catalyst} 4 mL and water in excess.

While MAA yield of FCC, alumina and MoO_3-ZrO_2/SiO_2 was less than 9 %, it exceeded

20 % over the Cs−HPA/SiO_2 and 30 % for the zeolite Y at 280 °C. Increasing of the reaction temperature by 20 °C enhances the PMMA degradation about 20 % (Figure 4.6) according to the TGA data. Nevertheless, increasing the temperature in the reactor up to 300 °C decreased MAA yield 1.5 times for all the catalysts (Figure 4.12).

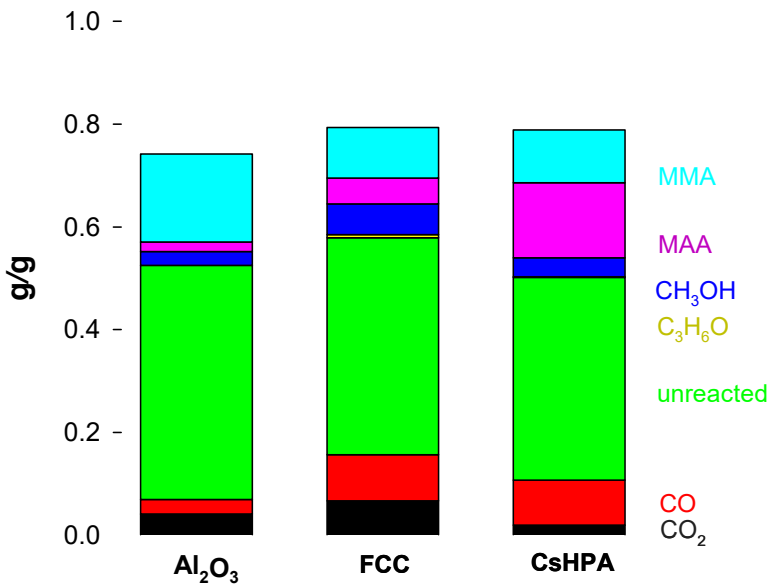

Figure 4.12 Products composition at 300 °C, V_{catalyst} 4 mL and water in excess.

PMMA injected in γ-Al_2O_3 at 230 °C slumped (defluidized) the fluidized bed and the polymer agglomerated the catalyst. TGA results obtained at 230 °C confirmed that this phenomena might occur (Figure 4.6). PMMA starts degrading in the range 270 °C to 290 °C (Figure 4.5). At 280 °C, about 10 % to 20 % of PMMA pyrolyzed. Other literature reports on PMMA TGA degradation often have several shoulders so the DTG has multiple peaks [149]. The absence of additional peaks in the DTG here may be related to the operating procedure of the instrument and the source of the PMMA. Based on a high resolution TGA technique, we detected a slight shoulder at 260 °C in our DTG peaks with mass loss of 5 % before the main DTG peak.

In all experiments with water in excess and a catalyst volume of 4 mL, the yield of MAA over γ-Al_2O_3 was in the range of 1 % to 3 %. The low crystallinity of γ-Al_2O_3 [150] and its high water adsorption capacity [57] decreases the strength of the bond between hydrogen and ester. Also, secondary adsorption of the reaction products on the catalyst surface prevents the adsorption of esters to it [151, 152].

At the same conditions, the yield of MAA over MoO_3−ZrO_2/SiO_2 was in the range 5 % to

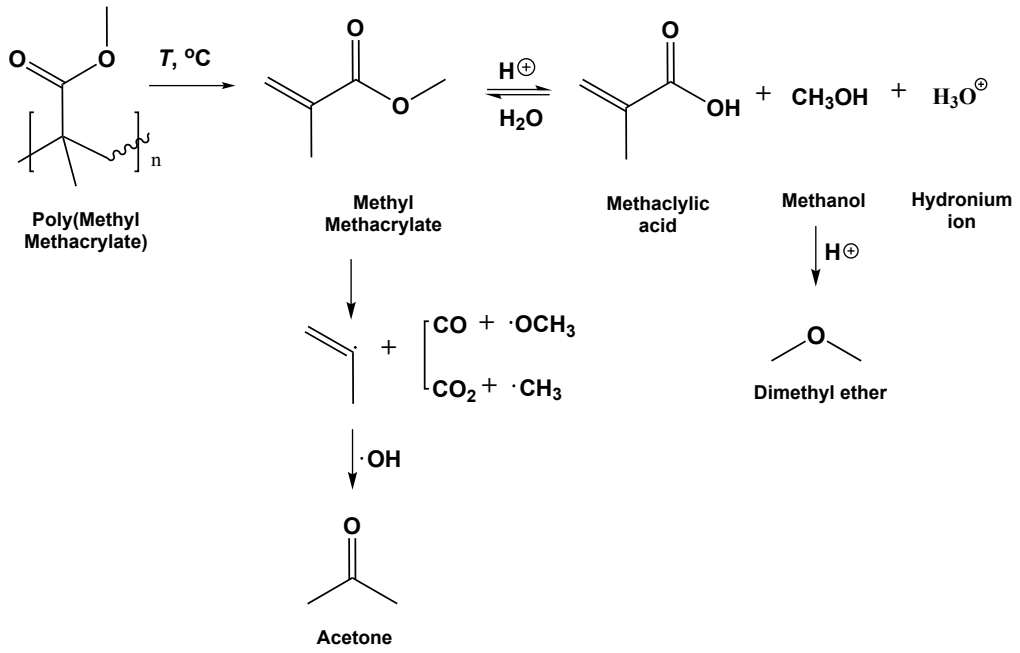

Figure 4.13 Mechanism of PMMA degradation and side reactions resulting formation of CO, CO_2, acetone and CH_3O- radical [4] leading to methanol formation on protonated sides of catalyst.

8 %. Selectivity of this catalyst was sensitive to temperature. Dropping temperature from 350 °C to 280 °C increased selectivity by 1.5 times. The pure silicon oxide has weak Brønsted acidity [153], while the acidity of a mixture of SiO_2 and ZrO_2 oxides, calcined at temperatures above 500 °C, significantly increases due to an increase in the density and strength of the Brønsted acid sites [57, 142]. This also defines the reduced poisoning effect of water on SiO_2-ZrO_2 oxides due to higher hydrophobic effect of SiO_2 comparing to γ-Al_2O_3 [57].

The activity of FCC catalyst towards MAA yield was similar to the MoO_3-ZrO_2/SiO_2 in all the range of temperatures and catalyst volumes. Selectivity of FCC was the opposite to MoO_3-ZrO_2/SiO_2 and dropped from 9 % to 0 % when increasing temperature from 280 °C to 350 °C. According to XRD diffractograms, the FCC catalyst has a faujasite crystalline structure, the spatial structure of the crystal lattice which has high density of Brønsted acid sites (Figure **??**) [62]. However, basic lanthanum oxide impregnated on the zeolite surface stabilizes the FCC catalyst and, simultaneously, reduces the strength of its acid sites [154]. The strong oxidative activity of FCC cracked the MMA to CO when the reactor operated with the highest catalyst volume.

Zeolite Y and $Cs-HPA/SiO_2$ have the highest strength and density of Brønsted acid sites and these catalysts represented the highest activity towards MAA yield and selectivity at

280 °C and 350 °C. From this we can conclude that catalyst acidity is the major factor for MMA hydrolysis.

4.4.4 Reaction mechanism

PMMA is the only polymer that almost completely depolymerizes via a radical mechanism to MMA. The initial molecular weight, chain length, and spatial arrangement of individual groups in the polymer chain play a significant role in PMMA degradation [155]. MMA polymerization depends on temperature, initiator among other factors and follows a radical or anionic mechanism Comonomers affect the polymer structure, the molecular weight, type of defects in the polymer chain, and the termination mechanism. [149] The impurities generated during the depolymerization depend on the polymer, but also on the depolymerization process itself. The samples used in the work are for injection grade, and so contain comonomers.

The degradation of PMMA (Figure 4.5) resulted in only one DTG peak with the maximum at 370 °C, which supports the random chain scission mechanism [4].

In the second stage of our process, MMA hydrolyzes to MAA and methanol.

$$H_2C{=}C(CH_3)COOCH_3 + H_2O \rightarrow H_2C{=}C(CH_3)COOH + CH_3OH \tag{4.9}$$

Thus, methanol is an indicator of methacrylic acid formation. However, the concentrations of methanol were much lower than expected by stoichiometry over alumina and FCC (Figure 4.14). Above 300 °C, MMA decarboxylates to CO (with only a minor amount of CO_2) and methoxy- CH_3O- and CH_3- radicals (Figure 4.13) [4, 22, 126]. These radicals react with protons or OH- groups from other species to form to methanol. Nevertheless, the amount of methanol identified by GC-FID over strongly acid catalysts ($Cs_xH_{1-x}PW_{12}O_{40}/SiO_2$ and zeolite Y) was an order of magnitude lower than the MAA compared to other catalysts with a lower acidity. We attribute this effect to dehydration of methanol over Brønsted acid sites to form dimethyl ether [156, 157]. We confirmed experimentally that the zeolite Y catalyst dehyrates methanol to dimethyl ether at 280 °C [158]. According to previous studies, acidic γ-Al_2O_3 is also reactive to produce some dimethyl ether [159].

4.5 Conclusions

Despite large scale pilot plant trials in the 1980s to depolymerize PMMA, this process remains an elusive commercial target due to the impurities produced that have a similar boiling point to methyl methacrylate (101 °C). This introduces unacceptable separation costs. Methacrylic

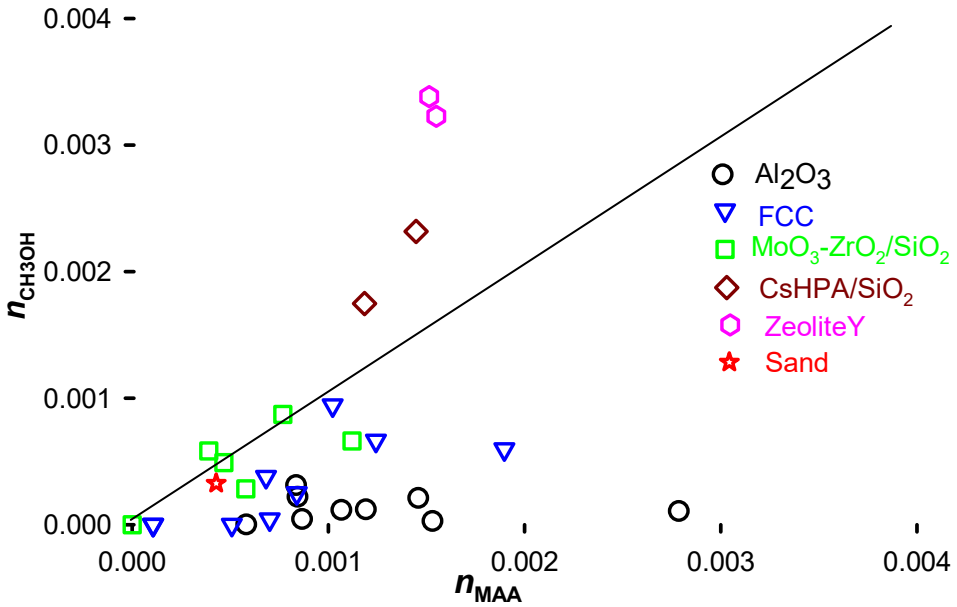

Figure 4.14 Yield MeOH versus MAA. The parity line is what we expect based on the MMA hydrolysis stoichiometry.

acid is a promising alternative to MMA as it has a much higher boiling point (161 °C). In a fluidized bed process, catalyst provides the heat to drive the thermolysis reaction while at the same time catalyzes MMA hydrolysis to MAA. However, the thermolysis reaction operates best above 350 °C while selectivity to MAA is better at lower temperatures. So, tandem reactors might be a practical alternative to a one-pot approach: thermolysis at high temperature first followed by catalytic hydrolysis to MAA. Among the 6 systems studied, sand produced more MMA presumably due to its higher heat capacity and superior fluidization properties. In the micro-fluidized bed, the yield of MAA increased with catalyst inventory (1:2 gram PMMA to gram catalyst up to 1:10 gram PMMA to gram catalyst) but in all cases the fraction of unreacted PMMA exceeded 50 % below 300 °C, which is closer to the optimal temperature for the catalytic hydrolysis. Based on MMA hydrolysis stoichiometery, we expected to see as much MeOH as MAA. This was the case for zeolite, Cs-HPA, MoO_3-ZrO_2/SiO_2 and sand but is was much lower over the alumina catalyst. We attributed this difference due to dehydration of MeOH to DME. The TGA experiments confirm that particle size below 0.5 mm improve mass and heat transfer rates. Among the five catalyst tested, zeolite Y gave the highest MAA yield and exceeded 30 %. The characteristics of zeolite Y that facilitate MAA yield include its high acidity, crystallinity and surface area and large pore structure. We anticipate improved yields in larger diameter fluidized beds with a larger shear that will

reduce agglomeration and improve heat transfer and thus control coke formation.

CHAPTER 5 ARTICLE 2 : ZEOLITE Y HYDROLYSES METHYL METHACRYLATE TO METHACRYLIC ACID IN THE GAS PHASE

Olga V. Chub, Jean-Luc Dubois, Gregory S. Patience. Chemical Engineering Journal, Submitted: 6 July 2022

5.1 Abstract

Polymethyl methacrylate (PMMA) depolymerizes to its monomer methyl methacrylate (MMA) below 400 °C but the accompanying byproducts have similar boiling points, which incurs excessive separation costs rendering the process economic challenging. Hydrolysing MMA to methacrylic acid (MAA) is a potentially economic alternative since its boiling point is 61 °C higher. Zeolites are among a class of heterogeneous catalyst with Brønsted acidity that protonate the ester carbonyl group in the much less common gas-phase route to acids. Here, for the first time, we report the hydrolysis kinetics of MMA to MAA in the gas phase over a Y/SiO_2 zeolite with a $960\,m^2\,g^{-1}$ surface area. MMA conversion in an 8 mm fixed bed reactor averaged 94 % above 200 °C and a yield of 85 %. Operating the reactor in excess water vapour shifts the equilibrium conversion towards the products. Surface reaction between adsorbed MMA and water is the rate controlling step. Heterogeneous supports control the hydrophobic properties, and thereby activity and stability. Introducing zeolites in the matrix of a silica gel allows access to all external zeolite centres compared to spray-drying with Ludox where the SiO_2 shell covers the external catalyst surface. Nuclear magnetic resonance spectroscopy with magic angle spinning technique (MAS-NMR) and ultra-violet visible (UV-Vis) detected Brønsted acidity. The apparent activation energy of the reversible reaction was $106\,kJ\,mol^{-1}$.

5.2 Introduction

Producing chemicals from waste and bio-based feedstocks reduces the burden on the environment, and is also economically attractive when it costs less than petroleum or reduces the number of processing steps. C_2-C_4 building blocks serve as raw materials to produce methyl methacrylate (MMA) [160, 161]. Industrial giants such as Röhm GmbH (Germany), ChiMei Corporation (Taiwan), Mitsubishi Chemical Holdings Corporation (Japan), Sumitomo Chemical (Japan), SABIC (Saudi Arabia), LG Chem (South Korea), Trinseo (US), Kuraray (Japan), Kolon Industries (South Korea), Toray Industries (Japan), Lotte Chemical Corporation (South Korea), and Plaskolite (US) are manufactuers of PMMA [162]. Mitsubishi

Rayon (MRC), Nippon Shokubai Kagaku Kogyo, Japan Methacrylic Monomer, Thai MMA, and Asahi developed the idea of partially oxidizing isobutylene to MMA and MAA [1, 88]. The C_2-C_4 schemes involve multi-step processes to produce MMA or methacrylic acid (MAA) and have a much lower environmental footprint compared to the acetone cyanohydrin (ACN) process, which is the primary commercial route [1, 163]. Drawbacks include low MMA/MAA yields and short catalyst lifetime, so optimizing the catalyst composition has been a compelling research endeavour [52].

Depolymerization of end-of-life poly(methyl methacrylate) (PMMA) is a well-studied route to produce recycled methyl methacrylate (r-MMA) and, then, to re-polymerize it to r-PMMA [22]. However, the concomitant formation of reaction by-products with similar boiling points to MMA negatively affect the quality of r-PMMA and increases the separation cost [4, 8, 21, 71]. The objective of the European "MMAtwo" program was to reduce primary fossil fuel consumption by at least 30 % and CO_2 emissions by 20 % by recycling scrap PMMA, improving existing recycling schemes, and developing novel approaches [67, 164].

In this context, we studied hydrolysis MMA to MAA as an alternative monomer/specialty chemical derived from PMMA depolymerization [165]. The ester hydrolysis is the reverse reaction of esterification, which has been studied since the 1920s [105]. The activation of the ester molecule is the limiting step. Brønsted acids catalyze the reaction to form carboxylic acids [51, 52]. More studies have been published in the open literature for liquid phase hydrolysis [166–168] while here we develop a gas-phase heterogeneous catalytic reaction. Reaction rates are faster in the gas phase and we expect that by-product yields will be lower as solvation reactions are minimized [53]. Super acids like Ce salts of hetero-poly acids and zeolites are the preferred catalysts because of their high activity and stability with respect to water vapour at low temperature [57–59]. Previous studies tested Al_2O_3, ZrO_2-MoO_3/SiO_2, Cs-HPA, FCC and zeolite Y and demonstrated that hydrolysis activity to MAA from MMA increased with acidity [165]. MAA yield and selectivity is directly proportional to the strength of the zeolite acid sites and hydrophobicity that is defined by crystallinity and Si/Al ratio [58, 60–62]. Among the acid catalysts, MAA yield over zeolite Y was 33 % compared to 19 % over Cs-HPA.

Because of the higher yield, we selected zeolite Y to study the gas-phase MMA hydrolysis kinetics in a fixed bed. We tested a range of temperatures to estimate the reaction kinetics and MAA stability at high temperature. Based on this preliminary set of data, we propose a second order reversible model (1st order in MMA and H_2O) and identify the equilibrium conversion.

5.3 Experimental

5.3.1 Materials

Tetraethoxy silane (tertaethyl orthosilicate, TEOS (99 %), ethanol (99.8 %), isopropanol (99.5 %), hydrochloric acid (32 g g^{-1} in water) and poly(ethylene glycol)-block-poly(propylene glycol) -block-poly(ethylene glycol) (Pluronic P_{123}), methyl methacrylate (99 %) all were purchased from Sigma Aldrich. Zeolite Y (hydrogen form, micro-sieve) (CBV780, Faujasite) was from Zeolyst. Argon (0.999 mol mol^{-1}) and calibration mixture CO (0.1 mol mol^{-1}), CO2 (0.1 mol mol^{-1}) purchased from Air Liquid.

5.3.2 Catalyst synthesis

The Si (TEOS) precursor was pre-hydrolyzed in an acidic medium [150]: a magnetic stirrer agitated a solution of 40 mL of TEOS, 29 mL of isopropanol, and 4.8 mL of an HCl solution (90 mL of distilled H_2O and 0.1 mL of 32 % HCl) for three days at room temperature. Then, 19 g of P_{123} was added to the pre-hydrolyzed TEOS solution at room temperature for an additional 20 h. After that, 10.4 g of zeolite Y was added to the solution of Si precursor with P_{123} (pH=2) at 40 °C for another 2 h. Then, 11.2 mL of NH_4OH was added and the mixture began to gel after about 2 min. We placed the gel in a plastic container to let it age for seven days at 40 °C. We then put the sample in a furnace that ramped the temperature to 120 °C at the heating rate of 1 °C min^{-1} and it remained at this temperature for 4 h. After that, the sample calcined at 550 °C for 6 h.

5.3.3 Characterization

The standard techniques characterized catalyst properties: N_2 porosimeter Gemini VII 5.02 (Micrometrics) measured the Brunauer–Emmett–Teller (BET) surface area and pore size distribution; an Altamira AMI 300 HP chemisorption analyzer assessed the catalyst surface acid sites by NH_3 desorption; a Jeol JSM-7600TFE scanning electron microscope (SEM) imaged the morphology, and an Oxford Instruments X-Max 80 Energy Dispersive Spectroscopic (EDS) detector determined the distribution of the active phase on the sample surface and estimated its mass ratio; an Evolution 220 (Micrometrics) UV-Visible spectrophotometer equipped with the integrating sphere of 60 mm recorded diffuse reflectance spectra (UV–visible DRS) in the range 200 nm to 900 nm at room temperature; a Bruker Avance 600 WB spectrometer scanned ^{1}H DQ MAS-NMR spectra; X-ray photo-electron spectroscope (XPS) (VG ESCALAB 250Xi) with mono Al Kα 1486.68 eV source, 900 µm spot size, 0.1 % detection limit and 10 nm penetration depth, and 1.3×10^{-6} Pa pressure in the cham-

ber analyzed the catalyst surface composition. A LECO CS744 analyzer (LECO), equipped with an IR detector, quantified the mass of carbon deposited on the catalyst and operated at 1300 °C to 1400 °C. An Agilent 7890A gas chromatograph (GC) equipped with a DB-Wax column (0.25 mm ID, 30 m of length, 0.25 µm of film diameter) connected to an Agilent 5975C VL MSD mass spectrometer identified the liquid reaction products. In the analytical method, the oven temperature rose to 40 °C in 4 min, then ramped to 100 °C at 4 °C min^{-1}, followed by a 10 °C min^{-1} ramp up to 200 °C and maintained at this temperature for 10 min. The autosampler injected 0.1 µL aliquots of liquid via a 10 µL micro-syringe from Supelco. The solution (1:100 dilution in ethanol) passed through a 0.2 µm filter to remove any solid residues. An HPR-20 TMS (Hiden Analytical) mass spectrometer (MS) equipped with a quartz inert capillary recorded CO and CO_2 at the reactor outlet at a frequency of 3 Hz, ionization energy 70 eV. Two HPLC pumps AZURA P 4.1S from Knauer, flow rate range from 0.001 mm min^{-1} to 10 mm min^{-1}, equipped with a pressure sensor and a maximum delivery pressure of 40 MPa, maximum viscosity 0.1 Pa s, injected MMA and water in the heated line. The pump was calibrated before the experiments with water (calibration coefficient $k = 1.01$, $R^2 = 1$) and MMA (calibration coefficient $k = 1.01$, $R^2 = 0.99$) at ambient conditions.

5.3.4 MMA hydrolysis tests

The activity of catalyst was evaluated in an 8 mm ID quartz tube 740 mm long. The catalyst bed height was 10 mm and positioned in the middle of the quartz tube. The catalyst operated as a fixed bed at 101 kPa from 160 °C to 300 °C. The reactor operated at a velocity of $U_g = 40\,mm\,s^{-1}$, which is high enough to fluidize the powder ($U_{mf} \leq 20\,mm\,s^{-1}$). Our previous studies demonstrated that plug flow approximation becomes poorer with increasing gas velocity above U_{mf} [169]. The catalyst (2) was sandwiched between glass wool (3), which restricted its movement so bubbles would not form and thus the flow regime would continue to be plug flow. A thermocouple (type K, chromel/alumel, the thermocouple precision was ± 1.5 K) in the middle of the catalyst bed monitored the reaction temperature (Figure 5.1). Argon flowed through the feed line and two HPLC pumps fed pure methyl methacrylate (MMA) and water to the line, which was heated to 130 °C to vaporize the liquids. The reaction products condensed in a liquid trap of ethanol cooled in an ice bath. The mass spectrometer monitored the m/Z ratios corresponding to CO (28) and CO_2 (44). We excluded the m/Z of CH_4 and H_2 as methane is known to form only above 300 °C [11, 22] and in our previous TGA experiments the H_2 fragment was barely perceptible. Before each experiment, we calibrated the mass-spectrometer with a standard gas mixture of 0.1 mol mol^{-1} CO and 0.1 mol mol^{-1} CO_2 in Ar. We then calculated the sensitivity coefficients and concentrations [170]. Presumably, the carbon must be coming from MMA as MAA was stable up to 350 °C.

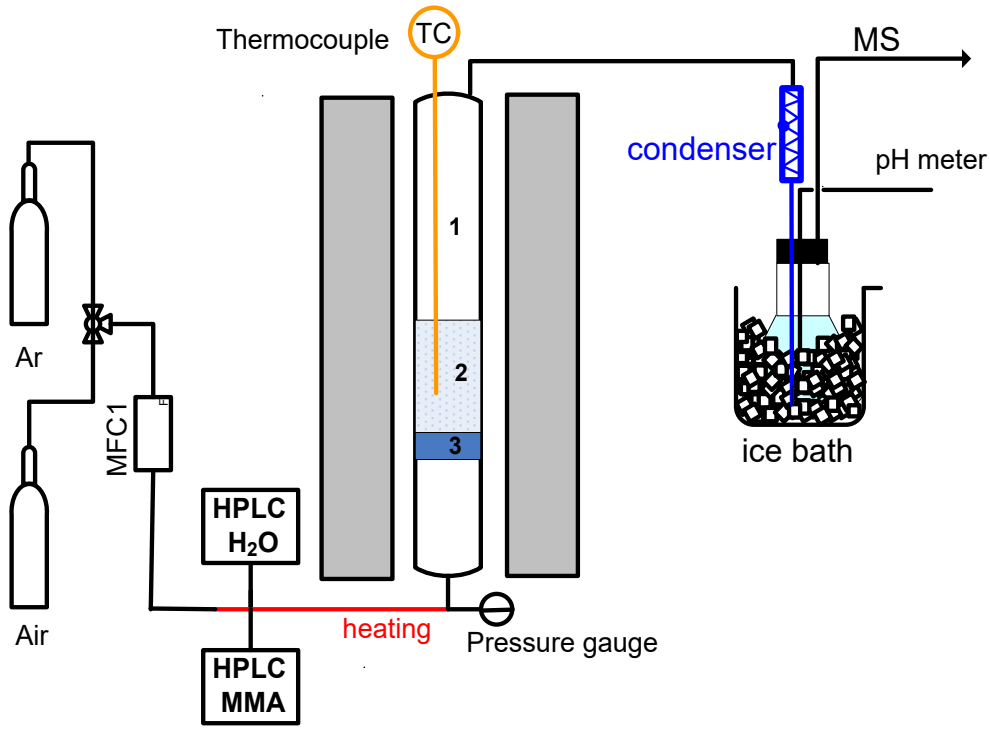

Figure 5.1 The experimental setup consisted of an 8 mm ID quartz tube housed in an electrical furnace, two HPLC pumps, quench, pH meter to monitor the acid concentration with time, Ar as the carrier gas, and air to regenerate the catalyst after an experiment.

5.4 Results and discussion

5.4.1 BET

The shape of the isotherm generated by the porosimeter resembles type IV(a) with H2(b) hysteresis, which corresponds to condensation of adsorbate in big pores (Figure 5.2). This hysteresis type is typical for materials with a wide range of pore distribution [137, 171]. The Brunauer–Emmett–Teller (BET) surface area of fresh zeolite Y/SiO_2 catalyst was 960 $m^2\,g^{-1}$ with a total pore volume at $p/p_0 = 0.99$ of 1.3 $cm\,g^{-3}$. The pore size was less than 96 nm and the pore distribution ranged from 0.8 nm to 78 nm. We might expect capillary condensation in zeolites when they operate at high partial pressure of water (and MMA). As a rough estimate, MMA would fill pores 0.5 nm in diameter at 250 °C and a 1:1 mixture of MMA and H_2O according to the Kelvin–Laplace equation [172]:

$$\ln \frac{P}{P\circ} = 2\frac{\sigma V_{\mathrm{m}}}{rRT} \tag{5.1}$$

where, $P\circ$ is the saturated vapour pressure, σ is the surface tension, V_{m} is the molar volume of water, and r is the droplet radius. So according to Eq. 5.1 since the droplet radius would be smaller for water, we assume capillary condensation is negligible. Furthermore, since the feed gas contained Ar as an inert carrier, partial pressures are even lower and so the condensation is even less probable.

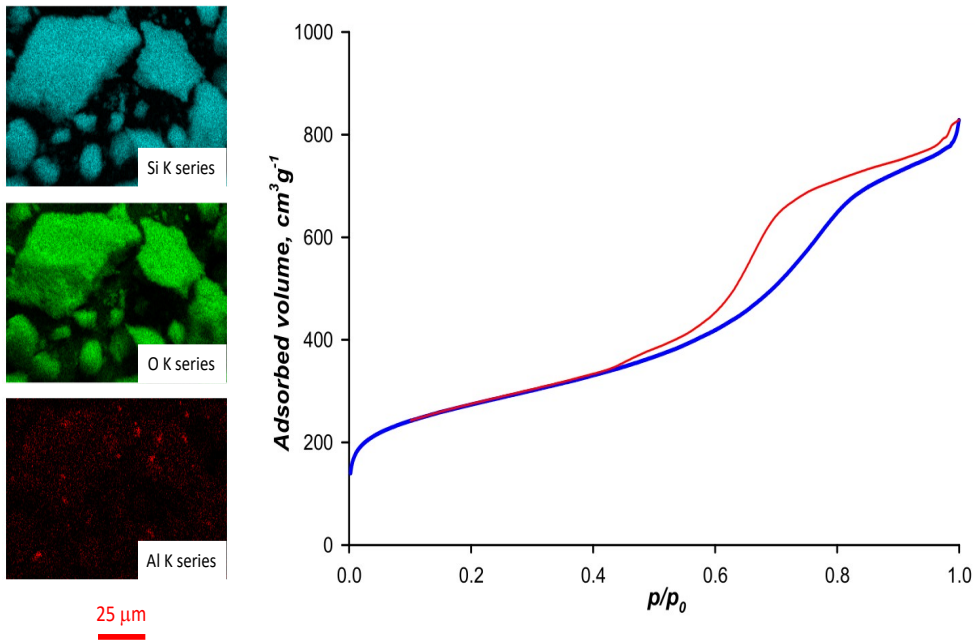

Figure 5.2 EDS mapping of silicon, aluminum and oxygen in the catalyst sample (on the left) and N_2 adsorption-desorption isotherms (on the right).

5.4.2 SEM

The catalyst particles are irregularly shaped agglomerates with visible inclusions of zeolite micro-particles (Figure 5.3). The high-resolution images ($\times$1000 magnification) did not show any visible porosity. EDS spectra (Figure 5.2) revealed that Si and oxygen were distributed homogeneously while Al appeared as a distinct spots. The size of the zeolite crystals were nominally less than 5 µm. The measured Si content was $0.38\,\mathrm{g\,g^{-1}}$ and it was $0.619\,\mathrm{g\,g^{-1}}$ for oxygen while it was only $0.001\,\mathrm{g\,g^{-1}}$ for Al (Figure 5.2).

5.4.3 DR-UV–vis

The absorbance spectra of zeolite Y micro-sieves has a broad intense peak at wavelengths from 200 nm to 550 nm with two shoulders at 250 nm and 340 nm related to charge trans-

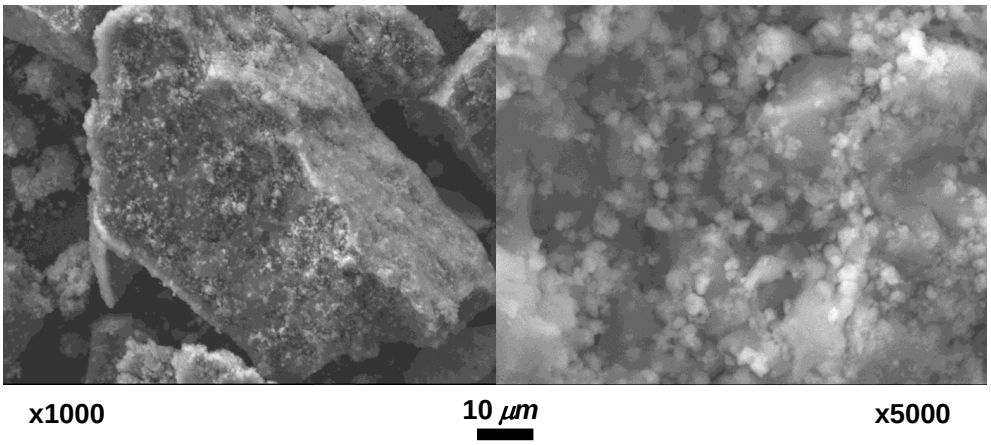

Figure 5.3 SEM image of zeolite Y encapsulated in silica gel. The white inclusions are zeolite Y.

fer processes in different Al−O coordination. The shoulder at 250 nm corresponds to the crystalline properties of zeolite and its high absorbance infers low Al content in zeolite [173].

The shoulder at 340 nm is associated with an Al extra-lattice responsible for catalyst acidity. This structure represents a more energetically favoured transition of a more polarized Al−O species that provides the catalytic activity of zeolite Y [173]. The lower the density of Al species in the zeolite lattice, the higher the induced charge transfer between alumina and oxygen and higher acidity of catalyst [173].

Encapsulating zeolite in silica gel caused a hypochromic shift. The silica gel barely absorbs electromagnetic radiation in the range of 250 nm to 900 nm [174]. However, the shoulders corresponded to two different types of Al−O species in the zeolite that are still evident after calcination at 550 °C. The 340 nm shoulder intensity is weaker compared to the initial zeolite Y, which suggests a partial dehydroxylation of −OH groups during calcination. The Kubelka-Munk function (Eq. 5.2) established the band gap of 2.5 eV (Figure 5.4, inclusion) for both zeolite Y and zeolite Y/silica gel.

$$F(R^{'}) = \frac{(1 - R^{'})^2}{2R^{'}} = \frac{k^{'}}{s} \tag{5.2}$$

where $R^{'}$ - reflectance, $k^{'}$, s - absorption and scattering coefficients, respectively.

The spectra of the catalyst after 30 min of reaction at different temperatures compared with fresh one and the carbon (reference) represented the increase of absorbance with temperature and concentration of coke on the catalyst surface (Figure 5.5). UV-vis spectrum at 300 °C has the same shape as pure carbon, which suggests that carbon covered all the catalyst

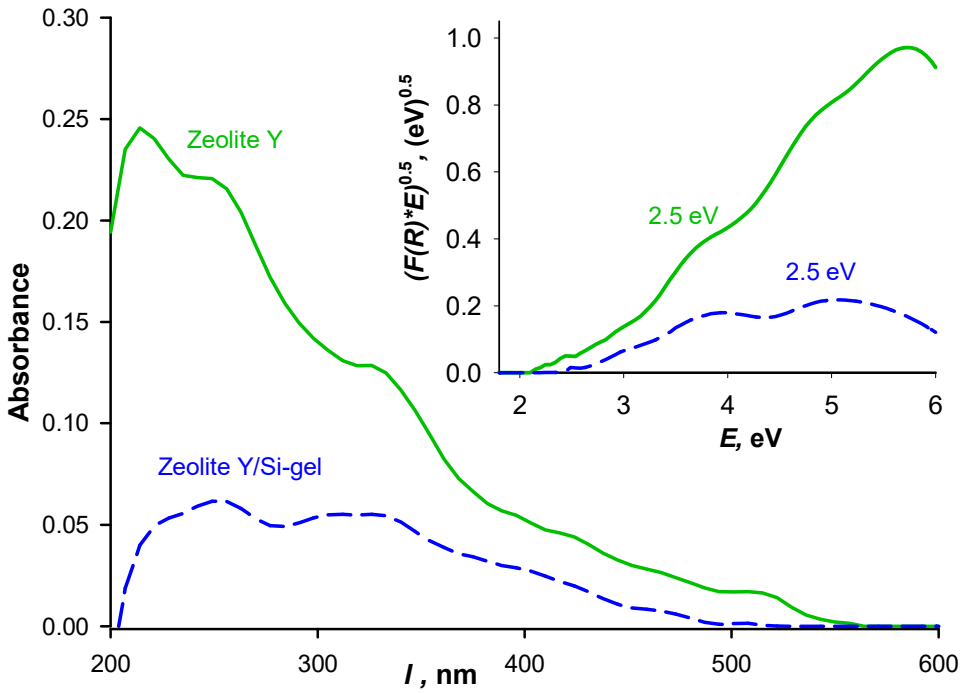

Figure 5.4 DR UV-visible spectra of absorbance vs wavelength and Kubelka-Munk function multiplied proton energy ($(F(R') \cdot E^{0.5})$ vs E) (inclusion) for zeolite Y particles size less than 1 µm (green, line) and zeolite Y encapsulated in silica gel (blue, dash)

surface [175]. Results of LECO analysis confirmed that carbon formed at 200 °C and was as much as 4 % by mass.

5.4.4 XPS

An X-ray photo-electron spectroscopy (XPS) registered binding energies of Si_2p, Al_2p, O_1s and C_1s (Table 5.1). We observed no chemical shift in Si_2p in the zeolite matrix compared to the one in silica gel. Thus, Si_2p could be plotted with a single doublet. The binding energy for Si_2p agrees with the results reported earlier for several zeolite structures [176, 177].

The O_1s envelope is asymmetric and we related it to two types of oxygen in our sample. We attribute the main peak (533.1 eV) to oxygen in zeolite and silica gel, and the peak with a higher binding energy (534.9 eV) to chemisorbed water. The binding energy of adsorbed water, 535.1 eV, reported previously is in good agreement with our results [178, 179]. The binding energy for Al_2p corresponds to bridging bonds characteristic of zeolite structures [180]. Based on XPS, the concentration of alumina was less than 0.1 % (atomic), which is the detection limit. The total concentrations of silica and oxygen in the sample were 31.2 % and 61.2 %, respectively, which corroborates the SEM-EDS measurements.

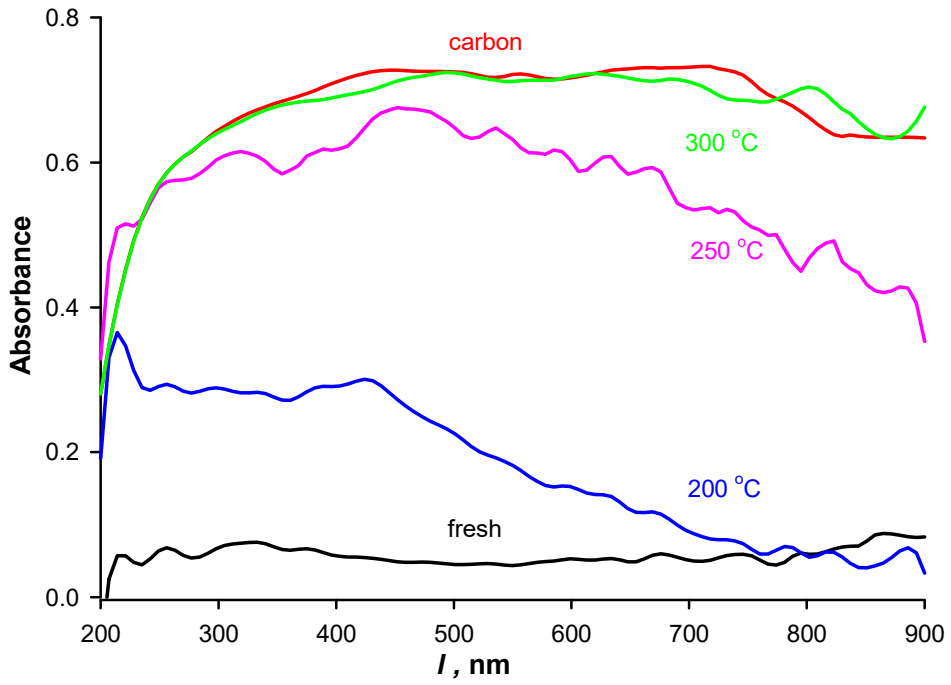

Figure 5.5 DR UV-Visible spectra of absorbance vs wavelength for fresh zeolite Y micro-sieve encapsulated in silica-gel (black) and after the reaction at different temperatures 200 °C (blue), 250 °C (pink), 300 °C (green). Spectrum of carbon black (red) represented as a reference.

Table 5.1 Identification and quantification of elements in zeolite Y/SiO_2 catalyst

Name	Structure	Binding energy, eV	FWHM†, eV	Atomic %
Al_2p	Al(OH)Si	74.3	3.02	0.1
$Si_2p_{3/2}$	SiO_2, Al(OH)Si	103.3	1.61	31.2
O_1sA	SiO_2	533.1	1.94	61.2
O_1sB	H_2O	534.9	1.94	4.8
C_1sA	C−C, C=C	284.1	1.49	1.9
C_1sB	C−O	285.5	1.49	0.6
C_1sC	C=O	287.2	1.49	0.1

† FWHM - Full Width at Half-Maximum

In addition, we identified carbon species on the catalyst surface which in total was around 2.6 % and comprised of a combination of C−C and C−O bonds. Since the surface is partly covered by carbon species, it becomes partly hydrophobic. Assuming a homogeneous distribution then only as much as 14 % of the surface is covered by carbon.

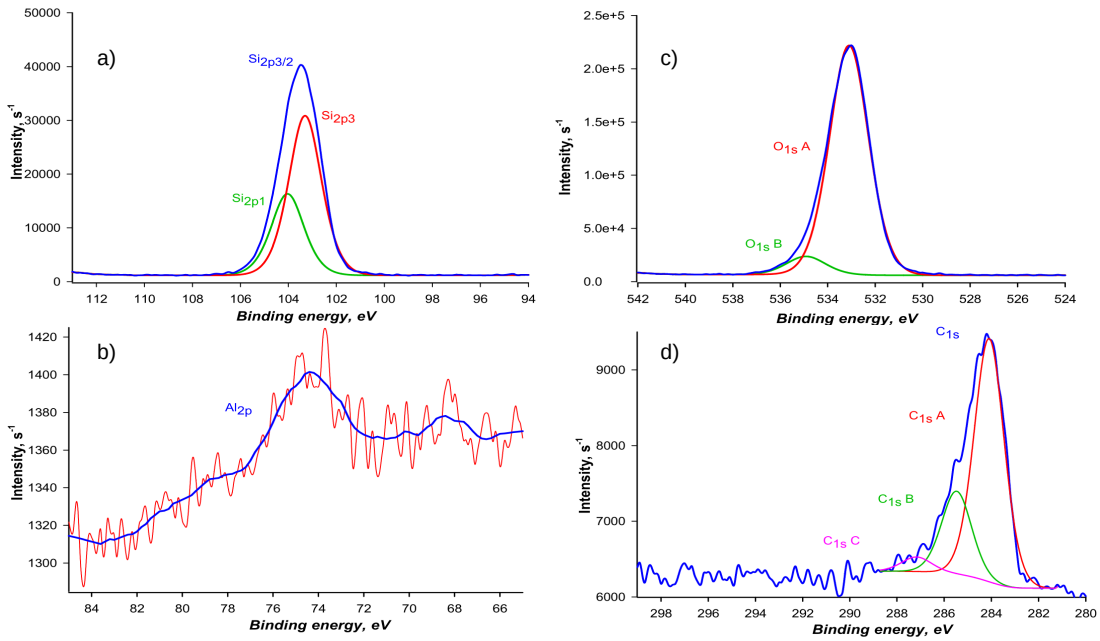

Figure 5.6 XPS spectrum of Si_2p (a), Al_2p (b), O_1s (c) and C_1s ions.

5.4.5 MAS-NMR

The magic angle spinning nuclear magnetic resonance (MAS-NMR) spectra, scanned for ^1H nuclei, analyzed protonic acid sites in catalyst sample [62, 181]. For zeolite Y, the typical chemical shifts belong to the range 0 ppm to 10 ppm [5]. The ^1H DQ MAS-NMR spectrum in our study revealed several chemical shifts at 1.58 ppm, 2.02 ppm, 2.86 ppm, 4.57 ppm and 6.22 ppm (Figure 5.7). We also observed a broad weak peak in the range 0 ppm to 10 ppm that accounted for about 10 % of overall peak. Previous studies suggest that it belongs to the anisotropic interactions in the sample explained by its heterogeneity [62]. We ascribe this effect to amorphous SiO_2 and crystalline zeolite Y structures in the catalyst. The chemical shift 0.9 ppm belongs to undisturbed AlOH species located in supercages of zeolite crystals the shift at 2.86 ppm belongs to extra-framework or in-cavities AlOH species. The shifts 1.58 ppm and 2.02 ppm refer to silanol groups at the external surface of the zeolite clusters and as framework defects [5, 182–184]. We also assign these peaks to the silanol groups of silica gel. The chemical shift 4.57 ppm is specific for protonated zeolite forms and belongs to SiO_3HAl bridging bonds in small cages confirming the presence of the Br∅nsted acid sites in the sample [5, 182]. We assigned the narrow peak at 6.22 ppm to different carbonyl groups adsorbed on the catalyst surface. The proton concentration in the ^1H MAS-NMR spectrum is proportional to the area under the peak and the acidity strength is proportional to the chemical shift [181]. This confirms the low concentration of alumina in the catalyst.

In addition, the n_{Si}/n_{Al} defines the electro-negativity of the framework and, therefore, the strength of BrØnsted acid sites.

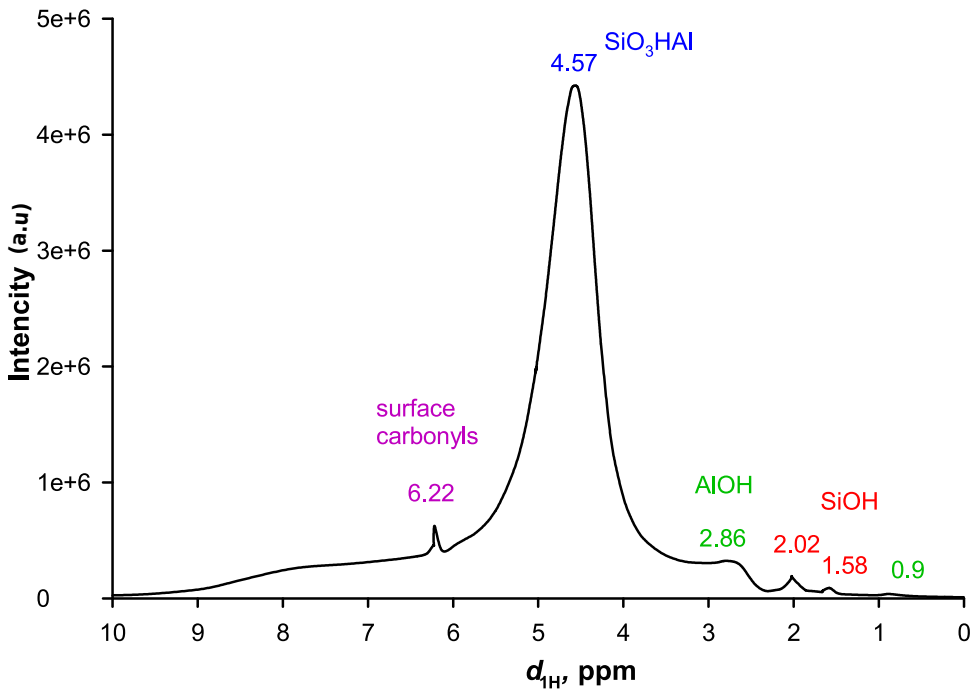

Figure 5.7 ^{1}H MAS-NMR spectrum of catalyst. The chemical shifts 0.9 ppm, 2.86 ppm belong to AlOH species located in supercages of zeolite and extra-framework, respectively; 1.58 ppm and 2.02 ppm represent AlOH external to the framework or defects located at silanol groups; 4.57 ppm belongs to SiO_3HAl species [5]. The chemical shift 6.22 ppm is due to adsorbed carbonyl groups on the catalyst surface.

5.4.6 TPD

The amount of acid centres on the catalyst surface was measured by adsorption/desorption of ammonia in a fixed bed quartz U-reactor. Ammonia saturated the sample at 50 °C for 60 min after preliminary drying of the sample in an inert to remove excess water and to clean the sample surface [185]. Then, the excess of adsorbed ammonia flashed at 60 °C in a flow of He. Temperature-programmed desorption of ammonia identified acid sites in the heating range 60 °C to 550 °C in a flow of He. The zeolite Y/SiO_2 had a low-temperature peak at 115 °C. The total amount of adsorbed ammonia per gram of catalyst was 66 µg (Figure 5.8). Ammonium interacts with all acid sites of the catalytic surface [62,186]. The content of silica gel in the catalyst sample is much higher than that of the zeolite that sits on the surface as separate clusters, which was confirmed by SEM (Figure 5.3). We assign the observed peak

to the ammonium adsorbed on acid centres of the silica gel. Previous studies show that silica gel by itself has weak Lewis acidity [186–188], which agrees with this assignation.

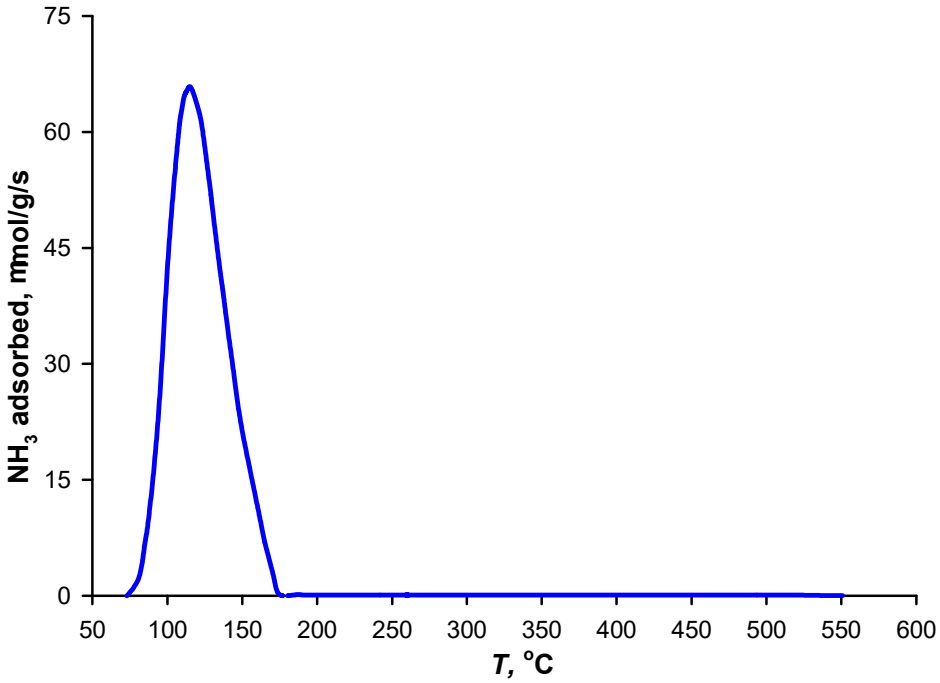

Figure 5.8 NH_3-TPD curve of zeolite Y encapsulated in silica gel

5.4.7 MMA hydrolysis to MAA

In the industrial plants, in the first step to produce MMA, PMMA depolymerizes to monomer. To accelerate the depolymerization rate, and thus minimize vessel sizes and investment, commercial plants operate above 350 °C [8]. Here, we explore the appropriate conditions for MMA hydrolysis that is in equilibrium with the esterification of MAA with methanol (Eq. 5.3). High temperatures increase the hydrolysis rate but MMA decomposition to CO_2 and coke [165] also increases. When MMA decomposes to CO_2 we would expect it to form a C_3 radical which may end up as propane, or propylene, or finally coke [165]. However, we did not specifically look for C_3 fragments in the MS signal since we operated below 350 °C.

$$H_2C{=}C(CH_3)COOCH_3 + H_2O \rightleftharpoons H_2C{=}C(CH_3)COOH + CH_3OH \tag{5.3}$$

Higher concentrations of water vapour improves the products yield as it shift the equilibrium conversion to the right (Eq. 5.3).

Here, we completed a set of experiments to scope out the expected conversion and yield from 160 °C to 300 °C with a high concentration of water vapour to simulate the expected conditions of a commercial operation (Table 5.2). Furthermore, we operated the reactor below 200 °C at partial MMA conversion to estimate the activation energy, E_{a} and reaction rate, k. This reduced set of experiments provides a framework for future work that will be dedicated to understanding the entire reaction mechanism.

In a first series of tests at 200, 250, and 300 °C the reactor operated with 0.14 g of catalyst and 20 mL min^{-1} of Ar as the carrier gas (Table 5.2, rows 1–3). The experimental system limited the range of feed flow rates as the pressure rise in the gas lines became too high to pump liquids to the evaporator at high rates. As a consequence, we only varied the feed rate of the Ar by a factor of 2. In this second series, with the higher Ar flow rate, we charged 0.17 g of catalyst to the reactor to maintain a constant contact time (Table 5.2, rows 4–6) [124]. The total molar flow rate of the reactants, $\dot{n}_{\mathrm{t}}$, in the two series was 3.1 mmol min^{-1} and 4.0 mmol min^{-1}. The Ar flow only represented from 26 % to 41 % of the total flow. The maximum contribution to the overall flow of MMA was less than 4 %, while the water vapour made up the remainder (55 % to 71 %). The superficial gas velocity, u, varied from 40 mm s^{-1} to 63 mm s^{-1}:

$$u = \frac{\dot{n}_{\mathrm{t}}}{\tilde{\rho} \times \frac{\pi}{4} D^2} \tag{5.4}$$

where, $\tilde{\rho}$ is the molar density (P/RT) and D is the reactor diameter. At these conditions, the contact time, τ, varied from 0.16 s to 0.22 s, depending on the temperature.

At the end of the test sequence, we conducted experiments at an Ar flow rate of 20 mL min^{-1} and 160 °C, 180 °C, 200 °C, and 250 °C to evaluate the reaction kinetic (Table 5.2, rows 7–9).

The expressions for the conversion and selectivity are:

$$X_{\mathrm{MMA}} = (1 - \frac{n_{\mathrm{MMA,out}}}{n_{\mathrm{MMA,in}}}) \cdot 100 \tag{5.5}$$

$$S_{\mathrm{i}} = \frac{n_i}{n_{\mathrm{MMAin}} - n_{\mathrm{MMAout}}} \cdot 100 \tag{5.6}$$

Yield of species i (Y_{i}: (MAA, MeOH, acetone, CO_2 and coke), is the product of conversion, X_{MMA}, and selectivity, S_{i}. Based on the stoichiometry of the reaction (Eq. 5.3), we would expect as much MeOH as MAA but MeOH is systematically higher, which suggests a series reaction in which MMA reacts to form MeOH, CO_2 and coke. The selectivity of CO_2 was never more than 0.2 %. The selectivity to coke reached 4 % above 180 °C while it was less than 0.6 % at 160 °C and 180 °C. The trend in acetone selectivity was the opposite: at 160 °C

to 180 °C it was around 9 % and 6 %, respectively, while it was rarely much above 2 % at the higher temperatures. The acetone formation mechanism may proceed from MMA hydrolysis to 2-hydroxy-isobutyric acid. The acid would then decompose to acetone and formic acid The formic acid would form CO_2 and H_2. Already a process has been patented to make MMA via 2-hydroxyisobutyrate [189]. The mass balance, δ, is generally less than 8 % but was higher during the kinetic runs, when we detected more acetone (experiments 6 and 7, Table 5.2).

$$\delta = 100 - \frac{(4n_{\mathrm{MAA}} + n_{\mathrm{MeOH}} + n_{\mathrm{coke}} + n_{\mathrm{CO2}} + 3n_{\mathrm{acetone}})/5}{n_{\mathrm{MMA,in}} - n_{\mathrm{MMA,out}}} \cdot 100 \tag{5.7}$$

Table 5.2 Experimental conditions and MAA and MeOH selectivity and yield

					Mole (%)		Y (%)		X (%)	δ (%)
No.	T °C	u mm s^{-1}	τ s	m_{cat} g	Ar	H_2O	MAA	MeOH	MMA	
1	203	41	0.2		28	69	77	88	94	0
2	249	44	0.18	0.14	28	68	77	88	95	-2
3	301	49	0.16		28	69	80	88	93	0
3	201	52	0.19		44	54	70	79	88	-4
4	251	56	0.18	0.17	44	54	76	87	93	0
5	302	63	0.16		43	54	73	83	98	-2
6	163	37	0.22		28	69	29	33	32	+14
7	181	39	0.21		28	69	52	57	71	-10
8	203	40	0.20	0.14	28	70	93	97	96	+6
9	248	44	0.18		28	70	87	98	97	+7

At 200 °C, MMA conversion exceeds 90 % (Figure 5.9) and MAA yield was about 80 %, which is much higher than for the fluidized bed tests [165]. We attribute the improved performance of the fixed bed to the high catalyst surface area compared to the fluidized bed catalyst: The zeolite Y fluidized catalyst was spray dried with Ludox and formed a SiO_2 shell that reduced the accessibility of the active phase.

Since the conversion was so high, we caution drawing definitive conclusions regarding the mechanism. Mechanisms depend on species adsorption and desorption rates and irreversible reactions like coke, all of which depend on temperature. For example, in the partial oxidation of methanol to formaldehyde, coke forms on FeMoO catalyst at 375 °C but at at 325 °C water adsorbs on the catalyst surface [190]. Conversion is also determined by the feed concentrations of the reacting gases, and the reaction rate drops as they approach equilibrium conditions.

Feeding high concentrations of water vapour favors the forward reaction, according to Le Chatelier's principle, and so we fed it in excess. Here we assumed an equilibrium constant, K_{eq}, based on the primary reaction network (ignoring, coke, CO_2, and acetone) (Eq. 5.3):

$$K_{\mathrm{eq}} = \frac{[\mathrm{MAA}][\mathrm{MeOH}]}{[\mathrm{MMA}][\mathrm{H_2O}]} \tag{5.8}$$

K_{eq} is calculated based on Gibbs energy, $\Delta_{\mathrm{r}}G^{\circ}$, and is a function of the Gibbs free energy of reaction at standard conditions, $\Delta_{\mathrm{r}}G^{\circ}$, and a reference temperature:

$$\Delta_{\mathrm{r}}G = \Delta_{\mathrm{r}}G^{\circ} + RT \ln K_{\mathrm{eq}} \tag{5.9}$$

At equilibrium, the $\Delta_{\mathrm{r}}G \Rightarrow 0$ and the equilibrium constant is:

$$\ln K_{\mathrm{eq}} = -\frac{\Delta_{\mathrm{r}}G^{\circ}}{RT} \tag{5.10}$$

We estimated the standard Gibbs energies ($\Delta_{\mathrm{r}}G^{\circ}$) for MMA hydrolysis based on the reaction stoichiometry (Eq. 5.3, Table 5.3). Since the reaction proceeds at atmospheric pressure, we assume ideal gas behavior [191]. Q' represents the shift of the reaction from the equilibrium state when compared to K_{eq} [191] and is determined by the ratio of the actual concentrations of the reaction products to the reagents:

$$Q' = \frac{[\mathrm{MAA}][\mathrm{MeOH}]}{[\mathrm{MMA}][\mathrm{H_2O}]} \tag{5.11}$$

Thus, when $Q' \ll K_{\mathrm{eq}}$ the reaction favors products, and when $Q' \gg K_{\mathrm{eq}}$ the reaction favors reagents. The system is at equilibrium when $Q' = K_{\mathrm{eq}}$. In our system $K_{\mathrm{eq}} \approx 1$ and $Q' \ll K_{\mathrm{eq}}$ at all the temperatures (Table 5.3).

Table 5.3 Thermodynamic parameters of MMA hydrolysis

T	ΔH°	ΔS°	ΔG°	K_{eq}	Q'
°C	kJ	kJ K^{-1}	kJ		
433			202	0.9455	0.0055
453			211	0.9456	0.0159
473	9	-0.445	220	0.9457	0.0264
523			242	0.9459	0.0249

Conversion was less than 40 % at 160 °C and plateaued at 95 % conversion above 200 °C,

which may indicate mass transfer limitations, equilibrium, or perhaps even strong adsorption (Figure 5.9). To estimate the reaction rate, we considered the three experiments at low temperature (experiments 6, 7, and 8) and fit the data to a first order model (Eq. 5.12) We normalized the reaction rate constant, k_0 to 200 °C (Eq. 5.13). Since the water vapor concentration is far in excess, we assume it is invariant with reactor length.

$$r = (k \cdot \tilde{\rho}_{\mathrm{H_2O}})\tilde{\rho}_{\mathrm{MMA}} \tag{5.12}$$

$$k = k_0 \cdot \exp\left[-\frac{E_\mathrm{a}}{R}\left(\frac{1}{T} - \frac{1}{T_0}\right)\right] \tag{5.13}$$

The best fit value of the activation energy, E_a, and first order rate constant, $k_{200\,^\circ\mathrm{C}}$, were $97\,000\,\mathrm{J\,mol^{-1}}$ and $730\,\mathrm{L\,mol^{-1}\,s^{-1}}$ (or $k \cdot \tilde{\rho}_{\mathrm{H_2O}} = 12\,\mathrm{s^{-1}}$), respectively. For gas solids systems, this is considered a fast reaction, and implies that mass transfer would be the limiting step in a fluidized bed [158]. We assumed internal diffusion resistance was negligible as the particle size was less than 100 µm [50]. We calculated the Weisz-Prater criterion as C_WP = Actual reaction rate/Diffusion rate base on the equation:

$$C_\mathrm{WP} = -r \cdot \rho \cdot \frac{R^2}{(De \cdot C_\mathrm{AS})} \tag{5.14}$$

In the range from 160 °C to 300 °C $C_\mathrm{WP} \ll 1$ which implies that internal diffusion resistance is negligible.

When the inert carrier gas flow rate was doubled (in experiments 1 and 4 the total molar flow rates, n_t, increased from $3.1\,\mathrm{mol\,min^{-1}}$ to $4\,\mathrm{mol\,min^{-1}}$) conversion decreased from 93 % to 88 %, which is consistent with a first order model ($\tau_1/\tau_2 \approx \ln(1 - X_1)/\ln(1 - X_2)$) which indicates that mass transfer resistance was negligible at 200 °C.

To test the hypothesis that the reaction is controlled by equilibrium, we derived a model assuming that both MMA and MAA are chemisorbed on vacant catalytic sites, X, to form MMA · X and MAA · X. We consider the adsorption, reaction, and desorption equilibrium steps:

$$\mathrm{MMA + X} \underset{k_{-1}}{\overset{k_1}{\rightleftharpoons}} \mathrm{MMA \cdot X} \tag{5.15}$$

$$\mathrm{MMA \cdot X + H_2O} \underset{k_{-2}}{\overset{k_2}{\rightleftharpoons}} \mathrm{MAA \cdot X + CH_3OH} \tag{5.16}$$

$$\mathrm{MAA \cdot X} \underset{k_{-3}}{\overset{k_3}{\rightleftharpoons}} \mathrm{MAA + X} \tag{5.17}$$

from which we write the following rate equations, where C_v is the concentration of vacant

sites:

$$\tilde{\rho}_{\mathrm{MMA}} C_{\mathrm{v}} = \frac{k_1}{k_{-1}} [\mathrm{MMA} \cdot \mathrm{X}] = K_1 [\mathrm{MMA} \cdot \mathrm{X}] \tag{5.18}$$

$$\tilde{\rho}_{\mathrm{H_2O}} [\mathrm{MMA} \cdot \mathrm{X}] = \frac{k_2}{k_{-2}} \tilde{\rho}_{\mathrm{CH_3OH}} [\mathrm{MAA} \cdot \mathrm{X}] = K_2 \tilde{\rho}_{\mathrm{CH_3OH}} [\mathrm{MAA} \cdot \mathrm{X}] \tag{5.19}$$

$$[\mathrm{MAA} \cdot \mathrm{X}] = \frac{k_3}{k_{-3}} \tilde{\rho}_{\mathrm{MAA}} C_{\mathrm{v}} = K_3 \tilde{\rho}_{\mathrm{MAA}} C_{\mathrm{v}} \tag{5.20}$$

In the case the reaction step is rate limiting, we express the reaction rate as a function of gas-phase concentration and concentration of the the chemisorbed sites ([MMA · X, [MAA · X])

$$r = k_2 [\mathrm{MMA} \cdot \mathrm{X}] \tilde{\rho}_{\mathrm{H_2O}} - k_{-2} [\mathrm{MMA} \cdot \mathrm{X}] \tilde{\rho}_{\mathrm{CH_3OH}} \tag{5.21}$$

$$= k_2 \left(\tilde{\rho}_{\mathrm{MMA}} \tilde{\rho}_{\mathrm{H_2O}} C_{\mathrm{v}} - \frac{\tilde{\rho}_{\mathrm{MAA}} \tilde{\rho}_{\mathrm{CH_3OH}} C_{\mathrm{v}}}{K_2} \right) \tag{5.22}$$

Since the adsorption and desorption steps are in equilibrium, the total number of sites, C_{T} equals the sum of the vacant sites and those adsorbed by MMA and MAA:

$$C_{\mathrm{T}} = C_{\mathrm{v}} + [\mathrm{MMA} \cdot \mathrm{X}] + [\mathrm{MAA} \cdot \mathrm{X}] \tag{5.23}$$

We rewrite this equation as a function of the total number of sites

$$C_{\mathrm{v}} = \frac{C_{\mathrm{T}}}{1 + K_1 \tilde{\rho}_{\mathrm{MMA}} + \tilde{\rho}_{\mathrm{MAA}} / K_3} \tag{5.24}$$

Finally, we re-express the rate equation with the number of vacant sites and then simplify the equation to

$$r = \frac{k_2'}{1 + K_1 \tilde{\rho}_{\mathrm{MMA}} + K_2 \tilde{\rho}_{\mathrm{MAA}}} \left(\tilde{\rho}_{\mathrm{MMA}} \tilde{\rho}_{\mathrm{H_2O}} - \frac{\tilde{\rho}_{\mathrm{MAA}} \tilde{\rho}_{\mathrm{CH_3OH}}}{K_{\mathrm{eq}}} \right) \tag{5.25}$$

where $K_{\mathrm{eq}} = K_1 K_2 K_3$, and $k_2' = k_2 C_{\mathrm{T}} K_1$. The design equation for a plug flow reactor is

$$Q \tilde{\rho}_{\mathrm{MMA,0}} \frac{\mathrm{d}X}{\mathrm{d}V} = k_2' \left(\tilde{\rho}_{\mathrm{MMA}} \tilde{\rho}_{\mathrm{H_2O}} - \frac{\tilde{\rho}_{\mathrm{MAA}} \tilde{\rho}_{\mathrm{CH_3OH}}}{K_{\mathrm{eq}}} \right) \tag{5.26}$$

We simplify this expression assuming MMA and MAA are weakly chemisorbed and $\tilde{\rho}_{\mathrm{H_2O,\,0}} >> \tilde{\rho}_{\mathrm{MMA}} X$

$$Q \frac{\mathrm{d}X}{\mathrm{d}V} = k_2' \tilde{\rho}_{\mathrm{H_2O,\,0}} \left(1 - X - \frac{X^2}{K_{\mathrm{eq}} \theta} \right) \tag{5.27}$$

where $\tilde{\rho}_{\mathrm{MMA,0}}$ and $\tilde{\rho}_{\mathrm{H_2O,0}}$ are the inlet concentrations, and $\theta = \tilde{\rho}_{\mathrm{MMA,0}} / \tilde{\rho}_{\mathrm{H2O,0}}$.

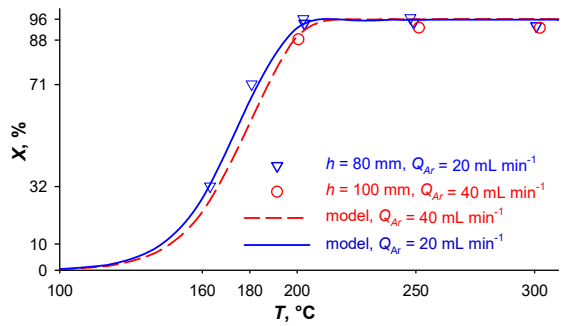

Figure 5.9 MMA conversion as a function of temperature. Experimental data are illustrated with symbols while the model fit at the two Ar feed rates are depicted with lines.

The kinetic model is a first attempt to characterize the data and identify the order of magnitude of several physico-chemical properties like the activation energy, rate constant, and equilibrium constant. Clearly more work is required to determine the confidence intervals but the standard deviation of the six experiments that reached equilibrium is $\pm 1\,\%$. The model fits the experimental data very well with at most an absolute error of $\pm 2\,\%$ for conversion and a standard deviation of $\pm 1\,\%$. Furthermore, it captures the shape from low conversion until it reaches what we presume is the equilibrium conversion (Figure 5.9).

The best fit activation energy is $E_\mathrm{a} = 106\,\mathrm{kJ\,mol^{-1}}$, which is $9\,\%$ higher than for the first order model that excludes the reverse reaction (Eq. 5.12), while the rate constant is $18\,\%$ higher ($k = 860\,\mathrm{L\,mol^{-1}\,s^{-1}}$ or $k \cdot \tilde{\rho}_{\mathrm{H_2O}} = 14\,\mathrm{s^{-1}}$).

Several studies have reported data on the liquid phase reaction as the esterification of carboxylic acids to esters is more common than gas-phase esterification (Table 5.4). Grzesik et al. (2007) [55] achieved $60\,\%$ conversion of methacrylic acid at $75\,^\circ\mathrm{C}$ after $300\,\mathrm{min}$ in a batch reactor. Sulphuric acid was as efficient reaching the same conversion at $70\,^\circ\mathrm{C}$ after $300\,\mathrm{min}$ while the heterogeneous catalyst Dowex 50WX only reached $30\,\%$ conversion in the esterification of acrylic acid with ethanol [56]. Methacrylic acid esterified in the liquid phase over NKC-9 from $50\,^\circ\mathrm{C}$ to $95\,^\circ\mathrm{C}$ [50] with MeOH in $20\,\%$ excess with respect to MAA. After $300\,\mathrm{min}$ the conversion of MAA reached $80\,\%$ at $95\,^\circ\mathrm{C}$ at an $80\,\%$ MMA yield.

5.5 Conclusions

Zeolite Y hydrolyses MMA to MAA in the gas phase from $160\,^\circ\mathrm{C}$ to $< 300\,^\circ\mathrm{C}$ achieving a yield of 80 percent. The reaction rate is extremely fast ($k\tilde{\rho}_{\mathrm{H_2O}} = 14\,\mathrm{s^{-1}}$) and the activation energy is high at just over $100\,\mathrm{kJ\,mol^{-1}}$. Surface reaction between chemisorbed MMA and water limit

Table 5.4 Activation energies of liquid phase esterification of various acids

	E_a kJ mol^{-1}	Catalyst	Reaction
1	72	$H_3PW_{12}O_{40}$ [55]	MAA esterification with ethanol to ethyl methacrylate
	72	$H_3PMo_{12}O_{40}$	
2	35	H_2SO_4 [56]	Esterification of acrylic acid with ethanol in liquid phase
	31	Dowex 50WX	
	36	Amberlyst	
3	44	NKC-9 [50]	MAA esterification with MeOH
4	17	H_2SO_4 [192]	MAA esterification with n-propanol
5	64	$H_3PW_{12}O_{40}$ [54]	MAA esterification with MeOH
	69	$H_3PMo_{12}O_{40}$	

the reaction rate and the equilibrium conversion is about 95 %. Coking was more prevalent above 200 °C, while at lower temperatures (and partial MMA conversion), acetone selectivity was as high as 10 %. This reaction is particularly interesting as an economic alternative to recover a specialty chemical from PMMA. MAA has a much higher boiling point and thus easier to recover in distillation trains (but it tends to polymerize when distilled). This work demonstrates that MAA is reasonably stable even at 300 °C, which will facilitate a tandem reaction system starting with PMMA depolymerization to MMA and its subsequent hydrolysis to MAA. The preliminary kinetic data suggest that the water hydrolyzes MMA to MAA and methanol and reaches an equilibrium conversion of at about 95 %. The reaction rate is extremely high above 200 °C but more experimental data is required to quantify any adsorption and desorption contributions and to confirm the high activation energy.

CHAPTER 6 ARTICLE 3 : TANDEM FLUIDIZED BED/MILLI-SECOND FIXED BED REACTOR PRODUCES METHACRYLIC ACID FROM POLY(METHYL METHACRYLATE)

Olga V. Chub, Jean-Luc Dubois, Gregory S. Patience. Applied Catalysis A: General, Published: 25 October 2022

6.1 Abstract

Producing monomers from end-of-life plastics is a sustainable alternative to petroleum as a feedstock. Fluidized beds are more effective than molten metal baths and agitated vessels to deconstruct poly(methyl methacrylate) (PMMA) to MMA because of their higher heat transfer rates. Here, we developed a tandem reactor to produce methacrylic acid (MAA). PMMA depolymerized to MMA in a fluidized bed of sand above 300 °C in the first step and then MMA hydrolyzed to MAA over zeolite Y suspended in glass wool at a contact time of 200 ms. MAA yield approached 48 % while MMA conversion was about 50 %. At high temperatures, cyclic hydrocarbons produced during the reaction condensed in the fixed bed hydrolysis section and reactor lines. Reacting PMMA to MAA in a tandem reactor is of industrial interest for end-of-life PMMA containing fillers and additives because of the higher MAA yield compared to reprocessing MAA in a single vessel.

6.2 Introduction

PMMA is a thermoplastic that was first synthesized in 1928 [193]. Its attractive physicochemical properties like high transparency, stiffness, and thermal stability, make it an ideal choice for applications in electronics, automotives, construction, and medicine [194–199]. The idea to depolymerize poly(methyl methacrylate) (PMMA) was conceieved the 1940s as a possibility to reduce the cost of manufacturing chemicals by replacing crude oil with plastic waste [64, 200–202].

Currently, more than 3 Mt of PMMA is produced annually worldwide, of which 10 % is synthesized in Europe, but only 3 % of this is recycled [4, 8]. PMMA is one of the few polymers that degrades by more than 90 % to its monomer [11, 20, 22, 66, 71, 203].

PMMA, is a thermoplastic polymer which is also known with its brand names of Plexiglas, Altuglas or Perspex has become a commodity polymer. Compared to other polymers it is still produced in small quantities worldwide, but it can be recycled through depolymerization back

to its monomer methyl methacrylate. Industry pyrolyzes PMMA to MMA in molten metal baths, extruders, various types of agitators, and fluidized and spouted bed reactors [8,15,16]. Among these reactor types, fluidized beds are more effective because of their short contact times, higher heat transfer rates, and isothermal temperature profile [47,70,126]. Although depolymerizing PMMA scraps and cuttings to methyl methacrylate (MMA) is practiced commercially, full recycle of PMMA plastics has been hindered by compounds produced during the thermolysis treatment that have similar boiling points to MMA and thus require energy intensive separation steps. Namely, known contaminants of regenerated MMA include methyl and ethyl acrylates and methyl isobutyrate. The acrylates are used as co-monomers in PMMA formulations, while methyl isobutyrate is created by the PMMA depolymerization process. Methyl acrylate has a lower boiling point than MMA, and can be separated by distillation. However, methyl isobutyrate and ethyl acrylate have close boiling points to MMA and are therefore difficult, if not impossible, to separate by distillation. At the same time, the carboxylic acids like acrylic acid, methacrylic acid and isobutyric acid have sufficiently different melting points to consider a separation by crystallization. Therefore, recycling of PMMA should be considered through combined depolymerization and hydrolysis. In this context, hydrolyzing MMA to methacrylic acid (MAA) will improve the process economics (as the MAA's boiling point is 61 °C higher), but to ensure profitability requires a process that minimizes side reactions while maximizing heat and mass transfer rates. In our previous study in a single fluidized bed reactor [165], we shifted the depolymerization of virgin PMMA towards formation of methacrylic acid (rather than methyl methacrylate as a final PMMA depolymerization product) through subsequent catalytic hydrolysis of methyl methacrylate. The process demonstrated high selectivity towards the acid at it's yield above 30 %. The catalyst acidity was a key factor to maximize the yield of MAA. In the fluidized bed, PMMA depolymerizes to monomer entirely at 350 °C [165]. However, compared to depolymerization, the hydrolysis of MMA to MAA, on the contrary, proceeds with greater efficiency at lower temperatures. In our next study, we hydrolyzed MMA to MAA in a fixed bed of an acidic zeolite Y. The yield of methacrylic acid reached 48 % below 250 °C and at excess of water which was about 100 °C lower than in the fluidized bed. We have found that the product yield is determined by the thermodynamics of the process and that the hydrolysis process is sensitive to the amount of water introduced.

In this context, tandem reactors allow separating the two reactions and customizing the reaction conditions of each of them. A fluidized bed is an ideal reactor type for the first step as the heat transfer rates are an order of magnitude greater than in fixed beds and the mechanical stresses introduced by the jets and the motion of the catalyst particles minimizes polymer-particle and polymer-polymer agglomeration. Even so, the scale-up of this reactor

type requires a close control of the polymer feed rates to minimize agglomeration, which results in a slumped bed and then gas bypassing and subsequent low yields. The preliminary studies demonstrated, that compared to catalytic pyrolysis of polyethylene, polypropylene, polystyrene, and polyethylene terephthalate in a single vessel, a tandem reactor that first pyrolyzes the solids then reacts the gas over HZSM-5 catalyst reduces coke and increases hydrocarbon yield [80]. Another example of a tandem reactor process is the hydrothermal treatment of high density polyethylene over a conical spouted bed followed by a fixed bed of Ni catalyst to produce syngas [204]. Despite of the advantages of realization of different processes in the tandem reaction systems compared to single reactors, there is no data in the open literature on reprocessing of PMMA to MAA in such reaction systems. Here, for the first time, we produced methacrylic acid from poly(methyl methacrylate) in a tandem reactor where polymer pyrolyzed in the fluidized bed to monomer in a lower reactor portion with its subsequent hydrolysis in a fixed bed of HY-catalyst suspended in glass wool, located in an upper reactor portion.

6.3 Experimental

6.3.1 Materials

Zeolite Y (CBV 780, hydrogen form, $0.0003\,\mathrm{g\,g^{-1}}$ Na_2O) in form of micro-sieves was from Zeolyst ($780\,\mathrm{m^2\,g^{-1}}$, Si/Al = 80/1). Silica gel was from Sigma Aldrich. The PMMA was supplied by Arkema (M_w= 100000) and milled in liquid nitrogen to $d_p \leq 100\,\mu\mathrm{m}$.

6.3.2 Catalyst Characterization

Zeolite morphology, elemental distribution, and mass ratios were identified by scanning electron microscope (SEM) (Jeol JSM-7600TFE) equipped with an EDS detector (Oxford Instruments X-Max 80). A gas chromatograph-mass spectrometer Agilent (GC-MS 7890A (DB-Wax column, 0.25 mm ID, 30 m long, 0.25 µm film diameter) connected to a 5975C VL MSD (Agilent) analyzed liquid reaction products. The induction combustion method evaluated the carbon in the catalyst (CS744 from LECO), equipped with an IR detector and iron and tungsten accelerators operating at 1300 °C to 1400 °C. An HPR-20 TMS mass spectrometer (Hidden Analytical) monitored CO and CO_2 signals at a frequency of 3 Hz. A laser particle size analyzer (LA-950, Horiba) with a dynamic range of 0.01 µm to 3000 µm recorded the particle size distribution (PSD) of sand and silica gel in water with a 0.6 % accuracy [205]. We report the D[4;3] volume moment mean.

6.3.3 Laboratory set-up

Before each experiment, PMMA and a fluidizing agent (sand or silica gel) (Figure 6.1, (4)) were loaded onto the glass wool distributor (3) in a lower portion of a 13 mmID quartz reactor (2). A fixed bed of zeolite Y (5) micro-sieve was located in the upper part of the quartz reactor. We minimized the pressure drop across the catalyst bed of the tiny ($d_p \leq$ 5 µm) particles by distributing the catalyst in the glass wool layers. The quartz reactor was placed in an electric furnace (1) equipped with three independently controllable zones. Two thermocouples measured temperature in both fluidized and fixed beds to control the conditions.

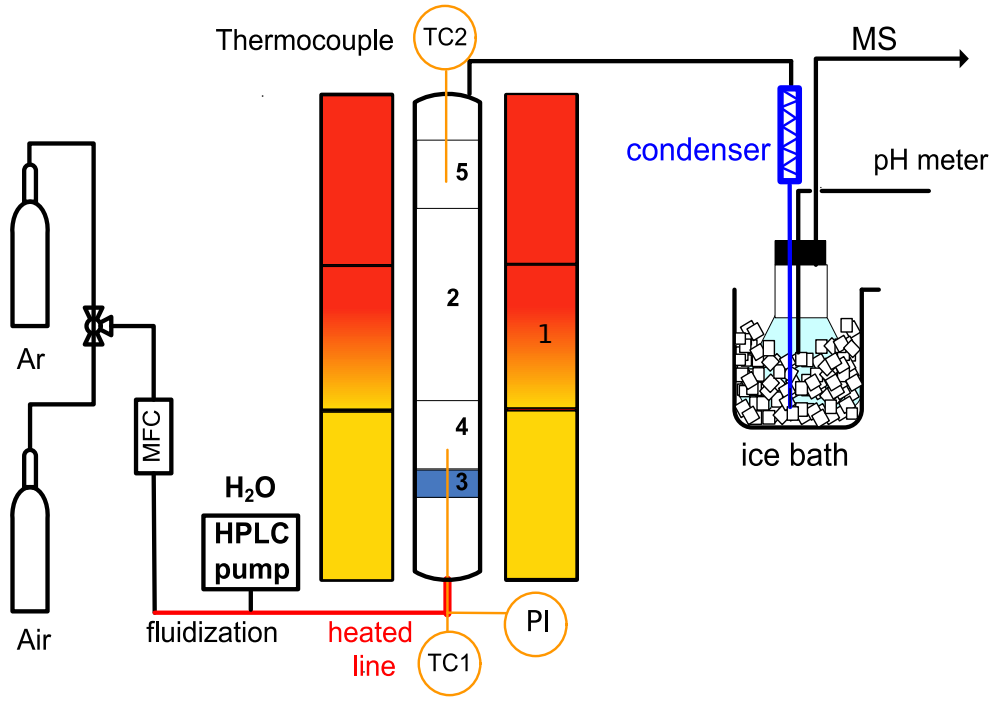

Figure 6.1 The tandem reactor system with a 13 mmID quartz reactor (2) located in an electrical furnace (1). The PMMA degraded in the lower fluidized bed (4) of inert (sand or silica gel) supported on the glass-wool distributor (3), and the MMA hydrolyzed in the upper fixed bed (5) of zeolite Y (hydrogen form).

At the beginning of an experiment, we heated the fluidized bed to 150 °C at a ramp of 5 °C min^{-1} to minimize undesirable temperature fluctuations. When the reactor reached 150 °C, the HPLC pump started to inject water through a line heated to 130 °C. The water vapor and pre-heated Ar (carrier gas) entered below the bed of sand (or silica gel) to fluidize it. We then increased the heating rate to reach the set-point temperature to depolymerize the PMMA that had been loaded with the fluidizing solids. The PMMA degradation products,

water vapor and Ar passed through the silica wool with zeolite Y. Volatile components in the effluent gas condensed in vessel filled with ethanol that was sitting in an ice bath. We sampled reaction products from 265 °C to 370 °C, at atmospheric pressure. The mass-spectrometer registered the gas-phase reaction products CO (28) and CO_2 (44).

6.4 Results and discussion

6.4.1 Powder characteristics

The catalyst had a high surface area (780 $m^2\,g^{-1}$) and a layered structure formed by sodalites-based fragments (≤1 µm or less, Fig. 6.2). The Si and O were the major elements in the zeolite structure while Al is localized in sodalite cages (Figure 6.2, EDS mapping) [206].

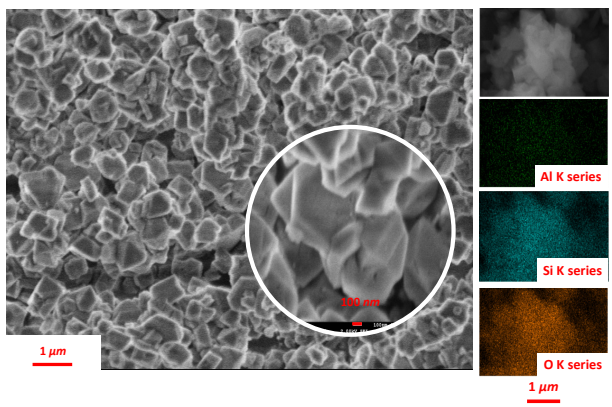

Figure 6.2 The scanning electron microscopy of zeolite Y catalyst (10^4 and $5{\cdot}10^4$ magnification) and distribution of silica, alumina and oxygen in the sample.

All the materials are of irregularly shaped (Figure 6.3), the minimum fluidization velocity of the silica gel is lower compared to sand (Table 6.1). The particle size of the PMMA was smaller than that of sand (d_{50} = 65 µm), and the density of the PMMA was almost half that of sand (1.18 $g\,m^{-3}$ vs 2.65 $g\,m^{-3}$).

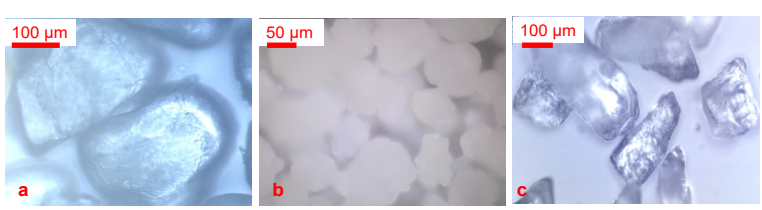

Figure 6.3 Optical images of sand (a), silica gel (b) and grinded PMMA (c).

Table 6.1 Physical properties of silica gel and sand.

Property	SiO_2	Sand
u_{mf}, $\mathrm{mm\,s^{-1}}$	3.3	5.1
ρ_{b}, $\mathrm{g\,cm^{-3}}$	0.77	1.35
ρ_{m}, $\mathrm{g\,cm^{-3}}$		2.65
d_{10}, µm	71	90
d_{50}, µm	100	117
d_{90}, µm	135	168
S_{sp}, $\mathrm{m^2\,g^{-1}}$	351	-
V_{pore}, $\mathrm{cm^3\,g^{-1}}$	1.4	-
d_{pore}, nm	9	-

6.4.2 Degradation of PMMA in a tandem reactor

We first poured sand into the reactor, and then, PMMA on the top of it. The mass of the sand in all the experiments was 8.5 g, the PMMA mass was 1 g (1 mL). The volume of zeolite Y in experiments varied from 2 mL to 4 mL.

Previous studies demonstrated polydispersed particles fluidize easily when the gas velocity, U_{g}, is greater than the minimum fluidization velocity, U_{mf}, of the particles with the highest $U_{\mathrm{mf,max}}$. When U_{g} drops below $U_{\mathrm{mf,max}}$, these particles will segregate and accumulate at the top surface when their particle density, $\rho_{\mathrm{p},i}$ is lower than the bed density, ρ_{bed} or drop to the bottom when $\rho_{\mathrm{p},i} > \rho_{\mathrm{bed}}$ [207, 208]. The axial particles segregation is lower for narrow particle sizes distributions [209, 210]. All the PMMA particles were completely mixed with the sand after 30 s to 40 s at a volumetric gas flow rate of 40 mL min^{-1} and bed a 40 mm sand bed height. At these conditions, the fluidized bed operated in the bubbling regime and the polymer particles were evenly distributed over almost the entire height of the sand, except underneath 6 mm to 10 mm, where larger sand particles segregated (Figure 6.4).

Previously, we demonstrated that the maximum methacrylic acid (MAA) yield was at 280 °C in fluidized bed of spray-dried acidic zeolite Y [165], while some of PMMA did not degrade. At the same time, PMMA totally degraded at 350 °C. In the current experiments, we aimed to reach higher temperature in the fluidized bed and lower temperature in the fixed bed to thermolyze all PMMA and maximize the yield of MAA by hydrolysis.

In the first set of experiments (Table 6.2, run 1), after the fluidized bed reached 265 °C, we slightly increased it to 280 °C and maintained it in the range of 265 °C to 286 °C for 41 min. The polymer started melting when the fluidized bed exceeded 120 °C. From 130 °C to 270 °C

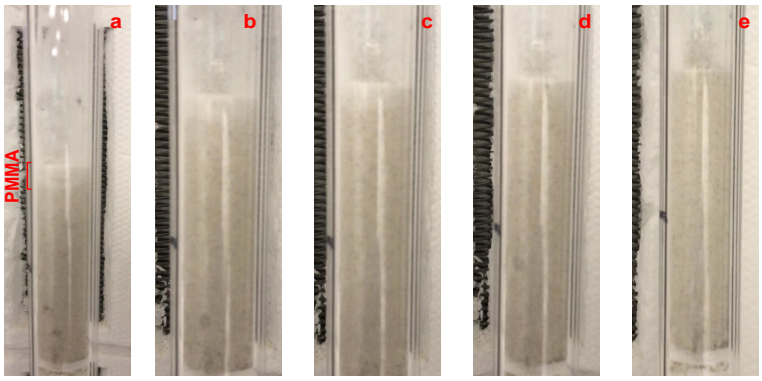

Figure 6.4 Time evolution of PMMA powder (d_p of 65 µm) back-mixing with sand at argon flow rate 40 mL min^{-1}; a - 0 s, b - 5 s, c - 10 s, d - 20 s, e - 30 s.

the sand bed defluidized with PMMA (Figure 6.5, a).

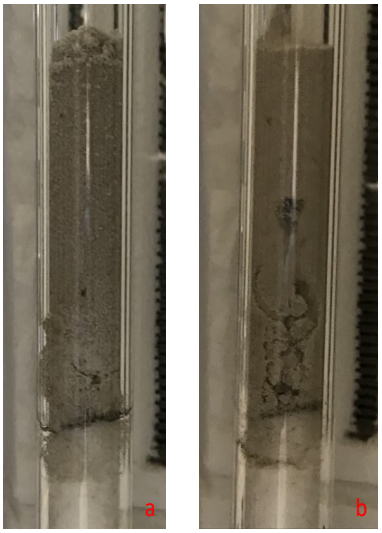

Figure 6.5 Defluidized bed of sand and PMMA in a temperature range from 130 °C to 270 °C (a) and agglomerates of sand and PMMA on the bottom at recommencement of fluidization above 280 °C.

The previous studies considered the defluidization as a result of particle adhesion between molten PMMA and the fluidizing medium or between the PMMA particles [211, 212]. The mechanism of particle agglomeration correlates with material properties, reaction conditions and reactor geometry [115, 134]. We assume that molten PMMA covered the surface of sand particles that agglomerated the particles. However, the defluidization of the bed did not collapse the bed entirely and gas continued to pass through the channels inside the bed of sand and molten polymer.

At temperatures close to the beginning of polymer degradation (270 °C), the sand near the bottom began to fluidize with limited movement of particles. When a significant part of the polymer reacted, the sand bed gradually returned to the fluidized state. However, from 265 °C to 286 °C, some small agglomerated particles of sand and polymer localized in the lower bed portion (Figure 6.5, b). Earlier studies supported our observations that local defluidization phenomena does not cause the reactor shutdown but channeling and, in the end, radial temperature and concentration gradients [116, 213].

In the same experiment, the temperature in the fixed bed reached 168 °C at the beginning, and the bed continued heating with the time up to 248 °C. The average temperature in the fixed bed was 242 °C (Table 6.2) while in the fluidized bed it varied by ±11 °C during the experiment.

Table 6.2 Average temperatures (°C) in the fluidized and fixed beds.

No.	Fluidized bed (sand)	Fixed bed (zeolite Y)
1	274	242
2	278	245
3†	327	305
4	370	350

† silica gel served as a fluidizing agent

The methacrylic acid yield was 46 % with 94 % selectivity and the carbon balance closed to within 3.7 % (Table 6.3). This is higher than the MAA yield over zeolite Y in a single fluidized bed of 33 % at similar temperature conditions [165]. The yield of methanol was 48 % with 97 % selectivity, which is expected since for every mole of MMA a mole of MeOH is produced. We estimated conversion of MMA in the fixed bed based on the weight of introduced PMMA recalculated to the moles of equivalent MMA as following:

$$X_{\mathrm{MMA}} = (1 - \frac{n_{\mathrm{MMAout}}}{n_{\mathrm{PMMAin}} - n_{\mathrm{carb}}/5}) \cdot 100 \tag{6.1}$$

here, n_{MMAout} is moles of MMA condensed after the reaction, n_{carb}—total moles of carbon detected by the LECO from solids withdrawn from the fluidized bed.

At these conditions, the total conversion of PMMA to MMA (accounting unreacted MMA in the fixed bed) was about 48 %. The selectivities of reaction products were calculated with respect to total PMMA converted to MMA as followed:

Table 6.3 Experimental conditions and MAA and CH_3OH yields.

No.				Inlet		Conv	Yield					Δ C
	m_{cat}	u	τ,	Ar	H_2O	X_{MMA}	MAA	MeOH	CO	CO_2	Coke	
	g	mm s^{-1}	ms	mole%		%			%			%
1	0.5	70	100	7	91	48	46	48	1	≤0.5	1	+3.7
2	1.0	73	300	13	85	53	48	50	2	1	≤0.5	+4.4
3	0.5	59	200	32	64	38	33	28	5	1	2	+4.7
4	0.5	24	400	91	0	13	0.3	6	9	3	≤0.5	+14.8

$$S_{\mathrm{i}} = \frac{n_{\mathrm{i}} \cdot N_{\mathrm{carb}}}{5 \cdot (n_{\mathrm{PMMAin}} - n_{\mathrm{MMAout}})} \tag{6.2}$$

Where N_{carb} - number of carbon atoms in molecule, n_{PMMAin}, n_{MMAout} - moles of PMMA entered the fluidized bed and unreacted MMA after the fixed bed.

We estimated the products yield as

$$Y_{\mathrm{i}} = X \cdot S \tag{6.3}$$

The total amount of the coke at the end of experiment reached 7 %, the CO_2 and CO generated was below 5 %. More coke formed in the fixed bed than the fluidized bed and reached 0.006 g g^{-1} (coke:solids) in agglomerated particles and 0.002 g g^{-1} in the rest of the solids. The coke distribution in the zeolite Y differed slightly. The LECO analysis detected 0.03 g g^{-1} on the catalyst.

The Ar flow rate and mass of zeolite was double that of the first run (Table 6.2, run 2). As a result, pressure in the Ar line increased and the water feed rate dropped, so the contact time was three times higher. We heated the fluidized bed to 182 °C and then, maintained it at about 300 °C, while in the fixed bed the temperature varied between 167 °C and 263 °C over 36 min. Like run 1, lower bed defluidized at the temperature where the polymer melted. The bed began to fluidize with increasing temperature as the polymer degraded. The yield of MAA and methanol were similar to the run 1 – 48 % and 50 % respectively, and conversion increased by 5 %. The coke distribution between fluidized and fixed beds was also the same as in run 1.

We replaced the sand with silica gel in run 3 (Table 6.2, run 3) and increased the Ar flow rate to 150 mL min^{-1}. The temperature in the fluidized bed varied from 240 °C to 380 °C.

The fixed bed started at 169 °C and reached 370 °C after 30 min. The average temperatures were higher than in the first two runs. In our previous study [165], MMA yield was 33 % over spray-dried zeolite Y (hydrogen form) at 300 °C and a flow rate 70 mL min^{-1}. The yields of MAA and methanol 33 %in this study were similar to our previous results [165] (MAA yield) but dropped compared to the results of the run 1 and 2.

In the run 3, PMMA totally thermolyzed to MMA in the fluidized bed, however, only 38 % of MMA hydrolyzed to MAA. We observed more than 10 times higher coking over silica gel compared to sand (1.5 %) because of the adsorption of melted polymer and MMA in its pores. The high temperatures in the fluidized bed invariably led to undesirable and uneven heating of the fixed catalyst bed. As a result, higher temperatures and less water compared to the two previous runs resulted in more by-products formation and their condensation on the top of the fixed catalyst bed, reactor walls, and in the lines. We washed the reactor walls with ethanol which turned yellow; the qualitative GC-MS analysis detected cyclic organic compounds (Table 6.4).

The last experiment ran anhydrously (Table 6.2, run 4), at 370 °C with sand in the fluidized bed and 170 mL min^{-1} Ar and a contact time of 0.4 s in the fixed bed. PMMA thermally degraded without defluidizing as the heating rate was much higher. We observed only a trace of MAA (less than 0.3 %) and a methanol yield of 6 %, presumably due to MMA decarboxylation [165, 203]. MMA was the main reaction product with some byproducts similar to the run 3, which contributed to a poorer mass balance of 15 % (Table 6.4).

Table 6.4 The products composition after thermolysis of PMMA (run 3, 4) at 370 °C (boiling points from NIST database).

Name	Chemical formula	Boiling point (°C)
2-Propenoic acid, 2-methyl-, 3-hydroxypropyl ester	$C_7H_{12}O_3$	218±23
Benzene, 1,2,3-trimethyl-	C_9H_{12}	176
Benzene, 1-methyl-4-[(2-propenyloxy)methyl]-	$C_{11}H_{14}O$	-
1,3,8-p-Menthatriene	$C_{10}H_{14}$	56
Benzene, 1,2,4,5-tetramethyl-	$C_{10}H_{14}$	197
Phenol, 2,3,5-trimethyl-	$C_9H_{12}O$	234
(+)-(5S,10S)-3,4,4aR,7,8,8aR-Hexahydro-5,8a-dimethylnaphthalen-2(1H)-one	$C_{12}H_{18}O$	-
2,5-Furandione, 3-(1,1-dimethylethyl)-	$C_8H_{10}O_3$	440

Coke formed in the lower and upper portions of the fixed bed (0.04 g g^{-1} and 0.02 g g^{-1}, respectively) (Figure 6.6). Under the anhydrous conditions, most of the PMMA degraded as

the LECO only detected 0.001 g g^{-1} of coke on the sand. However, more coke was detected on the zeolite Y.

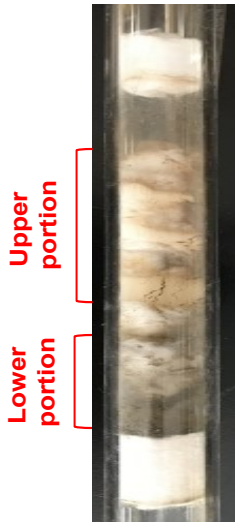

Figure 6.6 The distribution of coke in the fixed bed of zeolite Y located in the upper part of the tandem reactor.

The yield of MAA from MMA in a fixed bed reactor of zeolite Y reached 80 % at a temperature below 300 °C and a contact time of 200 ms [214]. In the present study, an increase in the contact time by a factor of three at similar temperatures from run 1 to run 2 had little effect on the conversion of MMA. Increasing the temperature to 300 °C in run 3 reduced the conversion by 1.3 times compared to run 1, while the contact time in run 3 was two times higher than in run 1. The MAA yield in this study was 1.6 times lower than compared to the previous study at comparable conditions [214]. We attribute this to the non-stationary operating conditions of the reactor. In each experiment, we heated the fluidized bed to a certain temperature but it oscillated by ± 10 °C during the run. At the same time, in the fixed bed at the beginning of the experiment the temperature was about 160 °C. Our previous study demonstrated that only 30 % of MMA hydrolyzed at this temperature. While the fixed bed was heating, less MMA reacted and so accumulated in the quench.

6.5 Conclusions

For decades, fluidized bed reactors demonstrated their utility over molten metal baths to degrade PMMA because of their superior heat and mass transfer rates. However, industry has yet to adopt this technology widely to recycle end-of-life plastics in part due to the substandard purity that may color the final product and the cost to separate the byproducts

from methyl methacrylate. Producing methacrylic acid rather than MMA is a compelling alternative as distillation costs will be lower since the boiling point of methacrylic acid is 161 °C versus 100 °C for MMA.

The laboratory tandem reactor first degraded PMMA to MAA in a fluidized bed and then water vapour hydrolyzed the MMA to MAA over an acidic zeolite Y catalyst in a fixed bed. The fluidized bed operated at 270 °C to 370 °C) while the fixed bed operated below 300 °C. The gas velocity was sufficiently high to blend the polymer in the sand particles but the bed slumped as the bed temperature reached the polymer melting point. Fortunately, the reactor continued to operate and the bed achieved a stable fluidization state when it reached 270 °C at which point the PMMA decomposed.

MMA hydrolyzes to MAA at a selectivity greater than 80 % below 250 °C and with excess of water vapour. At higher temperature and anhydrous conditions, aromatic compounds form. The highest yield of MAA in the tandem configuration was 48 %, at 50 % MMA conversion, which is 15 % higher than the MMA yield for PMMA degradation/MMA hydrolysis in a single vessel.

PMMA reacts over sand more than over silica gel and cokes less: 0.1 % vs. 1.5 %. Feeding water vapour seemed to suppress the reaction rate in the fluidized bed of sand and subsequently slumped the bed. Future work should explore injecting water vapour between the fluidized bed and fixed bed. This would maximize the PMMA degradation rate and at the same time provide an additional degree of freedom to control reaction temperature of the hydrolysis step. Furthermore, methacrylic acid yield would be higher due to the Le Chatelier principle.

CHAPTER 7 GENERAL DISCUSSION

Poly(methyl methacrylate) is a specialty thermoplastic polymer that has been commercialized in a short time since its invention at the beginning of 20th century and has established itself in the market due to its properties such as high strength and optical clarity, bio-compatibility, UV-resistance and low toxicity. The rapid growth in demand for PMMA over the past decades has led to an increase in its production volumes. which already surpassed 3.9 Mt yr^{-1} in 2020, with its annual growth of 5 % [8]. Among global plastic produced, less than 12 % is recycled, 25 % is incinerated, and the rest 60 % is land-filled (80 % in Canada) [6]. The rapid rise in oil prices since the second half of the 20th century within the gradual depletion of oil fields motivated the industry to find alternative sources for PMMA and MMA production. Recycling PMMA plastic wastes, rather than involving oil as raw material, has become one of the alternatives for obtaining the monomer. The contemporary industrial giants on the PMMA and MMA manufacturing market are targeting to minimize their capital and operating expenses and obtain a premium grade monomer.

Industry depolymerizes PMMA by pyrolysis mostly in molten metal baths, extruders, paddle reactors, reactors with mechanical agitation, or batch reactors (dry distillation). Fluidized beds (FB) operate at increased heat and mass transfer rates (about an order of magnitude higher compared to molten metal bath) due to good mixing of polymer with a fluidizing agent, approaching the maximal possible monomer recovery to 97 % which define their advantage among other reactor systems [**?**,11]. The conical spouted bed reactors (CSBR) are an alternative to FB and operate at a half lower pressure drop compared to FB, have extra short residence time and good density distribution due to wide range of particles size. However, the defluidization issues because of low bed/PMMA ratio and lower MMA yield favors fluidized bed reactors to be the most promising reactor types. Along with this, molten metal baths or extruders can not digest polymer scraps containing dyes, additives, fibers, etc. because of the impossibility of their fast separation during the reaction or, as in the case of an extruder, the risk of equipment breakage. And this is one of the reasons why industry ignores such polymer scraps. Kaminsky's group [47] in their research demonstrated that fluidized bed reactors are capable of processing polymers containing various additives (fibers, particles), which are then separated. On the other hand, the depolymerization of PMMA is accompanied by the release of co-monomers added during polymerization to improve its commercial properties and formation of by-products (responsible for unpleasant odor). These products present in the final product as traces, however some of them have similar to MMA boiling points and require significant investments for separation step Godia [21]. Thus, converting PMMA to

MAA may be a promising approach to optimize existing technologies and maximize the yield of MAA, since MAA has a 61 °C higher boiling point compared to MMA. In addition, scrap PMMA will be involved into the recycling process. In this regard, the configuration of the reactor for the conversion of PMMA to acid, as well as the type of catalyst for the hydrolysis stage, play a key role. This research provides investigations on the lab scale level using the virgin PMMA and addresses various questions about the conversion of PMMA to MAA, such as:

- the influence of temperature, feed flow rate, amount of water, and the catalyst/polymer ratio on the yield of MAA
- the reactor configuration to transform PMMA to MAA
- the influence of the catalyst physico-chemical properties on the yield of MAA
- the appropriate conditions for the catalytic hydrolysis of MMA to MAA in the fixed bed at equilibrium and identify the kinetic parameters
- influence of the preparation method on the catalyst activity
- the degradation behavior of PMMA at thermolysis

To answer the first question of the current study, we conducted experiments from 280 °C to 350 °C (Chapter 4). The MAA yield at 350 °C in the fluidized bed was low due to thermal instability of MMA and its decarboxylation with formation of CO_2, CO and acetone. The step-wise decrease in temperature led to an increase in MAA yield (33 %) at 280 °C. However, unreacted PMMA formed agglomerates with the catalyst.

The injection of PMMA at the 13 mm fluidized bed reactor was the first challenge in the process development. The PMMA material supplied from Arkema was 7 mm size pellets, and to prevent defluidization and the reactor shutdown, we milled the granules in a mill with adding of liquid nitrogen because of the dactyl properties of PMMA. To introduce PMMA powder in the reaction zone, we developed the method of pulse injection that consisted of placing of PMMA powder in the chamber under the reactor and supplying gas under a closed valve located below the PMMA chamber. After pressure reached its maximum, we opened the valve and PMMA injected in the FB of catalyst through the nozzle. This allowed us to quickly mix the PMMA with fluidizing catalyst. To prevent the nozzle blocking with the catalyst before the reaction start, we were loading catalyst on the glass-wool distributor while feeding fluidization gas at low flow rate. We also found that the stable fluidization take place at the PMMA:catalyst ratio 1 g:10 g. The large mass of loaded catalyst limited

the introduction of PMMA due to insufficient pressure under the PMMA chamber. Also we found that larger amount of PMMA in the chamber led to the blockage of the nozzle during its injection.

The first experiments on PMMA transformation to MAA ,where the acidic γ-Al_2O_3 served as a catalyst, demonstrated its low activity and selectivity which was comparable to the activity of sand. The wide peaks of the X-ray diffractogram at $2\theta = 67\,^\circ$, $46\,^\circ$ and $38\,^\circ$ confirmed the amorphous structure of γ-Al_2O_3. We also noticed that the Al_2O_3 produced more coke than sand because of its porous surface and adsorption of reaction products in pores. Testing of industrial FCC, Zeolite Y (acidic) catalysts as well as home-made $Mo-Zr/SiO_2$ and Keggin-type $Cs_xH_{(3-x)}PMo_{12}O_{40}$ /SiO_2 revealed that Zeolite Y (acidic) and Keggin-type $Cs_xH_{(3-x)}PMo_{12}O_{40}$ /SiO_2 are the most active towards MAA formation. However, to achieve the 2.5 mol of Cs by step-wise impregnation of silica gel with $H_3PMo_{12}O_{40}$ and Cs was difficult because of the adsorption of Cs on silica gel, which negatively affected the formation of the Keggin structure and catalyst activity. We spray-dryed zeolite Y micro-sieves with Ludox to enlarge particles for the lab scale applications in fluidized bed. Despite of better activity of this catalyst compared to others, the MAA yield did not exceed 33 %. The SEM study demonstrated that a shell of amorphous silicon oxide covered the catalyst particles during spray-drying. Thus, we correlated the catalyst activity mainly with defects on the particles' surface (chips, cracks on the surface).

We hypothesized that encapsulating the zeolite in a silica gel matrix would increase catalytic activity by providing a more accessible surface of zeolite active sites on the surface of the catalyst particles and in the pores and would be an alternative to spray drying (Chapter 5). The final catalyst had a higher surface area than zeolite Y micro-sieves and demonstrated high activity and selectivity in MMA hydrolysis in a fixed bed reactor of 8 mmID. The analysis of the catalyst acidity by the TPD method did not reveal any peaks related to Br∅nsted acidity because of its bonding with all types of sites over the zeolite and silica gel, but MAS-NMR and UV-Vis data confirmed the presence of acidic sites. We have demonstrated that faujasite-type acid zeolite Y is active and selective towards methacrylic acid. Zeolites Y are commercially produced in the form of particles of various geometries, and does not contain expensive components, which justifies their commercial use. The study of reaction kinetics in a wide range of temperatures and reagent concentrations is a good practice. However, the possibilities of conducting kinetic experiments in a wide range of reagents concentrations were technically limited in the 8 mm tube with a fixed catalyst bed because of the high pressure in the lines at evaporation of liquids, which in turn blocked liquid flow to the evaporator at higher reagent flow rates. Finally, we could increase the flow rate of Ar by a factor of 2.

In the last step of our study, we embraced the achievements of the previous two steps and hypothesized that the conversion of PMMA to MAA in a tandem reactor will increase the MAA yield compared to the fluidized bed and will be compatible with the performance of the fixed-bed (Chapter 6). In tandem reactor, PMMA is first thermolyzed in the fluidized bed of sand or silica gel, and then the MMA vapors updraft reacted with water vapor on the stationary bed of zeolite Y located in the upper reactor portion. We aimed to reach a higher temperature in the fluidized bed and lower – in the fixed bed. However, the implementation of the idea in a laboratory reactor was associated with the difficulty of maintaining a stationary and given temperature difference between the individual layers. Higher temperatures in the fluidized bed unavoidably caused the non-isothermal temperature raise in the fixed bed, which dropped the MAA yield in about 1.6 times (48 % vs 80 %). However, the MAA yield in the tandem reactor was 15 % higher than in the single fluidized bed.

CHAPTER 8 CONCLUSION

8.1 Conclusion

For the first time, we aimed to present MAA, rather than MMA, as an end product of the processing of PMMA to improve its quality and reduce the cost of additional purification. The development of such a recycling method demonstrates the possibility of introducing the scrap polymers in the recycling process in the pilot step.

We determined the reaction conditions that maximize MAA yield from PMMA in a micro-fluidized bed of 13 mm inner diameter. The TGA experiments demonstrated that the particle size below 0.5 mm are the most suitable for the reactor performance. The industrial and home-made catalysts such as γ-Al_2O_3, FCC, zeolite Y (faujasite), MoO_3-ZrO_2/SiO_2, $Cs_xH_{(3-x)}PMo_{12}O_{40}/SiO_2$ represented different activities at PMMA degradation while varying the catalyst volume, temperature regime, and water concentration in the FB reactor. The catalyst activity increased with the increase of its acidity. The zeolite Y was the most active and selective toward MAA at 280 °C (33 %). However, 50 % of PMMA was unreacted at this temperature. Sand possessed some catalytic activity in the depolymerization of PMMA in FB and only about 1 % of coke forms on its surface.

The yield of MAA increased with the decrease in the catalyst amount, and dropped with temperature raise to 350 °C because of particular MMA decarboxylation with formation of CO_2, CO and acetone as by-products. In addition, the yield of MeOH differs from stoichiometry. The most visible discrepancy we observed over the Al_2O_3 catalyst where part of methanol dehydrated to DME. The other catalysts like zeolite, Cs-HPA, MoO_3-ZrO_2/SiO_2, and sand represented the yield of MeOH is close to stoichiometry.

In the second step, the encapsulation of the acidic form of zeolite Y with a high Si/Al ratio into a silica gel matrix allowed to enlarge the micro-sieves of zeolite. For the first time, we studied the apparent kinetics of catalytic hydrolysis of MMA to MAA in a gas phase in an 8 mm ID fixed bed reactor. The reaction temperature varied in the range from 160 °C to 300 °C. The maximum MMA converted at 200 °C, however, further temperature increase dropped the MAA yield because of MMA decarboxylation.

The experimental data were approximated best by the first-order reaction by each reagent (the total second reaction order) in the temperature range 160 °C to 180 °C. Considering that hydrolysis is the reverse of esterification, we estimated reaction quotient (Q) which was much higher than the equilibrium constant (K_{eq}). This confirms that the reaction favors products

according to the principle of Le Chatelier. The estimated apparent activation energy E_{app} was 106 kJ mol^{-1}. The yield of MAA was about 85 % with the MMA conversion of 94 % at 200 °C and above which is more than 50 % much higher than at PMMA degradation in FB. Carbon forms over catalyst surface at about 6 % at temperatures 200 °C and higher.

The tandem reactor became a compromise solution for PMMA degradation to MAA between high-temperature thermolysis in the fluidized bed and relatively low-temperature regimes of hydrolysis in the fixed bed. We have demonstrated that sand is the most efficient fluidization agent to depolymerize PMMA as it maintains a uniform temperature in the reactor and generates almost no carbon compared to porous fluidizing agents. The yield of MAA in the upper fix bed of zeolite Y in the tandem reactor was 48 % at temperatures similar to a single FB which is 15 % higher compared to the single FB. It can be increased if maintain the isothermal conditions and particular temperature difference between both beds.

At the same time, acid zeolites are the most active and selective to methacrylic acid. The formation of by-products does not exceed 1 % at a low water concentration, which, with an excess of water, will not lead to the need to shut down the reactor and the need to flush the lines at the commercial process scale. The following factors determine the efficiency and potential benefits of future tandem reactors over a single fluidized bed reactors:

- lower cost of capital investments (no moving parts);
- ease of manufacture;
- use of one volume of the reactor for two processes;
- lower cost of reactor heating;
- longer life of the zeolite catalyst due to relatively low temperatures, absence of attrition;
- lower catalyst cost (no rare earth metals);
- the high selectivity of hydrolysis (lower costs by-products separation);
- possibility to recycle polymer containing solid additives.

8.2 Limitations of the solution proposed

While increasing the feed flow rate, the pressure in the heating line increased. This caused difficulty to supply the liquid in the 8 mmID reactor. This created restrictions on the variation of parameters in kinetics studies. In addition, continuous feeding of PMMA into the reactor required special equipment and high gas flow rates.

Another limitation refers to the design of the lab-scale tandem reactor to provide a certain temperature the difference in the lower reactor portion with a fluidized bed and the upper - with a fixed bed. When the the temperature in the fluidized bed is maintained at around 300 °C , the upper portion keeps at 250 °C due to the heated gases going up. However, the temperature difference is needed to be at least 100 °C to decompose PMMA and effectively maximize the MAA yield.

8.3 Recommendations for future research

Thermo-catalytic decomposition of PMMA into MAA in the one reactor volume was first proposed in the current research as an opportunity for chemical reprocessing of PMMA into valuable products (MAA) and to involve the scrap PMMA containing fillers and additives in the reprocessing. The restrictions on the operation of the lab-scale reactors create opportunities for the reactor scale-up. Some research groups are focused on studies of PMMA degradation in FB. Many studies reported their data on the optimization of such reaction parameters as PMMA/fluidizing agent ratio, solid/gas ratio, temperature regimes, and values of heat transfer parameters to provide a stable reactor performance, size of polymer particles, etc. However, the questions related to defluidization mechanisms in pilot-scale reactors are still not well understood. In this regard, exploring the hydrodynamics in the reactor at sublimation of continuously injected PMMA and water steam is of particular interest. Another step to improve the process could be to investigate the hydrodynamics coupled with chemical reaction and find the appropriate contact time for the maximization of MAA in a scaled reactor system.

The results of this study show that to degrade PMMA, the temperature should be in the range from 300 °C to 350 °C, and the effective temperature for MMA hydrolysis is in the range from 180 °C to 200 °C. Realization of the process in a tandem reactor for PMMA degradation maximized MAA yield compared to the single fluidized bed. However, it is necessary to provide a stable temperature difference between the fluidized and fixed beds to maximize the MAA yield. To improve the reactor performance, it can be a recommendation for the pilot-scale studies to inject water vapor directly under the fixed bed which will help the reaction quenching and maintain the stationary temperature in each bed.

The catalyst deactivates with the increase of the temperature and in time. The optimization of its composition to reduce coke formation and keep high acidity will help to minimize investments in industrial technology.

REFERENCES

[1] M. J. D. Mahboub, J. L. Dubois, F. Cavani, M. Rostamizadeh, and G. S. Patience, "Catalysis for the synthesis of methacrylic acid and methyl methacrylate," *Chemical Society Reviews*, vol. 47, no. 20, pp. 7703–7738, 2018.

[2] P. Nising, T. Zeilmann, and T. Meyer, "On the degradation and stabilization of poly (Methyl Methacrylate) in a continuous process," *Chemical Engineering and Technology*, vol. 26, no. 5, pp. 599–604, 2003.

[3] M. Menéndez, J. Herguido, A. Bérard, and G. S. Patience, "Experimental methods in chemical engineering: Reactors—fluidized beds," *The Canadian Journal of Chemical Engineering*, vol. 97, no. 9, pp. 2383–2394, 2019.

[4] E. K. Moens, K. D. Smit, Y. W. Marien, A. D. Trigilio, P. H. V. Steenberge, K. M. V. Geem, J.-L. Dubois, and D. R. D'Hooge, "Progress in reaction mechanisms and reactor technologies for thermochemical recycling of poly(methyl methacrylate)," *Polymers*, vol. 12, no. 8, p. 1667, 2020.

[5] M. Hunger, "Brønsted acid sites in zeolites characterized by multinuclear solid-state nmr spectroscopy," *Catalysis Reviews*, vol. 39, pp. 345–393, 2006.

[6] G. of Canada. (2022) Plastic waste and pollution reduction. [Online]. Available: https://www.canada.ca/en/environment-climate-change/services/managing-reducing-waste.html

[7] G. X. Xi, S. L. Song, and Q. Liu, "Catalytic effects of sulfates on thermal degradation of waste poly(methyl methacrylate)," *Thermochimica Acta*, vol. 435, no. 1, pp. 64–67, 2005.

[8] J. D. Tommaso and J.-L. Dubois, "Risk analysis on pmma recycling economics," *Polymers*, vol. 13, no. 16, p. 2724, 2021.

[9] V. Popescu, C. Vasile, M. Brebu, G. L. Popescu, M. Moldovan, C. Prejmerean, L. Stănuleţ, C. Trişcă-Rusu, and I. Cojocaru, "The characterization of recycled pmma," *Journal of Alloys and Compounds*, vol. 483, no. 1–2, pp. 432–436, 2009.

[10] D. S. Achilias, "Chemical recycling of polymers . the case of poly (methyl methacrylate)," presented at the Conference on Energy and Environmental

Systems, Chalkida, Greece, May 8-10 2006, pp. 271–276. [Online]. Available: https://www.researchgate.net/publication/242189669_Chemical_Recycling_of_Polymers_The_Case_of_Polymethyl_methacrylate

[11] W. Kaminsky, "Chemical recycling of plastics by fluidized bed pyrolysis," *Fuel Communications*, vol. 8, pp. 100 023–100 033, 2021.

[12] M. Newborough, D. Highgate, and P. Vaughan, "Thermal depolymerisation of scrap polymers," *Applied Thermal Engineering*, vol. 22, no. 17, pp. 1875–1883, 2002.

[13] C. Capone, L. D. Landro, F. Inzoli, M. Penco, and L. Sartore, "Thermal and mechanical degradation duringpolymer extrusion processing," *Polymer Engineering and Science*, vol. 47, no. 11, pp. 1813–1819, 2007.

[14] A. R. Prado, A. G. Leal-Junior, C. Marques, S. Leite, de Geovane L. Sena, L. C. Machado, A. Frizera, M. R. N. Ribeiro, and M. J. Pontes, "Polymethyl methacrylate (pmma) recycling for the production of optical fiber sensor systems," *Optics Express*, vol. 25, no. 24, p. 30051, 2017.

[15] A. Sasaki, N. Kikuya, T. Ookubo, and M. Hayashida, "Recovery method of pyrolysis product of resin," U.S. Patent US 8 304 573 B2, November, 6, 2012. [Online]. Available: https://patents.google.com/patent/US8304573/da

[16] G. Lopez, M. Artetxe, M. Amutio, G. Elordi, R. Aguado, M. Olazar, and J. Bilbao, "Recycling poly-(methyl methacrylate) by pyrolysis in a conical spouted bed reactor," *Chemical Engineering and Processing: Process Intensification*, vol. 49, no. 10, pp. 1089–1094, 2010.

[17] A. W. Siebert, D. Highgate, and M. Newborough, "Heat transfer characteristics of mechanically-stimulated particle beds," *Applied Thermal Engineering*, vol. 19, no. 1, pp. 37–49, 1999.

[18] A. Siebert, M. Newborough, and D. Highgate, "Heat transfer in mechanically-fluidized particle beds," *Chemical Engineering Research and Design*, vol. 80, no. 3, pp. 332–334, 2002.

[19] A. Sasaki and T. Tsuji, "Poly (methyl methacrylate) pyrolysis by two fluidized bed process," presented at the The 5th ISFR, Chengdu, China, October 11-14 2009, pp. 79–83.

[20] W. Kaminsky and C. Eger, "Pyrolysis of filled pmma for monomer recovery," *Journal of Analytical and Applied Pyrolysis*, vol. 58–59, pp. 781–787, 2001.

[21] C. B. Godiya, S. Gabrielli, S. Materazzi, M. S. Pianesi, N. Stefanini, and E. Marcantoni, "Depolymerization of waste poly(methyl methacrylate) scraps and purification of depolymerized products," *Journal of Environmental Management*, vol. 231, pp. 1012–1020, 2019.

[22] D. S.Achilias, "Chemical recycling of poly(methyl methacrylate) by pyrolysis. Potential use of the liquid fraction as a raw material for the reproduction of the polymer," *European Polymer Journal*, vol. 43, no. 6, pp. 2564–2575, 2007.

[23] F. Sasse and G. Emig, "Chemical recycling of polymer materials," *Chemical Engineering and Technology*, vol. 21, no. 10, pp. 777–789, 1998.

[24] T. Kashiwagi, J. E. Brown, A. Inaba, K. Hatada, T. Kitayama, and E. Masuda, "Effects of weak linkages on the thermal and oxidative degradation of poly(methyl methacrylates)," *Macromolecules*, vol. 19, no. 8, pp. 2160–2168, 1986.

[25] O. P. Korobeinichev, A. A. Paletsky, M. Gonchikzhapov, R. K. Glaznev, I. E. Gerasimov, Y. K. Naganovsky, I. K. Shundrina, A. Y. Snegirev, and R. Vinu, "Kinetics of thermal decomposition of pmma at different heating rates and in a wide temperature range," *Thermochimica Acta*, vol. 671, pp. 17–25, 2019.

[26] B. J. Holland and J. N. Hay, "The effect of polymerisation conditions on the kinetics and mechanisms of thermal degradation of pmma," *Polymer Degradation and Stability*, vol. 77, no. 3, pp. 435–439, 2002.

[27] M. Arshad, K. Masud, and M. A. et al., "The effect of albr3 additive on the thermal degradation of pmma a study using tg-dta-dtg, ir and py-gc-ms techniques," *Journal of Thermal Analysis and Calorimetry*, vol. 96, no. 3, pp. 873–881, 2009.

[28] I.-Y. Jeon and J.-B. Baek, "Nanocomposites derived from polymers and inorganic nanoparticles," *Materials*, vol. 3, no. 6, pp. 3654–3674, 2010.

[29] M. L. Saladino, T. E. Motaung, A. S. Luyt, A. Spinella, G. Nasillo, and E. Caponetti, "The effect of silica nanoparticles on the morphology, mechanical properties and thermal degradation kinetics of pmma," *Polymer Degradation and Stability*, vol. 97, no. 3, pp. 452–459, 2012.

[30] T. E. Motaung, A. S. Luyt, F. Bondioli, M. Messori, M. L. Saladino, A. Spinella, G. Nasillo, and E. Caponetti, "Pmma-titania nanocomposites: Properties and thermal degradation behaviour," *Polymer Degradation and Stability*, vol. 97, no. 8, pp. 1325–1333, 2012.

[31] Y. M. Lee and D. S. Viswanath, "Degradation of poly(methyl methacrylate) (pmma) with aluminum nitride and alumina," *Polymer Engineering and Science*, vol. 40, no. 11, pp. 2332–2341, 2000.

[32] M. Cochez, M. Ferriol, J. V. Weber, P. Chaudron, N. Oget, and J. L. Mieloszynski, "Thermal degradation of methyl methacrylate polymers functionalized by phosphorus-containing molecules. i. tga/ft-ir experiments on polymers with the monomeric formula CH2C(CH3)C(O)OCHRP(O)(OC2H5)2 (R = H, (CH2)4CH3, C6H5Br, C10H7)," *Polymer Degradation and Stability*, vol. 70, no. 3, pp. 455–462, 2000.

[33] A. Hamoudi, "Synthesis, analysis and thermolysis of copolymers of methyl methacrylate with alcali metal methacrylates," PhD dissertation, University of Glasgow, Scotland, Glasgow, Scotland, 1975. [Online]. Available: https://theses.gla.ac.uk/78707/1/13803962.pdf

[34] T. Kashiwagi, A. Inabi, and A. Hamins, "Behavior of primary radicals during thermal degradation of poly(methyl methacrylate)," *Polymer Degradation and Stability*, vol. 26, pp. 161–184, 1989.

[35] L. E. Manring, "Thermal degradation of saturated Poly(Methyl Methacrylate)," *Macromolecules*, vol. 21, no. 2, pp. 528–530, 1988.

[36] ——, "Thermal Degradation of Poly(methyl methacrylate). 2. Vinyl-Terminated Polymer," *Macromolecules*, vol. 22, no. 6, pp. 2673–2677, 1989.

[37] L. E. Manring, D. Y. Sogah, and M. G. Cohen, "Thermal Degradation of Poly(methyl methacrylate). 3. Polymer with Head-to-Head Linkages," *Macromolecules*, vol. 22, no. 12, pp. 4652–4654, 1989.

[38] B. J. Holland and J. N. Hay, "The kinetics and mechanisms of the thermal degradation of poly(methyl methacrylate) studied by thermal analysis-fourier transform infrared spectroscopy," *Polymer*, vol. 42, no. 11, pp. 4825–4835, 2001.

[39] M. Ferriol, A. Gentilhomme, M. Cochez, N. Oget, and J. L. Mieloszynski, "Thermal degradation of poly(methyl methacrylate) (pmma): Modelling of dtg and tg curves," *Polymer Degradation and Stability*, vol. 79, no. 2, pp. 271–281, 2003.

[40] J. Cheng, Y. Pan, J. Yao, X. Wang, F. Pan, and J. Jiang, "Mechanisms and kinetics studies on the thermal decomposition of micron poly (methyl methacrylate) and polystyrene," *Journal of Loss Prevention in the Process Industries*, vol. 40, pp. 139–146, 2016.

[41] R. Chen, R. Pan, and Q. Li, "Thermal degradation characteristics, kinetics and thermodynamics of micron-sized pmma in oxygenous atmosphere using thermogravimetry and deconvolution method based on gauss function," *Journal of Loss Prevention in the Process Industries*, vol. 71, p. 104488, 2021.

[42] W. Gao, J. Yu, J. Li, Q. Zhang, Q. Xie, X. Zhang, and D. Hu, "Experimental investigation on micro– and nano–pmma dust explosion venting at elevated static activation overpressures," *Powder Technology*, vol. 301, pp. 713–722, 2016.

[43] X. Zhang, W. Gao, J. Yu, Y. Zhang, J. Zhang, X. Huang, and J. Chen, "Effect of flame propagation regime on pressure evolution of nano and micron pmma dust explosions," *Journal of Loss Prevention in the Process Industries*, vol. 63, p. 104037, 2020.

[44] L. A. Pérez-Maqueda, J. M. Criado, and P. E. Sánchez-Jiménez, "Combined kinetic analysis of solid-state reactions: A powerful tool for the simultaneous determination of kinetic parameters and the kinetic model without previous assumptions on the reaction mechanism," *Journal of Physical Chemistry A*, vol. 110, no. 45, pp. 12 456–12 462, 2006.

[45] S. Khangkham, "Catalytic degradation of poly(methyl methacrylate) by zeolite and regeneration of coked zeolite by ozonation," PhD thesis, University of Toulouse, France, Toulouse, France, 2012. [Online]. Available: http://ethesis.inp-toulouse.fr/archive/00002077/

[46] S. Sakkosit, S. Damronglerd, and C. Ngamcharussrivichai, "Degradation of poly(methyl methacrylate) over zeolites in a batch reactor," in *Manufacturing Science and Technology III*, ser. Advanced Materials Research, vol. 622. Trans Tech Publications Ltd, 2 2013, pp. 1173–1177.

[47] W. Kaminsky, M. Predel, and A. Sadiki, "Feedstock recycling of polymers by pyrolysis in a fluidised bed," *Polymer Degradation and Stability*, vol. 85, no. 3, pp. 1045–1050, 2004.

[48] A. Laachachi, M. Ferriol, M. Cochez, D. Ruch, and J. Lopez-Cuesta, "The catalytic role of oxide in the thermooxidative degradation of poly(methyl methacrylate)-tio2

nanocomposites," *Polymer Degradation and Stability*, vol. 93, no. 6, pp. 1131–1137, 2008.

[49] N. Cinausero, N. Azema, J. M. L. Cuesta, M. Cochez, and M. Ferriol, "Impact of modified alumina oxides on the fire properties of pmma and ps nanocomposites," *Polymers for Advanced Technologies*, vol. 22, no. 12, pp. 1931–1939, 2011.

[50] R. Ran, J. Li, G. Wang, Z. Li, and C. Li, "Esterification of methacrylic acid with methanol: Process optimization, kinetic modeling, and reactive distillation," *Industrial & Engineering Chemistry Research*, vol. 58, no. 6, pp. 2135–2145, 2019.

[51] H. Hattori and Y. Ono, "4 - catalysts and catalysis for acid–base reactions," in *Metal Oxides in Heterogeneous Catalysis*, ser. Metal Oxides, J. C. Védrine, Ed. Elsevier, 2018, pp. 133–209.

[52] M. Kimura, T. Nakato, and T. Okuhara, "Water-tolerant solid acid catalysis of Cs2.5H0.5PW12O40 for hydrolysis of esters in the presence of excess water," *Applied Catalysis A: General*, vol. 165, no. 1–2, pp. 227–240, 1997.

[53] T. S. Glazneva, N. S. Kotsarenko, and E. A. Paukshtis, "Surface acidity and basicity of oxide catalysts: From aqueous suspensions to in situ measurements," *Kinetics and Catalysis*, vol. 49, no. 6, pp. 859–867, 2008.

[54] T. Witczak, M. Grzesik, J. Skrzypek, and M. Witczak, "Liquid-phase esterification of methacrylic acid with methanol catalyzed by heteropolyacid," *International Journal of Chemical Reactor Engineering*, vol. 8, no. 1, pp. 1–15, 2010.

[55] M. Grzesik and T. Witczak, "The influence of the catalyst on the kinetics of ethyl metacrylate synthesis," *Polish Journal of Chemical Technology*, vol. 9, no. 1, pp. 7–9, 2007.

[56] G. Jyoti, A. Keshav, J. Anandkumar, and S. Bhoi, "Homogeneous and heterogeneous catalyzed esterification of acrylic acid with ethanol: reaction kinetics and modeling," *International Journal of Chemical Kinetics*, vol. 50, no. 5, pp. 370–380, 2018.

[57] T. Okuhara, "Water-tolerant solid acid catalysts," *Chemical Reviews*, vol. 102, no. 10, pp. 3641–3666, 2002.

[58] Y. Izumi, "Hydration/hydrolysis by solid acids," *Catalysis Today*, vol. 33, no. 4, pp. 371–409, 1997.

[59] AvelinoCorma, H. Garcia, S. Iborra, and J. Primo, "Modified faujasite zeolites as catalysts in organic reactions: Esterification of carboxylic acids in the presence of hy zeolites," *Journal of Catalysis*, vol. 120, no. 1, pp. 78–87, 1989.

[60] T. A. Semelsberger, K. C. Ott, R. L. Borup, and H. L. Greene, "Role of acidity on the hydrolysis of dimethyl ether (dme) to methanol," *Applied Catalysis B: Environmental*, vol. 61, no. 3, pp. 281–287, 2005.

[61] K. Tanabe, M. Misono, Y. Ono, and H. Hattori, *New solid acids and bases: their catalytic properties*. Elsevier, 1989, vol. 51.

[62] E. Derouane, J. Védrine, R. R. Pinto, P. Borges, L. Costa, M. Lemos, F. Lemos, and F. R. Ribeiro, "The acidity of zeolites: Concepts, measurements and relation to catalysis: A review on experimental and theoretical methods for the study of zeolite acidity," *Catalysis Reviews: Science and Engineering*, vol. 55, no. 4, pp. 454–515, 2013.

[63] J. Vohlídal, "Polymer degradation: a short review," *Chemistry Teacher International*, vol. 3, no. 2, pp. 213–220, 2021.

[64] S. M. Al-Salem, P. Lettieri, and J. Baeyens, "Recycling and recovery routes of plastic solid waste (PSW): A review," *Waste Management*, vol. 29, no. 10, pp. 2625–2643, 2009.

[65] J. Kers, P. Kulu, D. Goljandin, and V. Mikli, "Reprocessing technology of composite plastic scrap and properties of materials from recycled plastics," *Proceedings of the Estonian Academy of Sciences: Engineering*, vol. 13, no. 2, pp. 105–116, 2007.

[66] D. S. Achilias, "Recent advances in the chemical recycling of polymers," *Journal of Organic Chemical Technology*, vol. 23, no. 12, p. 63, 2005.

[67] J.-L. Dubois, "New innovative process for recycling end-of-life PMMA waste. MMAtwo second generation methyl methacrylate. Conference: Plastic recycling technologies, AMI organizer, June 18-19th 2019, Dusseldorf, Germany," 2019.

[68] B. S. Kang, S. G. Kim, and J. S. Kim, "Thermal degradation of poly(methyl methacrylate) polymers: Kinetics and recovery of monomers using a fluidized bed reactor," *Journal of Analytical and Applied Pyrolysis*, vol. 81, no. 1, pp. 7–13, 2008.

[69] U. Arena and M. L. Mastellone, *Fluidized Bed Pyrolysis of Plastic Wastes*. Chichester, UK: John Wiley & Sons, Ltd, 2006, ch. 16, pp. 435–474. [Online]. Available: https://onlinelibrary.wiley.com/doi/book/10.1002/0470021543

[70] W. Kaminsky and J. Franck, "Monomer recovery by pyrolysis of poly(methyl methacrylate) (pmma)," *Journal of Analytical and Applied Pyrolysis*, vol. 19, pp. 311–318, 1991.

[71] W. Kaminsky, "Monomer recovery of plastic waste in a fluidized bed process," in *Feedstock Recycling and Pyrolysis of Waste Plastics: Converting Waste Plastics into Diesel and Other Fuels*. Hoboken, NJ: John Wiley & Sons, Ltd, 2006, ch. 24, pp. 627–640.

[72] T. L. Tsai, C. C. Lin, G. L. Guo, and T. C. Chu, "Effects of microwave-assisted digestion on decomposition behavior of polymethyl methacrylate (pmma)," *Materials Chemistry and Physics*, vol. 108, no. 2–3, pp. 382–390, 2008.

[73] I. D. Poree, K. P. Cameron, J. A. Bloem, F. D. Schlosser, and A. McGowan, "Process for decomposing a polymer to its monomer or monomers," US Patent US6 160 031A, Dec. 12, 2000. [Online]. Available: https://patents.google.com/patent/US6160031/zh

[74] G. Grause, M. Predel, and W. Kaminsky, "Monomer recovery from aluminium hydroxide high filled poly(methyl methacrylate) in a fluidized bed reactor," *Journal of Analytical and Applied Pyrolysis*, vol. 75, no. 2, pp. 236–239, 2006.

[75] E. Esmizadeh, S. Khalili, A. Vahidifar, G. Naderi, and C. Dubois, "Waste Polymethyl Methacrylate (PMMA): Recycling and High-Yield Monomer Recovery," *Handbook of Ecomaterials*, pp. 1–33, 2018.

[76] S. Khangkham, C. Julcour-Lebigue, S. Damronglerd, C. Ngamcharussrivichai, M. H. Manero, and H. Delmas, "Regeneration of coked zeolite from pmma cracking process by ozonation," *Applied Catalysis B: Environmental*, vol. 140–141, pp. 396–405, 2013.

[77] J. M. Arandes, I. Torre, P. Castano, M. Olazar, and J. Bilbao, "Catalytic cracking of waxes produced by the fast pyrolysis of polyolefins," *Energy & fuels*, vol. 21, no. 2, pp. 561–569, 2007.

[78] A. G. Buekens and H. Huang, "Catalytic plastics cracking for recovery of gasoline-range hydrocarbons from municipal plastic wastes," *Resources, Conservation and Recycling*, vol. 23, no. 3, pp. 163–181, 1998.

[79] S. Raseev, *Thermal and catalytic processes in petroleum refining. First edition.* CRC Press, 2003.

[80] Y. Xue, P. Johnston, and X. Bai, "Effect of catalyst contact mode and gas atmosphere during catalytic pyrolysis of waste plastics," *Energy Conversion and Management*, vol. 142, pp. 441–451, 2017.

[81] R. Narayanaswamy, K. K. Ramamurthy, and P. S. Sreenivasan, "Catalyst for the conversion of plastics to olefin and aromatic products," U.S. Patent US5 326 919A, 15 dec., 2015. [Online]. Available: https://patents.google.com/patent/US9175313B2/en

[82] N. Miskolczi, F. Ateş, and N. Borsodi, "Comparison of real waste (msw and mpw) pyrolysis in batch reactor over different catalysts. part ii: Contaminants, char and pyrolysis oil properties," *Bioresource Technology*, vol. 144, pp. 370–379, 2013.

[83] G. Audisio, F. Bertini, P. L. Beltrame, and P. Carniti, "Catalytic degradation of polymers: Part iii—degradation of polystyrene," *Polymer Degradation and Stability*, vol. 29, no. 2, pp. 191–200, 1990.

[84] J. Luche, T. Rogaume, F. Richard, and E. Guillaume, "Characterization of thermal properties and analysis of combustion behavior of pmma in a cone calorimeter," *Fire Safety Journal*, vol. 46, no. 7, pp. 451–461, 2011.

[85] J. Šesták and G. Berggren, "Study of the kinetics of the mechanism of solid-state reactions at increasing temperatures," *Thermochimica Acta*, vol. 3, no. 1, pp. 1–12, 1971.

[86] P. W. Vaughan and D. J. Highgate, "Depolymerization," US Patent US5 663 420A, September, 2, 1997. [Online]. Available: https://patents.google.com/patent/US5663420A/en

[87] J. Zhang, Y. Wang, X. Lu, and J. Yu, "Study on melting behavior of polymers during burning," *Fire Safety Science*, vol. 8, pp. 637–646, 2005.

[88] K. Nagai, "New developments in the production of methyl methacrylate," *Applied Catalysis A: General*, vol. 221, pp. 367–377, 2001.

[89] W. Bauer, "Methacrylic acid and derivatives," *Ullmann's Encyclopedia of Industrial Chemistry*, vol. 23, 2000.

[90] J. C. Dobson, "High yield process for the production of methacrylic acid esters," US Patent US5 393 918A, Feb., 28, 1995. [Online]. Available: https://patents.google.com/patent/US5393918A/en

[91] C.-S. Tsay, M. S. DeCourcy, I.-H. M. Chang-Mateu, H. G. Thompson, and D. E. Chase, "Apparatus and process for the high yield production of methyl methacrylate or methacrylic acid," US Patent US6 610 177B2, Dec., 12, 2002. [Online]. Available: https://patents.google.com/patent/US6610177B2/en

[92] M. S. Gibson, "Hydrolysis of methyl esters in dimethylsulfoxide for production of fatty acids," US Patent US5 440 061A, Aug., 08, 1995. [Online]. Available: https://patents.google.com/patent/US5440061A/en

[93] M. H. D. Butt and F. J. Waller, "Ester hydrolysis," US Patent US5 315 033A, May, 24, 1994. [Online]. Available: https://patents.google.com/patent/US5315033A

[94] D. Broell, H. Siegert, H. Hiltner, and T. Krauss, "Process for preparing methacrylic acid," US Patent US8 791 296B2, Jul., 29, 2014. [Online]. Available: https://patents.google.com/patent/US8791296B2/en?oq=US+8791296

[95] D. Packet, "Hydrolysis of mma to maa/a method for the direct hydrolysis of fatty acid esters to the corresponding fatty acids," US Patent EP1 352 891A1, October, 15, 2003. [Online]. Available: https://patents.google.com/patent/EP1352891A1/de?oq=EP+1352891+A1

[96] H. P. Lesutis, R. Gläser, C. L. Liotta, and C. A. Eckert, "Acid/base-catalyzed ester hydrolysis in near-critical water," *Chemical Communications*, no. 20, pp. 2063–2064, 1999.

[97] W. Long and C. W. Jones, "Hybrid sulfonic acid catalysts based on silica-supported poly(styrene sulfonic acid) brush materials and their application in ester hydrolysis," *ACS Catalysis*, vol. 1, no. 7, pp. 674–681, 2011.

[98] R. Goseki and T. Ishizone, "Poly(methyl methacrylate) (PMMA)," in *Encyclopedia of Polymeric Nanomaterials*. Berlin, Heidelberg: Springer Berlin Heidelberg, 2014, pp. 1–11. [Online]. Available: http://link.springer.com/10.1007/978-3-642-36199-9{_}244-1

[99] M. Mohammadi, H. Fazli, M. Karevan, and J. Davoodi, "The glass transition temperature of pmma: A molecular dynamics study and comparison of various determination methods," *European Polymer Journal*, vol. 91, pp. 121–133, 2017.

[100] S. Ray and R. P. Cooney, "Thermal degradation of polymer and polymer composites," in *Handbook of Environmental Degradation Of Materials: Third Edition*, 3rd ed. Elsevier Inc., 2018, pp. 185–206. [Online]. Available: http://dx.doi.org/10.1016/B978-0-323-52472-8.00009-5

[101] B. Singh and N. Sharma, "Mechanistic implications of plastic degradation," *Polymer Degradation and Stability*, vol. 93, no. 3, pp. 561–584, 2008.

[102] J. N. Brönsted, "Acid and basis catalysis," *Chemical Reviews*, vol. 5, no. 3, pp. 231–338, 1927.

[103] J. W. Huffman and P. G. Harris, "A Convenient Procedure For The Hydrolysis Of Hindered Esters," *Synthetic Communications*, vol. 6, no. 7, pp. 481–484, 1976.

[104] P. L. da Silva, L. Guimaraes, and J. R. Pliego Jr, "Revisiting the mechanism of neutral hydrolysis of esters: water autoionization mechanisms with acid or base initiation pathways," *The Journal of Physical Chemistry B*, vol. 117, no. 21, pp. 6487–6497, 2013.

[105] H. Shi, Y. Wang, and R. Hua, "Sharing active intermediate via a spontaneous theory calculation and supported by electrospray," *Physical Chemistry Chemical Physics*, vol. 17, pp. 30 279–30 291, 2015.

[106] S. M. Al-Salem, A. Antelava, A. Constantinou, G. Manos, and A. Dutta, "A review on thermal and catalytic pyrolysis of plastic solid waste (PSW)," *Journal of Environmental Management*, vol. 197, no. 1408, pp. 177–198, 2017. [Online]. Available: http://dx.doi.org/10.1016/j.jenvman.2017.03.084

[107] E. Szabo, M. Olah, F. Ronkay, N. Miskolczi, and M. Blazso, "Characterization of the liquid product recovered through pyrolysis of PMMA-ABS waste," *Journal of Analytical and Applied Pyrolysis*, vol. 92, no. 1, pp. 19–24, 2011.

[108] D. Hamad, "Experimental Investigation of Polyvinyl Alcohol Degradation in UV/H2O2 Photochemical Reactors Using Different Hydrogen Peroxide Feeding Strategies," thèse de doctorat, Ryerson University, Toronto, Canada, 2015. [Online]. Available: https://rshare.library.ryerson.ca/articles/thesis/Experimental_investigation_of_polyvinyl_alcohol_degradation_in_UV_H202_photochemical_reactors_using_different_hydrogen_peroxide_feeding_strategies/14665875

[109] C. Muhammad, J. A. Onwudili, and P. T.Williams, "Catalytic pyrolysis of waste plastic from electrical and electronic equipment," *Journal of Analytical and Applied Pyrolysis*, vol. 113, pp. 332–339, 2015.

[110] N. N. António, "Study of the mechanisms of thermal depolymerization of the poly(methyl methacrylate). Selection of solvent compatible with PMMA," Master's thesis, Universidade Technica de Lisboa, Lisbon, Portugal, 2007. [Online]. Available: https://fenix.tecnico.ulisboa.pt

[111] J. Mertinkat, A. Kirsten, M. Predel, and W. Kaminsky, "Cracking catalysts used as fluidized bed material in the Hamburg pyrolysis process," *Journal of Analytical and Applied Pyrolysis*, vol. 49, no. 1, pp. 87–95, 1999.

[112] K. A. Kun and R. Kunin, "The pore structure of macroreticular ion exchange resins," *Journal of Polymer Science Part C: Polymer Symposia*, vol. 16, no. 3, pp. 1457–1469, 1967.

[113] A. Dumain and C. Raufast, "Device for introducing a powder with catalytic activity into a fluidized-bed polymerization reactor," US Patent US4 687 381A, Aug., 18, 1987. [Online]. Available: https://patents.google.com/patent/US4687381A/en?oq=US+4687381

[114] C. B. Morales, T. J. Jamaleddine, F. Berruti, J. McMillan, and C. Briens, "Low-temperature experimental model of liquid injection and reaction in a fluidized bed," *Canadian Journal of Chemical Engineering*, vol. 94, no. 5, pp. 886–895, 2016.

[115] U. Arena and M. L. Mastellone, "Defluidization phenomena during the pyrolysis of two plastic wastes," *Chemical Engineering Science*, vol. 55, no. 15, pp. 2849–2860, 2000.

[116] G. Tardos and R. Pfeffer, "Chemical reaction induced agglomeration and defluidization of fluidized beds," *Powder Technology*, vol. 85, no. 1, pp. 29–35, 1995.

[117] J. L. Moseley and T. J. O'Brien, "A model for agglomeration in a fluidized bed," *Chemical Engineering Science*, vol. 48, no. 17, pp. 3043–3050, 1993.

[118] H. Arastoopour, C. S. Huang, and S. A. Weil, "Fluidization behavior of particles under agglomerating conditions," *Chemical Engineering*, vol. 43, pp. 3063–3075, 1988.

[119] P. G. Smith, *Applications of Fluidization to Food Processing.* John Wiley & Sons, 2007. [Online]. Available: https://onlinelibrary.wiley.com/doi/book/10.1002/9780470995426

[120] O. Levenspiel, "Tracer Technology. Modeling the Flow of Fluids," in *Fluid Mechanics and Its Application*, R. M. Madylam, Ed., 2012, vol. 96, pp. 1–135.

[121] Anna Yermakova, *Methods of Macrokinetics for Mathematical Modeling of Chemical Processes and Reactors.* Novosibirsk, Russia: Boreskov Institute of catalysis SB RAS, 2001.

[122] P. Valco and S. Vajda, *Advanced scientific computing in BASIC with applications in chemistry, biology and pharmacology, Data handling in science and technology.* Amsterdam: Elsevier, 1989, vol. 4.

[123] D. Stone and J. Ellis, "Calibration and Linear Regression Analysis: A Self-Guided Tutorial (Part 2)," pp. 1–7, 2001.

[124] O. Levenspiel, *Chemical Reaction Engineering*, 3rd ed. New York, USA: John Wiley & Sons, Inc., 1999.

[125] Y. Kikuchi, M. Hirao, T. Ookubo, and A. Sasaki, "Design of recycling system for poly(methyl methacrylate) (pmma). part 1: Recycling scenario analysis," *International Journal of Life Cycle Assessment*, vol. 19, no. 1, pp. 120–129, 2014.

[126] K. Smolders and J. Baeyens, "Thermal degradation of pmma in fluidised beds," *Waste Management*, vol. 24, no. 8, pp. 849–857, 2004.

[127] J. Brady, T. Drig, P. I. Lee, and J. X. Li, "Chapter 7 - polymer properties and characterization," in *Developing Solid Oral Dosage Forms: Pharmaceutical Theory and Practice: Second Edition*. Boston: Academic Press, 2017, pp. 181–223.

[128] C. Neveu, R. Sondjaja, T. Stöhr, and N. Iroff, "Lubricant and fuel additives based on polyalkylmethacrylates," *Polymer Science: A Comprehensive Reference*, vol. 10, pp. 453–478, 2012.

[129] K. Dahmen, T. Muller, R. Peppmoller, and N. Behlau, "Leather-treatment agents, process for their preparation, and their use for producing low-fogging leathers," U.S. Patent US6 048 467A, Aplil, 11, 1997. [Online]. Available: https://patents.google.com/patent/US6048467A/en

[130] L. A. Wall, "The mechanisms of pyrolysis, oxidation, and burning of organic materials," in *The Mechanisms of Pyrolysis, Oxidation, and Burning of Organic Materials*, vol. 13. National Bureau of Standards of Special Publication, 1972, pp. 1–199.

[131] M. M. Coleman and P. C. Painter, *Fundamentals of Polymer Science*, 2nd ed. CRC Press, 2018.

[132] A. Shrivastava, "7 - environmental aspects of plastics," in *Introduction to Plastics Engineering*, A. Shrivastava, Ed. William Andrew Publishing, 2018, pp. 207–232.

[133] H. Arisawa and T. Brill, "Kinetics and mechanisms of flash pyrolysis of poly(methyl methacrylate) (pmma)," *Combustion and Flame*, vol. 109, no. 3, pp. 415–426, 1997.

[134] M. Materazzi, *Clean Energy from Waste: Fundamental Investigations on Ashes and Tar Behaviours in a Two Stage Fluid Bed-Plasma Process for*

Waste Gasification, ser. Springer Theses. Springer, 2017. [Online]. Available: http://link.springer.com/10.1007/978-3-319-46870-9

[135] J.-L. Dubois, "PMMA depolymerization: Scale-up and Industrial implementation. MMAtwo Virtual Workshop on Polymer Recycling, September 2020."

[136] ——, "Guidelines for pmma depolymerization at pilot and industrial scale. mmatwo's webinar," 2022.

[137] R. Bardestani, G. S. Patience, and S. Kaliaguine, "Experimental methods in chemical engineering: specific surface area and pore size distribution measurements—BET, BJH, and DFT," *Canadian Journal of Chemical Engineering*, vol. 97, no. 11, pp. 2781–2791, 2019.

[138] H. Khan, A. S. Yerramilli, A. D'Oliveira, T. L. Alford, D. C. Boffito, and G. S. Patience, "Experimental methods in chemical engineering: X-ray diffraction spectroscopy—xrd," *Canadian Journal of Chemical Engineering*, vol. 98, no. 6, pp. 1255–1266, 2020.

[139] G. S. Patience, Ed., *Experimental methods and instrumentation for chemical engineers*, 2nd ed. B.V., Amsterdam: Elsevier, 2017.

[140] S. Soled, S. Miseo, G. McVicker, W. Gates, A. Gutierrez, and J. Paes, "Preparation of bulk and supported heteropolyacid salts," *Catalysis Today*, vol. 36, no. 4, pp. 441–450, 1997.

[141] N. Saadatkhah, M. G. Rigamonti, D. C. Boffito, H. Li, and G. S. Patience, "Spray dried SiO_2WO_3/TiO_2 and SiO_2 vanadium pyrophosphate core-shell catalysts," *Powder Technology*, vol. 316, pp. 434–440, 2017.

[142] H. J. Bosman, E. C. Kruissink, J. V. der Spoel, and F. V. den Brink, "Characterization of the Acid Strength of SiO2-ZrO2 Mixed Oxides," *Journal of Catalysis*, vol. 148, no. 2, pp. 660–672, 1994.

[143] D. O. Obada, D. Dodoo-Arhin, M. Dauda, F. O. Anafi, A. S. Ahmed, O. A. Ajayi, and I. A. Samotu, "Effect of mechanical activation on mullite formation in an alumina-silica ceramics system at lower temperature," *World Journal of Engineering*, vol. 13, no. 4, pp. 288–293, 2016.

[144] E. T. C. Vogt and B. M. Weckhuysen, "Fluid catalytic cracking: recent developments on the grand old lady of zeolite catalysis," *Chemical Society Reviews*, vol. 44, no. 20, pp. 7342–7370, 2015.

[145] S. Tatematsu, T. Hibi, T. Okuhara, and M. Misono, "Preparation process and catalytic activity of CsxH3-xPW12O40," *Chemistry Letters*, vol. 13, no. 6, pp. 865–868, 1984.

[146] F. J. S. Careaga, A. Porat, L. Briens, and C. Briens, "Pyrolysis shaker reactor for the production of biochar," *Canadian Journal of Chemical Engineering*, vol. 98, no. 11, pp. 2417–2424, 2020.

[147] B. A. Dar, M. Mohsin, A. Basit, and M. Farooqui, " Sand: A natural and potential catalyst in renowned Friedel Craft's acylation of aromatic compounds ," *Journal of Saudi Chemical Society*, vol. 17, no. 2, pp. 177–180, August 2013.

[148] M. A. Jackson, D. L. Compton, and A. A. Boatengb, " Screening heterogeneous catalysts for the pyrolysis of lignin ," *Journal of Analytical and Applied Pyrolysis*, vol. 85, no. 1–2, pp. 226–230, May 2009.

[149] K. D. Smit, Y. W. Marien, K. M. V. Geem, P. H. M. V. Steenberge, and D. R. D'hooge, "Connecting polymer synthesis and chemical recycling on a chain-by-chain basis: a unified matrix-based kinetic monte carlo strategy," *Reaction Chemistry and Engineering*, vol. 5, pp. 1909–1928, 2020.

[150] A. S. Shalygin, I. V. Kozhevnikov, E. Y. Gerasimov, A. S. Andreev, O. B. Lapina, and O. N. Martyanov, "The impact of si/al ratio on properties of aluminosilicate aerogels," *Microporous and Mesoporous Materials*, vol. 251, pp. 105–113, 2017.

[151] J. Van Den Brand, O. Blajiev, P. C. Beentjes, H. Terryn, and J. H. De Wit, "Interaction of ester functional groups with aluminum oxide surfaces studied using infrared reflection absorption spectroscopy," *Langmuir*, vol. 20, no. 15, pp. 6318–6326, 2004.

[152] A. R. Barron, "The interaction of carboxylic acids with aluminium oxides: Journeying from a basic understanding of alumina nanoparticles to water treatment for industrial and humanitarian applications," *Dalton Transactions*, vol. 43, no. 22, pp. 8127–8143, 2014.

[153] G. Mitran, S. Chen, K. L. Dolge, W. Huang, and D. K. Seo, "Ketonic decarboxylation and esterification of propionic acid over beta zeolites," *Microporous and Mesoporous Materials*, vol. 310, pp. 1–11, 2021.

[154] J. Lu, H. Hao, L. Zhang, Z. Xu, L. Zhong, Y. Zhao, D. He, J. Liu, D. Chen, H. Pu, S. He, and Y. Luo, "The investigation of the role of basic lanthanum (La) species on the improvement of catalytic activity and stability of HZSM-5 material for eliminating

methanethiol-(CH3SH),” *Applied Catalysis B: Environmental*, vol. 237, pp. 185–197, 2018.

[155] M. Lazzari, T. Kitayama, S. He, K. Hatada, and O. Chiantore, “The effect of stereoregularity on the thermal behavior of poly(methacrylic acid),” *Polymer Bulletin*, vol. 39, no. 1, pp. 85–91, 1997.

[156] T. Omojola, N. Cherkasov, and A. e. a. McNab, “ Mechanistic Insights into the Desorption of Methanol and Dimethyl Ether Over ZSM-5 Catalysts,” *Catalysis Letters*, no. 148, pp. 474–488, December 2018.

[157] F. Haase and J. Sauer, “ Interaction of methanol with Broensted acid sites of zeolite catalysts: an ab initio study,” *Journal of the American Chemical Society*, vol. 13, no. 117, p. 3780–3789, April 1995.

[158] M. Kaarsholm, F. Joensen, R. Cenni, J. Chaouki, and G. S. Patience, “MeOH to DME in bubbling fluidized bed: Experimental and modelling,” *Canadian Journal of Chemical Engineering*, vol. 89, no. 4, pp. 274–283, 2011.

[159] T. K. Phung, C. Herrera, M. A. Larrubia, M. Garcia-Dieguez, E. Finocchio, L. J. Alemany, and G. Busca, “Surface and catalytic properties of some γ-al2o3 powders,” *Applied Catalysis A: General*, vol. 483, pp. 41–51, 2014. [Online]. Available: https://www.sciencedirect.com/science/article/pii/S0926860X14004062

[160] P. F. H. Harmsen, M. M. Hackmann, and H. L. Bos, “Green buildingblocks for bio-based plastics,” *Biofuels, Bioprod. Biorefin.*, vol. 8, pp. 306–324, 2014.

[161] P. Sang-Hyun, T. Dishisha, S. Dayankac, J. Gerelsaikhan, S. Lundmark, N. Rehnberg, and R. Hatti-Kaul, “A new route for the synthesis of methacrylic acid from 2-methyl-1,3-propanediol by integrating biotransformation and catalytic dehydration,” *Green Chemistry*, vol. 14, pp. 1942–1948, 2012.

[162] Markets and Markets, “Polymethyl methacrylate (pmma) market by grade (general purpose, optical), form(extruded sheet, cast acrylic sheet, pellets, beads), end-use industry (signs & displays, construction, automotive, lighting fixtures, electronics, marine, healthcare) & region—global forecast to 2027,” 2022. [Online]. Available: https://www.marketsandmarkets.com/Market-Reports/polymethyl-methacrylate-pmma-market-715.html(accessed:June2022)

[163] O. H. Bailey, R. A. Montag, and J. S. Yoo, “Methacrylic acid synthesis,” *Applied Catalysis A: General*, vol. 88, no. 2, pp. 163–177, 1992.

[164] CEFIC. (2021) MMAtwo. Second generation of methyl methacrylate (MMA). [Online]. Available: https://www.mmatwo.eu/

[165] O. V. Chub, N. Saadatkhah, J.-L. Dubois, and G. S. Patience, "Fluidized bed poly (methyl methacrylate) thermolysis to methyl methacrylate followed by catalytic hydrolysis to methacrylic acid," *Applied Catalysis A: General*, p. 118637, 2022.

[166] P. Audri, P. V. Upara, U. Ratnaparkhi, and M. Sakhalkar, "Hydrolysis and esterification with acid catalysts," WO Patent WO 2012/164 573 A2, December 6, 2012. [Online]. Available: https://patents.google.com/patent

[167] J. W. Huffman and P. G. Harris, "A convenient procedure for the hydrolysis of hindered esters," *Synthetic Communications*, vol. 6, no. 7, pp. 481–484, 1976.

[168] I. Kim, J. Kim, and D. Lee, "A comparative study on catalytic properties of solid acid catalysts for glycerol acetylation at low temperatures," *Applied Catalysis B: Environmental*, vol. 148–149, pp. 295–303, 2014.

[169] A. Bérard, B. Blais, and G. S. Patience, "Experimental methods in chemical engineering: Residence time distribution—rtd," *The Canadian Journal of Chemical Engineering*, vol. 98, no. 4, pp. 848–867, 2020.

[170] P. Perreault, E. Robert, and G. S. Patience, "Experimental methods in chemical engineering: Mass spectrometry – ms," *The Canadian Journal of Chemical Engineering*, vol. 97, no. 5, pp. 1036–1042, 2019.

[171] M. Thommes, K. Kaneko, A. V. Neimark, J. P. Olivier, F. Rodriguez-Reinoso, J. Rouquerol, and K. S. Sing, "Physisorption of gases, with special reference to the evaluation of surface area and pore size distribution (iupac technical report)," *Pure and Applied Chemistry*, vol. 87, no. 9–10, pp. 1051–1069, 2015.

[172] K. P. Galvin, "A conceptually simple derivation of the kelvin equation," *Chemical Engineering Science*, vol. 60, no. 16, pp. 4659–4660, 2005.

[173] E. D. Garbowski and C. Mirodatos, "Investigation of structural charge transfer in zeolites by uv spectroscopy," *Journal of Physical Chemistry*, vol. 86, pp. 97–102, 1982.

[174] E. Péré, H. Cardy, O. Cairon, M. Simon, and S. Lacombe, "Quantitative assessment of organic compounds adsorbed on silica gel by ftir and uv–vis spectroscopies: the contribution of diffuse reflectance spectroscopy," *Vibrational Spectroscopy*, vol. 25, pp. 163–175, 2001.

[175] M. Sharif Sh., F. Golestani Fard, E. Khatibi, and H. Sarpoolaky, "Dispersion and stability of carbon black nanoparticles, studied by ultraviolet–visible spectroscopy," *Journal of the Taiwan Institute of Chemical Engineers*, vol. 40, no. 5, pp. 524–527, 2009.

[176] M. Johansson and K. Klier, "Surface acidity (brønsted and lewis) by high resolution x-ray photoelectron spectroscopy," *Topics in Catalysis*, vol. 4, pp. 99–108, 1997.

[177] T. L. Barr, "The nature of the relative bonding chemistry in zeolites: an xps study," *Zeolites*, vol. 10, no. 8, pp. 760–765, 1990.

[178] A. V. Naumkin, A. Kraut-Vass, S. W. Gaarenstroom, , and C. J. Powell. (2012) Nist x–ray photoelectron spectroscopy database. [Online]. Available: https://www.srdata.nist.gov/xps

[179] P. D. Schulze, S. L. Shaffer, R. L. Hance, and D. L. Utley, "Adsorption of water on rhenium studied by xps," *Journal of Vacuum Science and Technology A*, vol. 1, no. 1, pp. 97–99, 1983.

[180] R. B. Borade and A. Clearfield, "Characterization of acid sites in beta and zsm-20 zeolites," *The Journal of Physical Chemistry*, vol. 96, no. 16, pp. 6729–6737, 1992.

[181] V. Mastikhin, I. Mudrakovsky, and A. Nosov, "1h nmr magic angle spinning (mas) studies of heterogeneous catalysis," *Progress in nuclear magnetic resonance spectroscopy*, vol. 23, no. 3, pp. 259–299, 1991.

[182] A. Zheng, S. Li, S.-B. Liu, and F. Deng, "Acidic properties and structure–activity correlations of solid acid catalysts revealed by solid-state NMR spectroscopy," *Accounts of Chemical Research*, vol. 49, no. 4, pp. 655–663, 2016.

[183] L. Lakiss, C. Kouvatas, J.-P. Gilson, H. A. Aleksandrov, G. N. Vayssilov, N. Nesterenko, S. Mintova, and V. Valtchev, "Unlocking the potential of hidden sites in faujasite: New insights in a proton transfer mechanism," *Angewandte Chemie*, vol. 60, pp. 26 702–26 709, 2021.

[184] Z. Wang, T. Li, Y. Jiang, O. Lafon, Z. Liu, J. Trébosc, A. Baiker, J. P. Amoureux, and J. Huang, "Acidity enhancement through synergy of penta- and tetra–coordinated aluminum species in amorphous silica networks," *Nature Communications*, vol. 11, no. 1, pp. 259–299, 2020.

[185] M. Niwa and N. Katada, "New Method for the Temperature-Programmed Desorption (TPD) of Ammonia Experiment for Characterization of Zeolite Acidity: A Review," *The Chemical Record*, vol. 13, pp. 432–455, 2013.

[186] M. A. Abedin, S. Kanitkar, N. Kumar, Z. Wang, K. Ding, G. Hutchings, and J. J. Spivey, "Probing the surface acidity of supported aluminum bromide catalysts," *Catalysts*, vol. 10, pp. 869–883, 2020.

[187] M. Miura, Y. Kubota, T. Iwaki, K. Takimoto, and Y. Muraoka, "Nature of Acid Sites on the Surface of Silica-alumina. I. The Relation between the Acid Property of Sites and the Heat of Immersion," *Bulletin of the Chemical Society of Japan*, vol. 42, no. 6, pp. 1476–1480, 1969.

[188] Z. Si, D. Weng, X. Wu, J. Yang, and B. Wang, "Modifications of CeO2–ZrO2 solid solutions by nickel and sulfate as catalysts for NO reduction with ammonia in excess O2," *Catalysis Communications*, vol. 11, no. 13, pp. 1045–1048, 2010.

[189] H. Higuchi and K. Kida, "Process for producing methyl methacrylate," US Patent US5 087 737A, February 11, 1992.

[190] A. Godefroy, G. S. Patience, R. Cenni, and J.-L. Dubois, "Regeneration studies of redox catalysts," *Chemical Engineering Science*, vol. 65, no. 1, pp. 261–267, 2010.

[191] A. A. Gordus, "Chemical equilibrium: I. the thermodynamic equilibrium constant," *Journal of Chemical Education*, vol. 68, no. 2, p. 138, 1991.

[192] M. Grzesik, J. Skrzypek, and M. Witczak, "Kinetic models for esterification of methacrylic acid using n-propanol and isopropanol," in *Studies in Surface Science and Catalysis*. Elsevier Inc., 2001, vol. 133, pp. 541–545.

[193] A. W. Birley, R. J. Heath, and M. J. Scott, "Other amorphous thermoplastics," in *Plastics Materials: Properties and Applications*. Boston, MA: Springer US, 1988, pp. 60–71.

[194] U. Ali, K. J. B. A. Karim, and N. A. Buang, "A review of the properties and applications of poly (methyl methacrylate(pmma)," *Polymer Reviews*, vol. 4, no. 55, pp. 678–705, 2015.

[195] E. Pawar, "A review article on acrylic pmma," *IOSR Journal of Mechanical and Civil Engineering*, vol. 13, no. 2, pp. 1–4, 2016.

[196] M. S. Zafar, "Prosthodontic applications of polymethyl methacrylate (pmma): An update," *Polymers*, vol. 12, no. 10, pp. 1–35, 2020.

[197] M. Belkheir, M. Boutaleb, A. Mokaddem, and B. Doumi, "Predicting the effect of coconut natural fibers for improving the performance of biocomposite materials based on the poly (methyl methacrylate)—pmma polymer for engineering applications," *Polymer Bulletin*, vol. 79, pp. 5635–5665, 2022.

[198] M. Shi, J. D. Kretlow, P. P. Spicer, Y. Tabata, N. Demian, M. E. Wong, F. K. Kasper, and A. G. Mikos, "Antibiotic-releasing porous polymethylmethacrylate/gelatin/antibiotic constructs for craniofacial tissue engineering," *Journal of controlled release*, vol. 152, no. 1, pp. 196–205, 2011.

[199] R. Sharma, V. Mahto, and H. Vuthaluru, "Synthesis of pmma/modified graphene oxide nanocomposite pour point depressant and its effect on the flow properties of indian waxy crude oil," *Fuel*, vol. 235, pp. 1245–1259, 2019.

[200] N. Grassie and H. W. Melville, "Thermal degradation of polymethylmethacrylate," *Bulletin des Sociétés Chimiques Belges*, vol. 57, no. 4–6, pp. 142–153, 1948.

[201] E. D. Segui and B. C. Alarcon, "Process and device for the regeneration of monomers starting from polymethacrylate and, more especially, methyl polymethacrylate," US Patent US2 858 255A, October, 28, 1958. [Online]. Available: https://patents.google.com

[202] P. Bober, A. Oriňák, R. Oriňaková, P. Zamostný, J. Ladomerský, and A. Fedorková, "Hydrogen production by catalysed pyrolysis of polymer blends," *Fuel*, vol. 90, no. 6, pp. 2334–2339, 2011.

[203] Y. Ding, W. Zhang, X. Zhang, D. Han, W. Liu, and J. Jia, "Pyrolysis and combustion behavior study of pmma waste from micro-scale to bench-scale experiments," *Fuel*, vol. 319, p. 123717, 2022.

[204] A. Erkiaga, G. Lopez, I. Barbarias, M. Artetxe, M. Amutio, J. Bilbao, and M. Olazar, "Hdpe pyrolysis-steam reforming in a tandem spouted bed-fixed bed reactor for h2 production," *Journal of Analytical and Applied Pyrolysis*, vol. 116, pp. 34–41, 2015.

[205] H. Li, J. Li, J. Bodycomb, and G. S. Patience, "Experimental methods in chemical engineering: Particle size distribution by laser diffraction—PSD," *Canadian Journal of Chemical Engineering*, vol. 97, no. 7, pp. 1974–1981, 2019.

[206] X. Li, H. Han, W. Xu, S.-J. Hwang, P. Lu, A. Bhan, and M. Tsapatsis, "Enhanced reactivity of accessible protons in sodalite cages of faujasite zeolite," *Angewandte Chemie*, vol. 134, no. 5, p. e202111180, 2022.

[207] A. W. Nienow and D. J. Cheesman, "The effect of shape on the mixing and segregation of large particles in a gas-fluidised bed of small ones," in *Fluidization*, J. R. Grace and J. M. Matsen, Eds. New York: Plenum Press, 1980, pp. 373–380.

[208] M. Aerov and O. Todes, *Hydraulic and thermal fundamentals of the operation of devices with a stationary and fluidized granular layer*. Khimiya, Leningrad, 1968.

[209] H. Jiang, H. Chen, J. Gao, J. Lu, Y. Wang, and C. Wang, "Characterization of gas–solid fluidization in fluidized beds with different particle size distributions by analyzing pressure fluctuations in wind caps," *Chemical Engineering Journal*, vol. 352, pp. 923–939, 2018.

[210] C. L. Lin, T. H. Peng, and W. J. Wang, "Effect of particle size distribution on agglomeration-defluidization during fluidized bed combustion," *Powder Technology*, vol. 207, no. 1-3, pp. 290–295, 2011.

[211] M. L. Passos, M. A. S. Barrozo, and A. S. Mujumdar, *Fluidization Engineering Practice*, 2nd ed. Quebec, QC: Laval-Canada, 2014.

[212] Y. Zhong, J. Gao, Z. Guo, and Z. Wang, "Mechanism and prevention of agglomeration/defluidization during fluidized-bed reduction of iron ore," in *Iron Ores and Iron Oxide Materials*, V. Shatokha, Ed. London, UK: IntechOpen, 2018, p. 280. [Online]. Available: https://www.intechopen.com/books/6335

[213] P. Cai, I. J. Hartley, K. H. Lee, and L. L. Jacobsen, "Method of detecting and correcting local defluidization and channeling in fluidized-bed reactors for polymerization," US Patent US6 384 157B1, May, 16, 2000. [Online]. Available: https://patents.google.com

[214] O. Chub, G. S. Patience, and J.-L. Dubois, "Zeolite Y hydrolyses methyl methacrylate to methacrylic acid in the gas phase," 2022, submitted for publication. [Online]. Available: https://ssrn.com/abstract=4159276

[215] S. Vyazovkin, A. K. Burnham, J. M. Criado, L. A. Pérez-Maqueda, C. Popescu, and N. Sbirrazzuoli, "Ictac kinetics committee recommendations for performing kinetic computations on thermal analysis data," *Thermochimica Acta*, vol. 520, no. 1–2, pp. 1–19, 2011.

[216] S. Vyazovkin, K. Chrissafis, M. L. D. Lorenzo, N. Koga, M. Pijolat, B. Roduit, N. Sbirrazzuoli, and J. J. Suñol, "Ictac kinetics committee recommendations for collecting experimental thermal analysis data for kinetic computations," *Thermochimica Acta*, vol. 590, pp. 1–23, 2014.

[217] J. A. Conesa, A. Marcilla, J. A. Caballero, and R. Font, "Comments on the validity and utility of the different methods for kinetic analysis of thermogravimetric data," *Journal of Analytical and Applied Pyrolysis*, vol. 58-59, pp. 617–633, 2001.

[218] A. Y. Snegirev, V. A. Talalov, V. V. Stepanov, O. P. Korobeinichev, I. E. Gerasimov, and A. G. Shmakov, "Autocatalysis in thermal decomposition of polymers," *Polymer Degradation and Stability*, vol. 137, pp. 151–161, 2017.

[219] W. Kaminsky, "Recycling of polymers by pyrolysis," *Le Journal de Physique IV*, vol. 3, no. 7, pp. 1543–1552, 1993.

[220] J. M. Criado, L. A. Pérez-Maqueda, P. E. Sánchez, J. A. Perejón, and M. J. Diánez, "Sample controlled thermal analysis (SCTA): Applications to the kinetic analysis of solid state reactions and the synthesis of materials," in *Thermal Analysis Applied to Complex Systems: Slags, Glasses and Ceramics.* Amsterdam: Transworld Research Network, 2013, vol. 37, no. 2, pp. 109–142.

[221] P. E. Sánchez-Jiménez, L. A. Pérez-Maqueda, A. Perejón, and J. M. Criado, "Combined kinetic analysis of thermal degradation of polymeric materials under any thermal pathway," *Polymer Degradation and Stability*, vol. 94, no. 11, pp. 2079–2085, 2009.

[222] P. J. Barrie, "The mathematical origins of the kinetic compensation effect: 1. the effect of random experimental errors," *Physical Chemistry Chemical Physics*, vol. 14, pp. 318–326, 2012.

[223] J. Li and S. I. Stoliarov, "Measurement of kinetics and thermodynamics of the thermal degradation for non-charring polymers," *Combustion and Flame*, vol. 160, no. 7, pp. 1287–1297, 2013.

[224] S. Lomakin, J. E. Brown, R. S. Breese, and M. R. Nyden, "An investigation of the thermal stability and char-forming tendency of cross-linked poly (methyl methacrylate)," *Polymer degradation and stability*, vol. 41, no. 2, pp. 229–243, 1993.

[225] T. Fateh, F. Richard, T. Rogaume, and P. Joseph, "Experimental and modelling studies on the kinetics and mechanisms of thermal degradation of polymethyl methacrylate in

nitrogen and air," *Journal of Analytical and Applied Pyrolysis*, vol. 120, pp. 423–433, 2016.

[226] A. K. Burnham, R. K. Weese, and B. L. Weeks, "A distributed activation energy model of thermodynamically inhibited nucleation and growth reactions and its application to the beta–delta phase transition of HMX," *The Journal of Physical Chemistry B*, vol. 108, no. 50, pp. 19 432–19 441, 2004.

[227] D. W. Marquardt, "An algorithm for least-squares estimation of nonlinear parameters," *Journal of the Society for Industrial and Applied Mathematics*, vol. 11, no. 2, pp. 431–441, 1963.

[228] B. L. Denq, W. Y. Chiu, and K. F. Lin, "Kinetic model of thermal degradation of polymers for nonisothermal process," *Journal of Applied Polymer Science*, vol. 66, no. 10, pp. 1855–1868, 1997.

[229] J. J. Krishna, S. S. Kumar, O. Korobeinichev, and R. Vinu, "Detailed kinetic analysis of slow and fast pyrolysis of poly(methyl methacrylate)-flame retardant mixtures," *Thermochimica Acta*, vol. 687, p. 178545, 2020.

[230] K. Moinuddin, Q. S. Razzaque, and A. Thomas, "Numerical simulation of coupled pyrolysis and combustion reactions with directly measured fire properties," *Polymers*, vol. 12, no. 9, pp. 1–19, 2020.

[231] L. Jiang, X.-R. Yang, X. Gao, Q. Xu, O. Das, J.-H. Sun, and M. K. Kuzman, "Pyrolytic kinetics of polystyrene particle in nitrogen atmosphere: Particle size effects and application of distributed activation energy method," *Polymers*, vol. 17, no. 421, pp. 1–18, 2020.

[232] A. Barlow, R. Lehrle, J. Robb, and D. Sunderland, "Polymethylmethacrylate degradation-kinetics and mechanisms in the temperature range 340–460 c," *Polymer*, vol. 8, pp. 537–545, 1967.

APPENDIX A DEGRADATION KINETICS OF POLY(METHYL METHACRYLATE) AT NON-ISOTHERMAL CONDITIONS

Depolymerization end-of-life plastics to monomer is a sustainable alternative to petroleum as a feedstock. Poly(methyl methacrylate) (PMMA) is one of the few polymers that thermally degrades to monomer easily and fluidized bed reactors are effective contactors because of their high heat transfer rates. Industrial reactors operate at particles sizes of about 3 mm to 30 mm in form of pellets or crashed scrap polymer grains. However, the industrial fluidized beds are susceptible to slumping (defluidization) as the melted polymer forms agglomerates at some reaction conditions. Micronizing the plastic to a fine powder and its dispersing across the layer minimizes slumping on the one hand and increases the cost of investing in technology on the other. The reaction kinetics depend on temperature and to evaluate this contribution to chemical recycling process we pyrolyzed PMMA non-isothermally in a thermogravimetric analyzer (TGA) at heating ramps of $5\,^{\circ}\mathrm{C\,min^{-1}}$ to $40\,^{\circ}\mathrm{C\,min^{-1}}$. A high resolution ramp demonstrated that a single reaction mechanism likely accounts for $> 95\,\%$ of the change in mass of PMMA. A first order model predicted the micron-sized PMMA degradation (R^2>0.999) and the activation energy was in the range $160\,\mathrm{kJ\,mol^{-1}}$ to $180\,\mathrm{kJ\,mol^{-1}}$. The major reaction products was methyl methacrylate and an on-line mass spectrometer detected CO_2 and traces of acetone, methanol, water, dimethyl ether (DME), methacrylic acid (MAA), hydrogen, propene, ethane, methane, and ethylene in the effluent. Extrapolation of the results to heating rates up to $400\,^{\circ}\mathrm{C\,min^{-1}}$, inherent in industrial reactors, will allow optimizing their operation.

Introduction

PMMA is a thermoplastic that was developed in the early 1930s. Its attractive physicochemical properties like high transparency, stiffness, and thermal stability, make it an ideal choice for applications in electronics, automotives, construction, and medicine [194, 195]. More than 3 Mt of PMMA is produced annually worldwide, of which 10 % is synthesized in Europe, but only 3 % of this is recycled [4, 8]. Substituting fossil fuel with scrap polymer as a feedstock reduces the environmental burden while minimizing cost to produce PMMA [4]. Although depolymerizing PMMA scraps and cuttings to methyl methacrylate (MMA) is practiced commercially, full recycle of PMMA plastics has been hindered by byproducts that have similar boiling points to MMA and thus require energy intensive separation steps. Hydrolyzing MMA to methacrylic acid (MAA) improves the process economics (as the MAA's boiling point is 61 °C higher), but to ensure profitability requires a process that minimizes

side reactions while maximizing heat and mass transfer rates. Our previous study [165] on catalytic depolymerization of virgin PMMA with subsequent hydrolysis of its monomer to methacrylic acid demonstrated high selectivity towards acid formation, and other reaction products had lower boiling points.

Ultimately the process design will depend on the reaction kinetics, particularly the reaction rate constant and activation energy, which vary widely in literature reports.

MMA polymerizes to PMMA following either a free-radical or anionic mechanism. Free-radical polymerization produces high average chain lengths (1000) and dispersity ($\geq$ 1.5). Anionic polymerization produces shorter chains ($\leq$100) with a narrower dispersion (about 1) [4]. PMMA starts to degrade above the glass transition temperature [22] and chain length (which is determined by the polymerization method), spatial arrangement of the PMMA (isotactic, syndiotactic, or atactic) and dispersity (branching degree) affect how it depolymerizes [25, 26]. Co-polymers and stabilizers, added to PMMA during its preparation to achieve the desired technical specification, catalyze or inhibit the depolymerization process [27–32].

Literature reports that the least stable bonds break at the head-to-head linkage (160 °C) while unsaturated ends break at 270 °C and random scission occurs at 370 °C [24, 34–37]. Later studies demonstrated that the depolymerization process depends on molecular weight, physical properties, experimental conditions [25, 26, 38, 39]. Some studies demonstrated the decreasing of activation energy at decreasing the particle size in inert or in air [40–43] and shape [44], while Smolders and Baeyens (2004) [126] demonstrated that the specific surface area of sand particles in fluidized beds is the principal parameter restricting heat and mass transfer since the polymer melts in fluidized bed before thermolysis starts. The higher the specific surface area, the less the transport limitations regardless of particle size of injecting polymer.

Also, the degradation kinetics depend on how the data is collected and and the computational methods [215–218]. Much of the literature data has been measured in thermogravimetric analyzers (TGA) over a narrow range and low heating rates [39], which ensures the PMMA thermally equilibrates [216]. In fluidized bed reactors, PMMA particles of ambient temperature are injected into a bed of solids (with/without catalyst) by pulse injection [165] in the case of micron-size polymer (<100 µm), through double flap gate or a screw conveyor [20, 219] (about 5 mm pellets), or hopper equipped with pneumatic system (3 mm X 4 mm cylindrical pellets) [16]. Based on prior data [16, 20, 219], we hypothesize that PMMA enters the fluidized bed operating above 300 °C as a solid. At large PMMA particle sizes, this leads to a large thermal gradient within the particle, which can affect the degradation kinetics and change

the reaction path.

In this study, we varied the TGA heat ramp from $5\,\mathrm{K\,min^{-1}}$ to $40\,\mathrm{K\,min^{-1}}$ to evaluate the reaction kinetics of injection grade commercial PMMA while measuring the effluent gas composition. Furthermore, we conducted a high resolution ramp (HRR) to identify secondary and tertiary reaction pathways—head-to-head linkage breaks, unsaturated end breaks, and random scission.

Experimental

Materials

The injection mold grade poly(methyl methacrylate) pellets, ($d_\mathrm{p} = 6\,\mathrm{mm}$, from Arkema), we milled these solids in liquid nitrogen to a particle size less than $60\,\mu\mathrm{m}$ for TGA studies.

Methods

The micronized PMMA powder pyrolyzed in a TA-Q500 thermogravimetric operating with a flow of Ar at $60\,\mathrm{mL\,min^{-1}}$. The PMMA powder was placed on a platinum pan and a Platinel II® thermocouple positioned 2 mm above the sample registered the temperature of gas phase (heated by radiation from the furnace) above the sample with a $\pm 0.01\,\%$ of measurement precision. The nominal deviation between sample and reference was reported as $\pm 1\,^\circ\mathrm{C}$ but our data suggests that there is a time lag of 1.2 min so the difference between sample and reference temperature increases with ramp. All experiments were repeated to assess reproducibility. An HPR-20 TMS bench top mass spectrometer (Hidden Analytical) equipped with a quartz inert capillary analyzed the gas phase composition at the exit. The MS reported data at a frequency of 3 Hz.

Theory

PMMA degrade completely and solid residue is in the range of 0.1 % to 0.4 % [22]. Decomposition kinetics for a single reaction at ambient pressure represents the conversion extent function (α) and temperature (T) [215, 220, 221]:

$$\frac{\mathrm{d}\alpha}{\mathrm{d}t} = k(T) \cdot f(\alpha) \tag{A.1}$$

Introducing the reference temperature T_ref minimize correlation between $k(T_\mathrm{Ref})$ and E_a [222] and the Arrhenius equation transforms to:

$$k(T) = k_0 \cdot \exp\left[\frac{-E_\mathrm{a}}{R} \cdot \left(\frac{1}{T} - \frac{1}{T_\mathrm{ref}}\right)\right] \tag{A.2}$$

Conversion extent α is a function of sample weight change:

$$\alpha = \frac{m_0 - m_\mathrm{t}}{m_0 - m_\mathrm{inf}} \tag{A.3}$$

were, m_0, m_t and , m_inf is the initial, instantaneous and final sample weight correspondingly.

The function $f(\alpha)$ associates with a physical model of a process according to proposed reaction mechanism. Wide used empirical approaches imply model function in a form $(1 - f(\alpha))$ when considering the first order reaction, and Eq. A.4 when the reaction order (n) is different from the first [215, 217].

$$f(\alpha) = (1 - \alpha)^n \tag{A.4}$$

These simplified models formally estimate the apparent activation energy in homogeneous reactions without taking into account heat and mass transfer processes associated with phase transformations on the polymer surface, which depend both on the heating rate of the sample and on the size, dispersion and bulk density of its particles. Such processes result in ascending of the reaction rate at the beginning of the process (kinetics limitation region) and its descending at the end of the reaction (mass-transfer limitation region). A typical S-curve of α=$f(t)$ represents such behavior [215].

According to Sěstac [85], to avoid incorrect interpretation of experimental data, all the factors affecting processes of transport and nucleation should be included in the function $f(\alpha)$. Existing theories propose analytical Avrami-Erofeev model for accurate estimation of kinetic parameters in a wide range of kinetic mechanisms and reaction conditions [44, 85]. This model considers various nucleation mechanisms during polymer degradation (n varies from 1/4 to 3 [41]):

$$f(\alpha) = n(1 - \alpha)(-\ln(1 - \alpha))^{(n-1)/n} \tag{A.5}$$

or more general extended Prout–Tompkins model (at p=0) [215]:

$$f(\alpha) = \alpha^m (1 - \alpha)^n (-\ln(1 - \alpha))^p \tag{A.6}$$

These two approaches cover all possible reaction mechanisms and reaction conditions.

Results and discussion

PMMA degradation

High inert flow rates in a TGA increases heat and mass transfer rates between the sample

and gas phase and improves the removal of reaction products on the one hand but can be a source of uncertainty due to vibration of the platinum pan and a temperature lag on the other [216]. To identify the optimal flow rate, we treated 2.7 mg of PMMA at a heating rate of 25 °C min^{-1} in the range 20 mL min^{-1} to 80 mL min^{-1} in Ar. In these tests, the m/m_0 curve was independent of flow rate (no apparent shift towards an increase or decrease in temperature), indicating the heat transfer and kinetics at PMMA degradation were independent of inert flow rate. In all the subsequent experiments we fed 60 mL min^{-1} of Ar and repeated each run twice to assess reproducibility.

We applied the high resolution ramp (HRR) technique to identify the different types of bonds rupture while the polymer degrades. This technique varies the heating rate in response to a change in the mass loss rate: when the mass loss rate exceeds a threshold value, the temperature ramp decreases and the ramp increases when it is below the threshold. We observed two peaks on the derivative thermogravimetric curve (DTG). The small peak appeared at 260 °C to 270 °C (Figure A.1) as a shoulder of the major one (with the maximum in the range 280 °C to 420 °C). The small peak is characteristic of unsaturated end scission and the major peak describes the random scission [24]. The mass loss of the small peak is negligible ($\delta \leq 5\,\%$), so we assume a one step degradation by random chain scission. Such degradation behavior of PMMA can be explained by the polymer type. Since the PMMA we use in current study is of injection mould grade and its molecular weight is relatively low (100×10^3 g mol^{-1} [165]), the co-monomers in its composition prevent the low-temperature depolymerization.

Previous TGA studies on PMMA degradation focused on the formation of radicals to MMA [25,39,40,223]. Ferriol et al.(2003) reported degradation of PMMA synthesized by free-radical mechanism with high molecular weight (350×10^3 g mol^{-1} to 996×10^3 g mol^{-1}). Korobeinichev et al.(2019) degraded PMMA of 29×10^3 g mol^{-1} polymerized by free radical method.

Holland (2002) [26] reported slight decreasing of the apparent activation energy from 190 kJ mol^{-1} to 150 kJ mol^{-1} with increase of the reciprocal degree of polymerization (1/D) from 0 to 0.008. Thus, peroxide initiators or oxygen added during polymerization process, results in multi step depolymerization mechanism and increase the concentration of labile end groups. But anionically or free-radicals polymerized PMMA are as stable as thermally polymerized one [26].

Several studies reported that PMMA pyrolysis is accompanied by the formation of products in the gas phase like CO_2, CO, CH_4, and methanol above 350 °C, due to random scission and MMA decarboxylation [4, 133, 224]. In some studies, CO_2 was the major gas-phase product [34, 84, 225]. The analysis of time and temperature evolution of these reaction products is of interest for the subsequent study of the kinetics for industrial reactors.

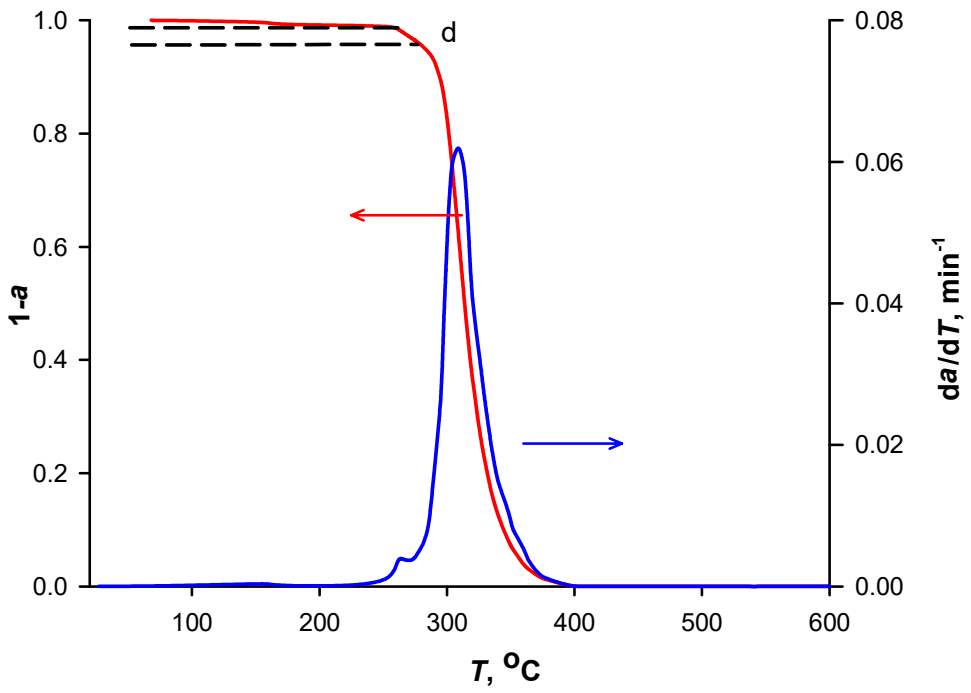

Figure A.1 TG and DTG curves obtained at HRR, 25 °C min^{-1}

At a heating rate of 10 °C min^{-1} in Ar, the PMMA began to lose mass at 270 °C, with a sharp mass loss in the range 300 °C to 400 °C and completely degraded by 420 °C. Half the PMMA reacts by 370 °C (Fig. A.2).

The mass spectrometer (MS) coupled with TGA analyzer registered raw signals at specific masses of: Ar (20), MMA (69), CO_2 (44), CO (28), CH_4 (13), methanol (31), acetone (43), water (18), MAA (86), dimethyl ester (DME) (45), propene (27), H_2 (2), ethane (30) and ethylene(26). The signals of N_2 (14) and O_2 (32) were added to identify any dilution to the concentration by ingress of air at the suction line or at the ferrule between the capillary and the head of the MS.

The time evolution of the mass loss derivative and MS signal of MMA confirms ester formation as a major product of PMMA degradation by random scission. Liquid by-products like acetone, methanol, dimethyl ether (DME), water and methacrylic acid appear as PMMA degradation and during MMA decarboxylation, $< 1\,\%$ (Fig. A.3).

The intensity of MMA peak was much higher compared to other gas-phase degradation products. The maximum concentration of MMA appears at the same time as the maxima for the by-products. We registered the MS spectra of CO_2, H_2, propene, ethane, ethylene and methane in the gas phase. According to the reaction mechanism, CO_2 formation refers to the

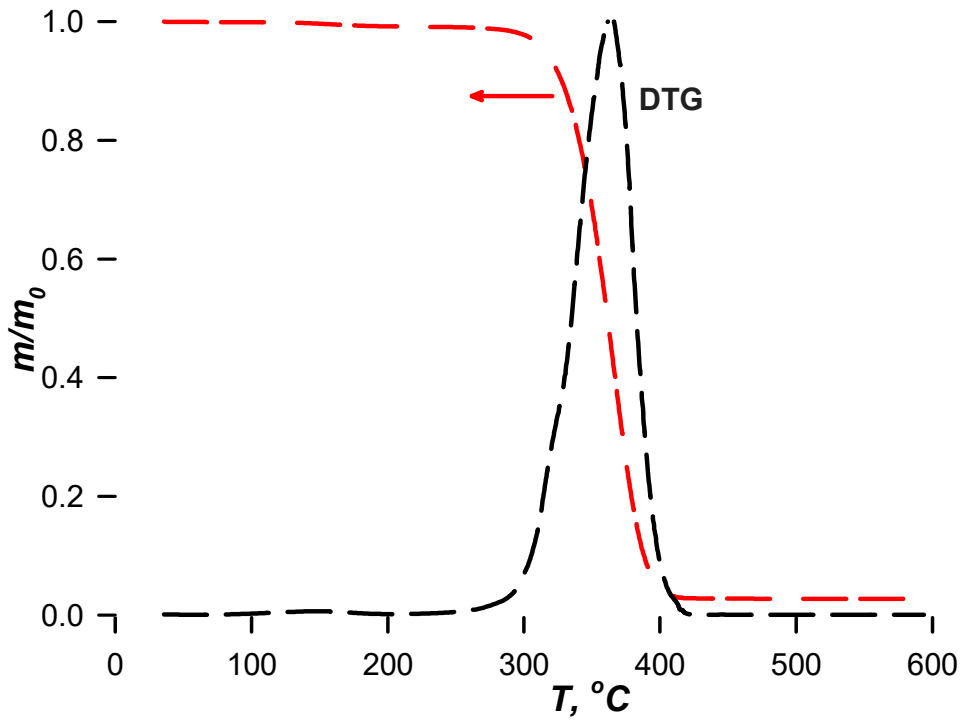

Figure A.2 TGA (red), DTG (black) curves correspond to mass-loss of PMMA at 10 °C min^{-1}.

beginning of decarboxylation of MMA when the temperature exceeds 300 °C (Figure A.1) [4, 165]. Also the presence of oxygen in the macro- molecular polymer chain leads to CO_2 formation [10]. The weak secondary peaks of CO_2 and H_2 emerge above 450 °C and are related to the degradation of the polymer residue. Fateh et al. [225] also reported secondary CO_2 peaks at higher temperature. The C_2-C_4 hydrocarbons (ethylene, ethane, propene) formation accompanied PMMA thermolysis in our study as well as reported in previous studies at PMMA degradation in fluidized bed reactors [20, 22, 126]. In these studies CO_2 appeared as the main degradation product in the gas phase, while the concentrations of the other compounds were less than 1 % to 4 % of the total.

Previous studies considered the degradation kinetics of PMMA over a narrow temperature range to minimize the confounding factor of heat transfer on the kinetics at high heating rates. Nevertheless, the data obtained over a wide range of polymer heating rates are most relevant to industrial reactor operation modes.

We recorded mass change from 24 °C to 700 °C at heating rates 5, 10, 15, 25 and 40 °C min^{-1} and a polymer mass 2.7 mg. At stable heating rates PMMA degraded in one step, the experimental TG curves (Figure **??**,Figure A.6) shifted to higher temperatures at the higher heating rates.

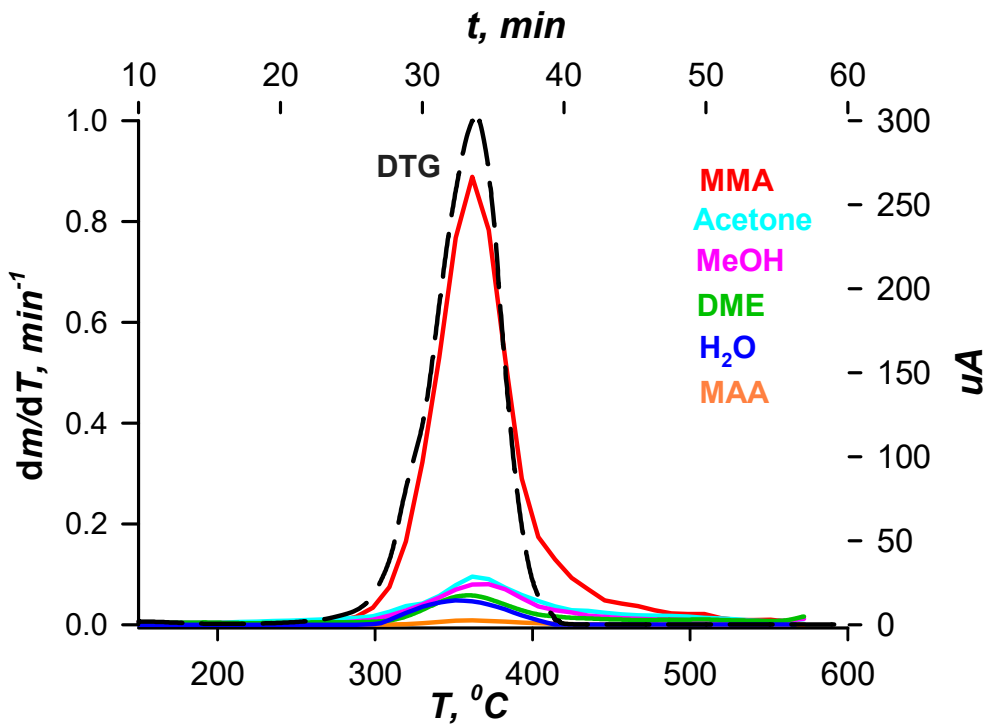

Figure A.3 The DTG curve (black, dashed line) and the MS spectra of liquid products of PMMA thermolysis registered at heating rate 10 °C min^{-1}: MMA (red), acetone (cyan), methanol (pink), dimethyl ether (DME) (green), water (light-blue), methacrylic acid (MAA)(orange).

Kinetic analysis

We approximated the experimental curves with the Avrami-Erofeev rate equation (Equation A.5), which is based on the assumption of random nucleation and the growth of nuclei. The physical meaning of which means the predominance of the phase transformation process over kinetics [226]. The identification of kinetic parameters k_0, E_{a} and n from experimental data (Figure A.5) solved by minimization of the objective function (Eq. A.7).

$$S = \sum_{i=1}^{N_{\mathrm{exp}}} (\alpha_{\mathrm{i}}^{\mathrm{exp}} - \alpha_{\mathrm{i}}^{\mathrm{calc}})^2 \cdot \mu_{\mathrm{i}} \rightarrow min \tag{A.7}$$

where $\alpha_{\mathrm{i}}^{\mathrm{exp}}$, $\alpha_{\mathrm{i}}^{\mathrm{calc}}$ are experimental and calculated conversion extents at referral temperature; μ_{i} - weight coefficient; N_{exp} - number of experiments.

Progress to the minimum was carried out by the Gauss-Marquardt method [227].

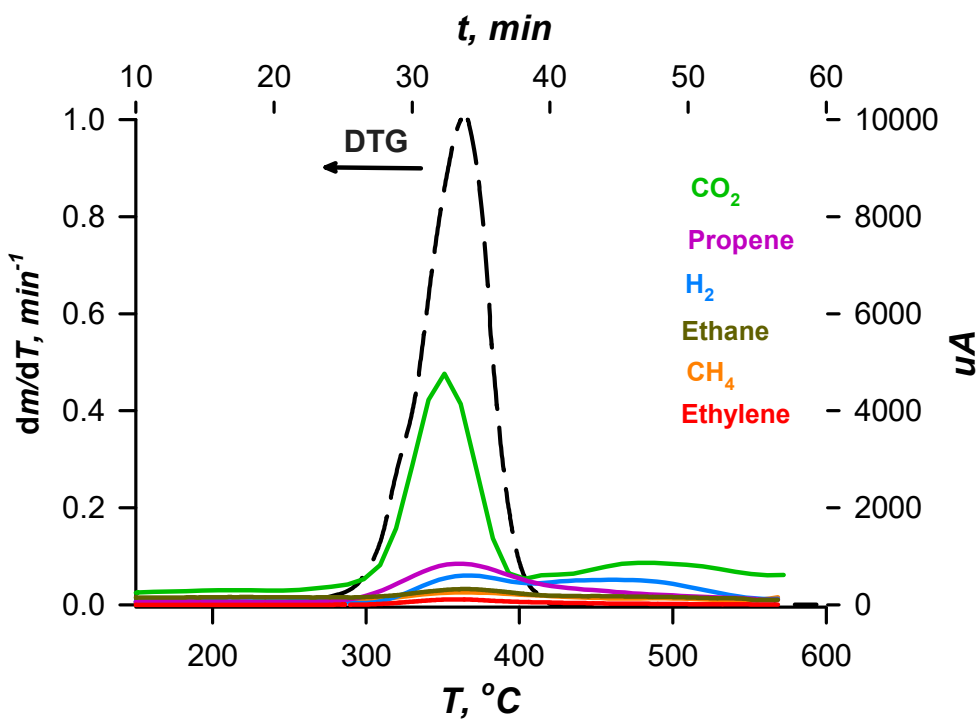

Figure A.4 The DTG curve (black dashed line) corresponds to the mass-loss of PMMA at $10\,^{\circ}\mathrm{C\,min^{-1}}$. The MS signals: CO_2 (green), propene (pink), hydrogen (light blue), ethane (dark yellow), methane (orange), and ethylene (red).

$$R^2 = \frac{\sum_{i=1}^{N_{\mathrm{exp}}}(m_{\mathrm{i}}^{\mathrm{exp}} - m_{\mathrm{i}}^{\mathrm{calc}})^2}{\sum_{i=1}^{N_{\mathrm{exp}}}(\overline{m^{\mathrm{exp}}} - m_{\mathrm{i}}^{\mathrm{calc}})^2} \tag{A.8}$$

Here, $m_{\mathrm{i}}^{\mathrm{exp}}$, $\overline{m^{\mathrm{exp}}}$ and $m_{\mathrm{i}}^{\mathrm{calc}}$ are experimental (i and averaged) and calculated masses of sample; N_{exp} - number of experiments.

The values of the n factor varied from 1/2 to 4 characterize the degree of phase transfer processes. The activation energy slightly varied over the heating rates (Table A.1), however, E_{a} significantly varied in different models. It decreased at increasing of n factor from $362\,\mathrm{kJ\,mol^{-1}}$ (at $n = 1/2$) to $48\,\mathrm{kJ\,mol^{-1}}$ (at $n = 4$) which is similar to results reported earlier $31\,\mathrm{kJ\,mol^{-1}}$ to $272\,\mathrm{kJ\,mol^{-1}}$ [228, 229] (Table A.1). We also minimized the objective function while simulating triplet: n, E_{a} and k_{eff}. The simulation results at $5\,^{\circ}\mathrm{C\,min^{-1}}$ and were close to the first order, from $10\,^{\circ}\mathrm{C\,min^{-1}}$ to $25\,^{\circ}\mathrm{C\,min^{-1}}$ the n factor varied slightly from 1, and at $40\,^{\circ}\mathrm{C\,min^{-1}}$ it exceeded 2 and the activation energy dropped almost twice.

Then, we simulated the kinetic parameters by first order and n-order models (Eq. A.5) to specify the kinetic parameters. Calculations by two models gave the similar results and the

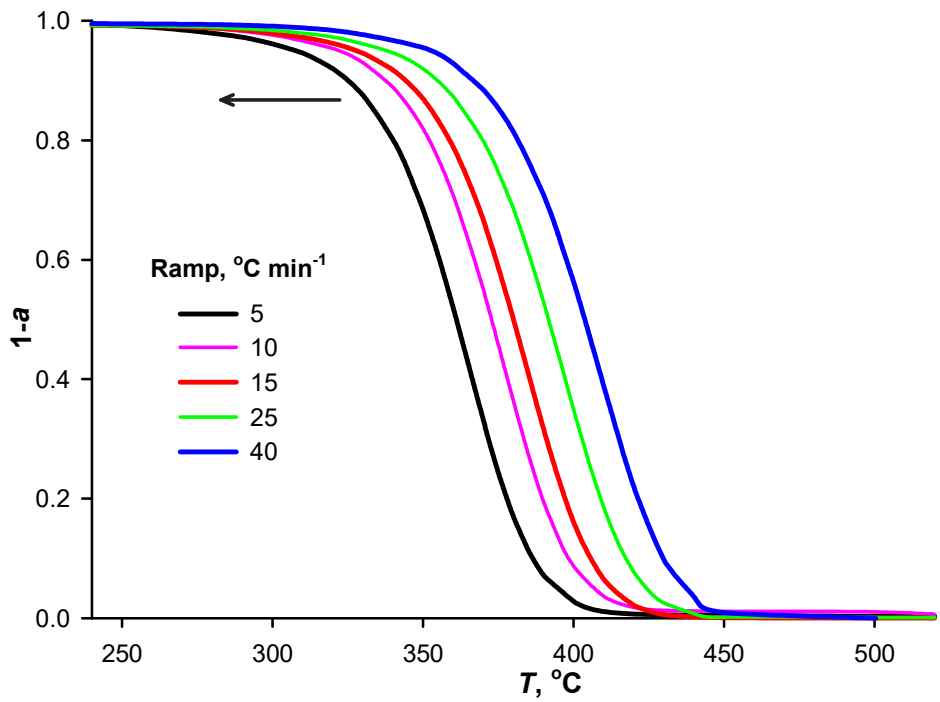

Figure A.5 TG curves of PMMA pyrolysis demonstrated at heating rates 5 °C min^{-1}, 15 °C min^{-1} and 40 °C min^{-1} and inert flow rate 60 mL min^{-1}.

average activation energy were 182 kJ mol^{-1} and 186 kJ mol^{-1} in all range of heating rates. The reaction rate constant at 370 °C was 0.015 min^{-1}. Previous studies reported the E_{a} = 183 kJ mol^{-1} and k_{eff} from 0.015 min^{-1} to 0.017 min^{-1} respectively [39, 218, 228, 230] for the PMMA pyrolyzed at non-isothermal conditions.

We employed the Coats-Redfern method [41, 231] to validate the kinetic model of first order.

$$\ln \frac{g(\alpha)}{T^2} = \ln \frac{AR}{\beta E_{\mathrm{a}}} - \frac{E_{\mathrm{a}}}{RT} \tag{A.9}$$

The linearized experimental data exploring the first reaction order allow to estimate the values of activation energies and frequency factor by plotting the $\ln(g(\alpha)/T^2)$ versus $1/T$ where $g(\alpha)$ = -ln(1-α). The activation energy averaged over the heating rates was about 160 kJ mol^{-1} and reaction rate constant at 370 °C was 0.017 min^{-1} ($R^2 = 0.998$) which allows us to approve domination of the first order model to characterize the degradation of micron-sized PMMA. The previous studies demonstrated the relationship between the E_{a} value and phase nucleation and nuclei growth processes which are high and small values respectively [226]. The activation energy necessary for degradation predicted as 160 kJ mol^{-1} is average compared to the results obtained by other models explored in current study. We presume

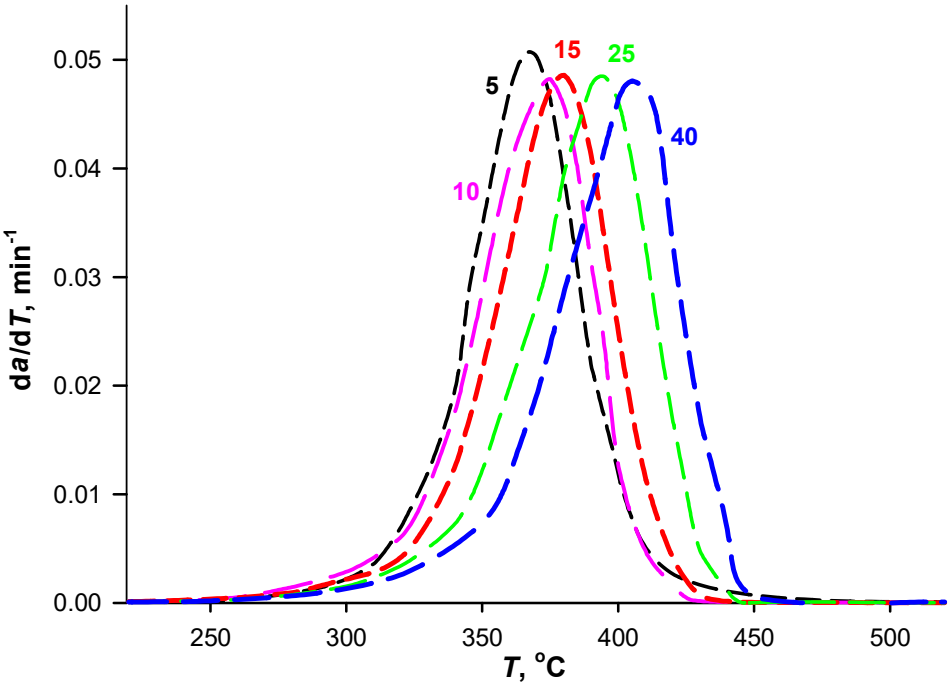

Figure A.6 DTG curves of PMMA pyrolysis demonstrated at heating rates 5 °C min^{-1}, 15 °C min^{-1} and 40 °C min^{-1} and inert flow rate 60 mL min^{-1}.

Table A.1 Apparent kinetic parameters obtained by different models

h °C·min^{-1}	Parameter	Model							
		1-order	n-order	A1/2	A3/2	A2	A3	A4	An
5	E_a, kJ·mol^{-1}	179	177	346	115	87	59	47	180
	Ln(k_{eff})	-4.22	-4.22	-4.49	-4.14	-4.09	-4.07	-4.08	-4.22
	n	1	0.98	0.5	1.5	2	3	4	0.99
	R^2	0.99	1	0.98	0.98	0.98	0.98	0.99	0.99
10	E_a, kJ·mol^{-1}	179	188	359	137	103	61	47	128
	Ln(k_{eff})	-4.89	-4.87	-5.77	-4.60	-4.50	-4.32	-4.29	-4.64
	n	1	1.11	0.5	1.5	2	3	4	1.4
	R^2	0.99	1	0.98	0.99	0.99	0.99	0.99	0.99
15	E_a, kJ·mol^{-1}	182	183	365	121	91	62	48	161
	Ln(k_{eff})	-5.24	-5.24	-6.50	-4.80	-4.60	-4.42	-4.35	-5.09
	n	1	1.01	0.5	1.5	2	3	4	1.13
	R^2	0.99	1	0.99	0.99	0.99	0.98	0.98	0.98
25	E_a, kJ·mol^{-1}	184	189	368	126	94	62	48	154
	Ln(k_{eff})	-5.85	-5.85	-7.73	-7.82	-4.92	-4.62	-4.50	-5.54
	n	1	1.06	0.5	1.5	2	3	4	1.19
	R^2	0.99	1	0.99	0.99	0.99	0.99	0.99	0.99
40	E_a, kJ·mol^{-1}	186	193	372	205	154	63	49	85
	Ln(k_{eff})	-6.44	-6.48	-8.94	-6.58	-6.06	-4.80	-4.63	-5.09
	n	1	1.09	0.5	1.5	2	3	4	2.19
	R^2	0.99	1	0.98	0.99	0.99	0.98	0.98	0.98

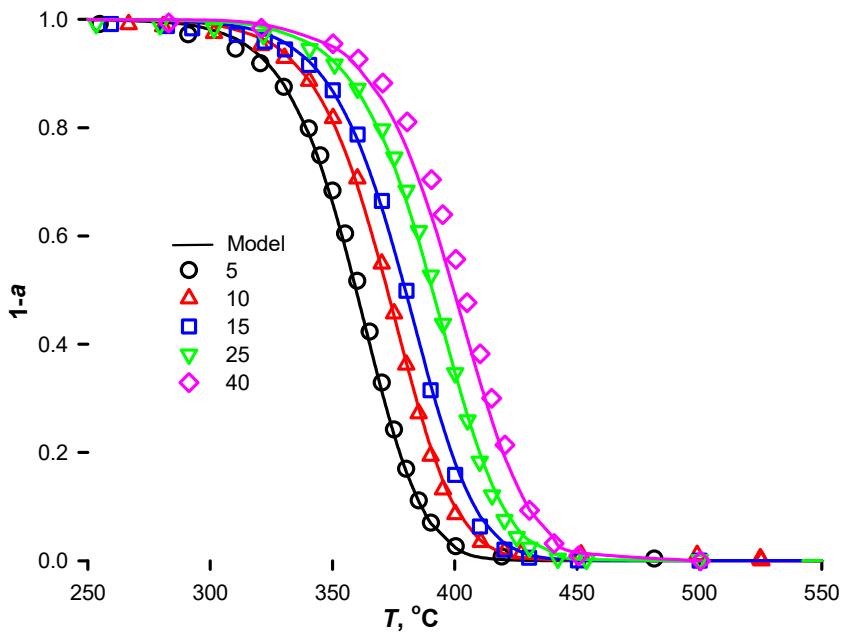

Figure A.7 Simulated results (lines) versus experimental (dots) for the first order model

that, since fine PMMA particles have a smaller volume and a large outer surface of the particles, they are easier to decompose and the effect of phase transitions from solid to liquid is negligible. Prior, Barlow also demonstrated that degradation of micron-sized PMMA in the temperature range from 340 °C to 460 °C is kinetically controlled and describes by the first order model [232].

At the same time, our previous study showed that the temperature lag in the decomposition of 6 mm pellets is only about 15 °C compared to micron-sized PMMA, and particles with a diameter of 0.5 mm to 1 mm decomposed at the same temperatures [165].

Most industrial plants operate well above 400 °C. In commercial, continuous reactors, the heating rate can reach several 100 °C min^{-1}. However, in batch reactor or rotating drums (dry distillation processes), the reactors are heated and cooled on daily basis. Heating to depolymerization temperature can take several hours, but the mass close to the wall of the reactor receives most of the energy, and the rest of the mass is heated by conduction through the polymer. This slow polymer mixing results in high heat and mass transfer limitations. In the fluidized beds, on the contrary, the active mixing of solid particles results in high heat exchange between solid particles and gas phase and temperature is equilibrated in the reaction volume. However, as we mentioned above, the transport restrictions influence when

large PMMA particles, injected at ambient conditions, contact with sand and melt. Smolders demonstrated that, the reaction rate constant is similar for the wide range of PMMA particles size from 100 µm to 1600 µm. In addition, in fluidized bed the reaction is kinetically controlled up to 460 °C [126] compared to the lead bath where transport limitations start already from 380 °C.

Based on the averaged kinetic parameters simulated by Coats-Redfern method, we extrapolated the simulation to the low (1 °C min^{-1}) and high heating rates assuming the fast PMMA pyrolysis (400 °C min^{-1}) (Figure A.8).

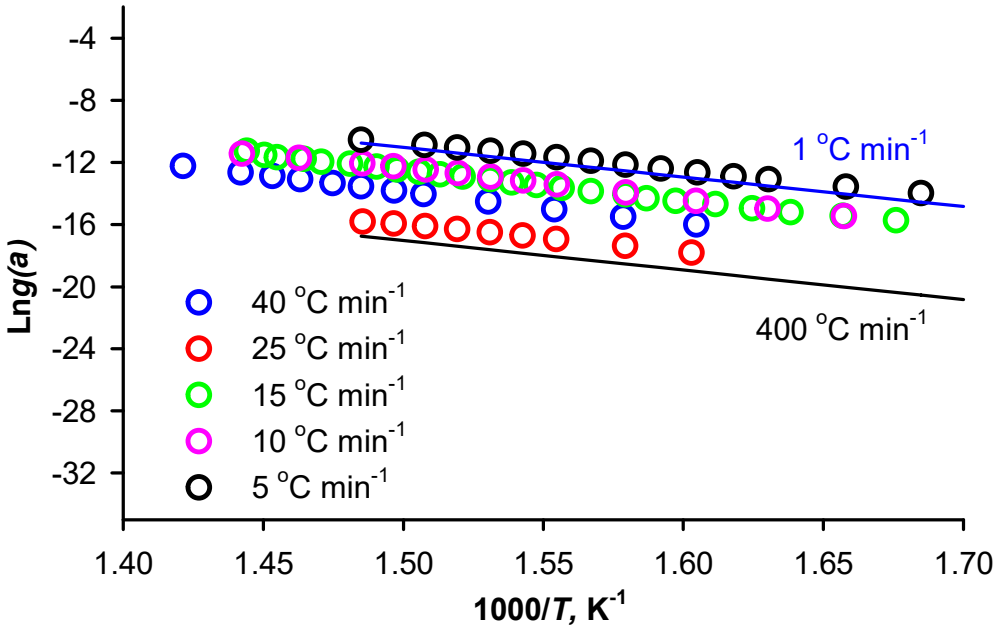

Figure A.8 The linearized experimental data by Coats-Redfern method at variation of heating rates from 5 °C min^{-1} to 40 °C min^{-1} (dots) and extrapolated curves: 1 °C min^{-1} - blue and 400 °C min^{-1} black assuming the pyrolysis of micronized PMMA.

Conclusion

Poly(methyl methacrylate) degraded in a wide range of heating rates 5 °C min^{-1} to 40 °C min^{-1} and PMMA thermolyzes by random scission. We observed MMA, acetone, methanol, dimethyl ether, water and methacrylic acid as liquid-phase products; and CO_2, propene, hydrogen, ethane, methane and ethylene as gas phase products of PMMA thermolysis. All reaction products appeared th the same time as MMA.

The MMA and CO_2 had higher intensity while other reaction products appeared in a very small amount due to decarboxylation of MMA followed by radicals reactions The micron-sized PMMA degraded in one step and first order model predicts well its degradation behavior.

The activation energy estimated by the first order model was $180\,\mathrm{kJ\,mol^{-1}} \pm 65\,\mathrm{kJ\,mol^{-1}}$ with $R^2 = 0.99$ and the results were confirmed by the Coats-Redfern model ($160\,\mathrm{kJ\,mol^{-1}}$ with $R^2 = 0.99$). The results obtained represent the interest for the design of industrial fluidized bed reactors.